MECHANISM OF PHOTOREDUCTION AND STEREOCHEMICAL ASPECTS OF AXIAL LIGATION IN SOME IRON-PORPHYRINS MONITORED BY RESONANCE RAMAN SPECTROSCOPY

NABO KUMAR CHAUDHURY
DEPARTMENT OF PHYSICS
SCHOOL OF PHYSICAL SCIENCES
NORTH-EASTERN HILL UNIVERSITY
SHILLONG - 793003

SYNOPSIS OF THE THESIS SUBMITTED
FOR THE DEGREE OF

DOCTOR OF PHILOSOPHY

To

THE NORTH-EASTERN HILL UNIVERSITY

SHILLONG - 793 001

INDIA

NOVEMBER, 1990

Physics

DS

535.846

CHA

SYNOPSIS

Porphyrin complexes have long been considered materials of great importance because of their ubiquitous properties and significant role in a variety of physico-chemical functions. Heme-proteins have therefore been investigated on multi and interdisciplinary levels. All these proteins containing an iron-porphyrin as the prosthetic group are responsible for oxygen transport (hemoglobin, myoglobin and cytochromes b, c), oxygen reduction (cytochrome oxidase), hydrogen peroxide utilization and destruction (peroxidases and catalases) and many other functions. The active site in each case contains, most often, an iron protoporphyrin-IX and obviously these diverse functions must be dictated by various stereochemical parameters like oxidation and spin states, the nature of axial ligands, state of coordination and, of course, the environment. The essential biochemical processes, however, require the reduced state of iron as in cooperative binding of oxygen in hemoglobin. In recent years, reduction of iron-porphyrin complexes has been achieved by chemical[1], electrochemical[2] or photochemical[3] methods and monitored by different spectroscopic techniques. But so far it has not been possible to delineate the various steps involved in the reduction and electron transfer processes in these systems. Therefore, in order to understand the functioning of heme-related proteins; it is important to delineate the basic mechanism of oxido-reduction processes including studies of the intermediate transient species involved in the activation process alongwith

possible structural changes which may take place during the biophysical changes.

Since vibrational spectroscopy is one of the very powerful tools to gain insight into the nature of chemical bonds and geometrical structure of molecules in solution, Raman spectra of metalloporphyrins have been extensively investigated.[4] Resonance Raman (RR) technique offers a means of selectively enhancing certain vibrational modes of the porphyrin chromophore only in a complex heme-protein which are sensitive probes of the changes in the oxidation, spin and coordination states of the central iron atom and reflect the structural and bonding changes as well. Therefore extensive RR studies on many heme-proteins and model complexes have been carried out in the recent past and have resulted in useful correlations between Raman frequencies and various stereochemical parameters.

This thesis describes systematic RR studies for understanding the mechanism of photoreduction of some iron-porphyrins in the presence of biologically relevant 2-methylimidazole (2-MeIm), 1,2-dimethylimidazole (1,2-Me_2Im) and imidazole (Im) as axial ligands and stereochemical aspects of axial ligation in these systems. We have measured action spectrum and have carried out systematic RR studies to explore the detailed mechanism of photoreduction process in iron porphyrins. We have performed similar studies at low temperatures upto ~20K which have further substantiated our proposed mechanism on

photoreduction and also revealed temperature dependent changes in axial ligation. Solvent dependence on the yield of photoreduction of iron porphyrin has been initiated with the aim of understanding the specific role of environment on the photoreduction process. Our RR studies on the stereochemical aspects of axial ligation in the photoreduced iron-porphyrins have revealed the coexistence of both the upright and tilted configurations of axial ligand Fe-N_{Im} bond with respect to the normal to the porphyrin plane. The different aspects of these studies are given in individual chapters.

This thesis is divided into seven chapters.

In Chapter I, we review RR and other related studies on iron porphyrins. Some of the important stereochemical parameters of iron porphyrins have been discussed because of their direct influence on the reactivities of porphyrin complexes as a whole. The increasing importance of photoreduction technique employed here for obtaining reduction of iron porphyrin complexes and in situ monitoring by RR technique have been emphasized over other conventional methods.

We have presented relevant theoretical background to understand the electronic absorption and resonance Raman (RR) spectra of iron porphyrins in Chapter II.

Chapter III presents pertinent details of the different experimental techniques that have been used in this study. A

brief description of the method of sample preparation, lasers and laser Raman spectrometer have been incorporated, apart from details of other instruments and accessories used in this work.

In Chapter IV, we present our detailed RR studies on the mechanism of photoreduction of iron protoporphyrin-IX dimethyl ester chloride in the presence of biologically relevant axial ligands.[5] In this study, we have discovered the important catalytic role of trace amount of alcohol (primary or secondary) as "directing ligand", which facilitates the ligation of nitrogenous bases to the fifth coordination site by replacing the tightly bound halide ion from the coordination sphere of iron porphyrins. The dependence of photoreduction on excitation wavelength and coincidence of the maximum of quantum yield of photoreduced species with the Soret transition has been observed, indicating that photoreduction process is driven by absorption in the Soret region. From the action spectra of Fe^{III}PPDME(2-MeIm) complex obtained by irradiation with a white light source for different times in the presence of a short-cut filter L-38, we have obtained the rate constant for photoreduction as k_R^{-1}= 10 minute. We have identified ligand free, four coordinated, Fe^{II}PPDME as the transient species involved in the photoreduction of Fe^{III}PPDME(2-MeIm) complex from concentration dependent RR studies of photoreduction on axial ligand (2-MeIm). On the basis of these results, a mechanism for photoreduction of iron porphyrins has been proposed. Light irradiation in the Soret region excites the Fe^{III}PPDME(2-MeIm) complex to the $e_g(\pi^*)$ or to

the antibonding d_z2 orbital where ligated 2-MeIm dissociates donating its charge to the iron centre. The resulting 2-MeIm$^+$ then diffuses away from the coordination sphere of iron porphyrins. The ligand free, Fe^{II}PPDME, transient species is stabilized by coordination with another 2-MeIm molecule from solution giving five coordinated, high spin, reduced Fe^{II}PPDME(2-MeIm) complex as the final photoreduced species.

In Chapter V, we discuss our RR studies on Fe^{III}PPDME(1,2-Me_2Im) complex at low temperatures. In this temperature dependent RR study[6], we have observed photoreduction of this complex in soft dimethyl sulfoxide (DMSO) matrix at ~100K by excitation in the Soret absorption region and have characterized the photoreduced product as six coordinated, intermediate spin, Fe^{II}PPDME(DMSO)$_2$ complex. Non-photoreducibility in the hard glassy DMSO matrix at ~20K indicates that the long-range quantum-mechanical electron tunneling plays insignificant role while the short-range electron transfer is the primary process involved in the photoreduction of iron porphyrin complexes. Temperature dependent changes in the axial ligation have been observed where in cold solution at ~250K 1,2-Me_2Im coordinates at the fifth ligand position by replacing DMSO. The photoreduced species has been characterized as five coordinated, high spin, Fe^{II}PPDME(1,2-Me_2Im) complex at this temperature. We also report our preliminary RR studies on the solvent dependent yield of photoreduction where it appears that the yield of photoreduction depends on the polarity of the

solvent which facilitates the solvent-induced dissociation of ion-pairs created by electron transfer, although other solvent parameters also play important role.

In Chapter VI, we give the details of stereochemical aspects of axial ligation in the photoreduced iron-porphyrins.[7] During concentration dependent RR studies on axial ligands of FeOEP and FePPDME complexes, we have observed doublet structure in the Fe-N_{Im} stretching region in these complexes with 2-MeIm and 1,2-Me_2Im as axial ligands due to coexistence of the upright and tilted configurations of the Fe-N_{Im} bond with respect to the normal to the porphyrin plane. With 2-MeIm complexes of iron porphyrins, the upright configuration is the predominant species. The frequency of the Fe-N_{Im} stretching mode shows an upshift with increase in the concentration of 2-MeIm axial ligand due to H-bonding between the N_δ-proton of free 2-MeIm and ligated 2-MeIm. However, a larger frequency shift in the case of Fe^{II}PPDME(2-MeIm) complex is attributed to non-bonded interactions between the vinyl groups of Fe^{II}PPDME complex and methyl groups of ligated 2-MeIm. With more sterically hindered ligand 1,2-Me_2Im, we have once again observed that the non-bonded repulsive interaction is responsible for stabilizing the upright configuration of Fe-N_{Im} bond in the Fe^{II}PPDME(1,2-Me_2Im) complex, where as in the Fe^{II}OEP(1,2-Me_2Im) complex, it is the tilted configuration which is the predominant species.

Chapter VII presents summary and conclusions from our RR studies described in this thesis for understanding the mechanism of photoreduction of iron porphyrins and stereochemical aspects of axial ligation. Suggestions for extension of this work in future studies are also made which may help to confirm our proposed mechanism of photoreduction and other aspects discussed in this thesis.

References

1. Donhoe, R.J.; Atamian, M.; Bocian, D.F. *J. Am. Chem. Soc.* 109, 5593, 1987.

2a. Seely, G.R.; Talmadge, K. *Photochem. Photobiol.* 3, 195, 1964.

b. Kim, D.; Miller, L.A.; Rakhit, G.; Spiro, T.G. *J. Phys. Chem.* 90, 3320, 1986.

c. Bottomely, L.A.; Kadish, K.M. *Inorg. Chem.* 20, 1348, 1981.

3a. Bortocci, C.; Maldotti, A.; Traversso, O.; Bignozzi, C.A.; Carassitti, V. *Polyhedron*, 2, 97, 1983.

b. Bizet, C.; Morliere, P.; Brault, D.; Delgado, O.; Bazin, M.; Santus, R. *Photochem. Photobiol.* 34, 315, 1981.

4a. Spiro, T.G. in *"Iron Porphyrins"* Lever, A.B.P.; Gray, H.B. Eds., Adision-Wesley, Reading, M A Part II, p. 91, 1983.

b. Kitagawa, T.; Ozaki, Y. *"Structure and Bonding"*, 64, 71, 1987.

5a. Verma, A.L.; Chaudhury, N.K.; Saini, G.S.S. in *"Recent Trends in Raman Spectroscopy"* Banerjee, S.B.; Jha, S.S. Eds., World Scientific Publishing Co., Singapore, p. 192, 1989.

b. Verma, A.L.; Chaudhury, N.K.; Saini, G.S.S. *"XIIth International Conference on Raman Spectroscopy"* Durig, J.R.; Sullivan, J.F. Eds., John Wiley and Sons, New York, p. 592, 1990.

c. Verma, A.L.; Saini, G.S.S.; Chaudhury, N.K. *Proc. Ind. Acad. Sci. (Chem. Sci.)* 102, 291, 1990.

5d. Verma, A.L.; Chaudhury, N.K. *J. Raman Spectrosc.* (Submitted).

6. Chaudhury, N.K.; Saini, G.S.S.; Verma, A.L. (Submitted).

7. Chaudhury, N.K.; Saini, G.S.S.; Verma, A.L. *Inorg. Chem.* (Submitted).

MECHANISM OF PHOTOREDUCTION AND STEREOCHEMICAL ASPECTS OF AXIAL LIGATION IN SOME IRON-PORPHYRINS MONITORED BY RESONANCE RAMAN SPECTROSCOPY

Chaudhuri

NABO KUMAR CHAUDHURY

DEPARTMENT OF PHYSICS

SCHOOL OF PHYSICAL SCIENCES

NORTH-EASTERN HILL UNIVERSITY

SHILLONG - 793003

THESIS SUBMITTED

FOR THE DEGREE OF

DOCTOR OF PHILOSOPHY

To

THE NORTH-EASTERN HILL UNIVERSITY

SHILLONG - 793 001

INDIA

NOVEMBER, 1990

Physics

D E D I C A T E D T O T H E

M E M O R Y

O F

M Y F A T H E R

PHONE :
GRAMS : NEHU

North-Eastern Hill University

Bijni Complex, Bhagyakul, Shillong 793003 (Meghalaya)

Prof. A.L. Verma
Dean,
School of *Physical Sciences*

CERTIFICATE

I certify that the thesis entitled ***"MECHANISM OF PHOTOREDUCTION AND STEREOCHEMICAL ASPECTS OF AXIAL LIGATION IN SOME IRON-PORPHYRINS MONITORED BY RESONANCE RAMAN SPECTROSCOPY"*** *submitted by Shri* ***Nabo Kumar Chaudhury*** *for the degree of* ***Doctor of Philosophy*** *of the North-Eastern Hill University, Shillong, embodies the record of original research work carried out by him under my supervision.*

He has been duly registered and the thesis presented is worthy of being considered for the Award of Ph.D. Degree.

This work has not been submitted to any other University for any Degree.

A.L. Verma
19.11.90

Dated, November 1990 ***(A.L. Verma)***

Shillong. *Thesis Supervisor*

Phone :
Grams : NEHU

North - Eastern Hill University

Bijni Complex
Bhayakul, Shillong - 793003 (Meghalaya)

Department of ... Physics

CERTIFICATE

This is to certify that Shri **Nabo Kumar Chaudhury** has cleared the following four courses as a requirement for Ph.D. programme obtaining grade A in all of them.

Course	Grade
1. Molecular Physics and Group Theory	A
2. Molecular Biophysics	A
3. Magnetic Resonance (Theory and Technique)	A
4. French Language	A

19/11/92

(Y.S.T. Rao)
Professor and Head
Department of Physics
School of Physical Sciences
North-Eastern Hill University
Shillong - 793 003

A C K N O W L E D G E M E N T

First and foremost, I take great pleasure, in expressing my deepest sense of gratitude to ***Prof. A.L. Verma*** *for introducing me to this subject and for his constant guidance, encouragement and help throughout the entire course of my Ph.D. programme.*

I am grateful to ***Prof. Y.S.T. Rao, Prof. C.S. Shastry*** *and* ***Dr. K. Kumar*** *for their help and encouragement during my M.Sc. and Ph.D. programmes.*

I also take this opportunity to thank ***Dr. T. Chakraborty, Mr. G.S.S. Saini, Mrs. P.K. Shantha*** *and all my colleagues for their manifold cooperation and encouragement.*

My most sincere thanks are due to ***Mr. A.K. Rathore,*** *who spared his valuable time and help in typing this thesis in addition to his assistance in obtaining Raman spectra.*

I am also extremely grateful to the Council of Scientific and Industrial Research, New Delhi, Department of Atomic Energy, Bombay and Department of Science and Technology, New Delhi for providing financial assistance during the period of this work.

Last but not the least, it gives me immense pleasure to place on record the blessings of my beloved father bestowed on me and the debt that I owe to my family members for their ungrudging patience and continuous encouragement.

19.11.90

(NABO KUMAR CHAUDHURY)

C O N T E N T S

SYNOPSIS

Porphyrin complexes have long been considered materials of great importance because of their ubiquitous properties and significant role in a variety of physico-chemical functions. Heme-proteins have therefore been investigated on multi and interdisciplinary levels. All these proteins containing an iron-porphyrin as the prosthetic group are responsible for oxygen transport (hemoglobin, myoglobin and cytochromes b, c), oxygen reduction (cytochrome oxidase), hydrogen peroxide utilization and destruction (peroxidases and catalases) and many other functions. The active site in each case contains, most often, an iron protoporphyrin-IX and obviously these diverse functions must be dictated by various stereochemical parameters like oxidation and spin states, the nature of axial ligands, state of coordination and, of course, the environment. The essential biochemical processes, however, require the reduced state of iron as in cooperative binding of oxygen in hemoglobin. In recent years, reduction of iron-porphyrin complexes has been achieved by chemical[1], electrochemical[2] or photochemical[3] methods and monitored by different spectroscopic techniques. But so far it has not been possible to delineate the various steps involved in the reduction and electron transfer processes in these systems. Therefore, in order to understand the functioning of heme-related proteins, it is important to delineate the basic mechanism of oxido-reduction processes including studies of the intermediate transient species involved in the activation process alongwith

possible structural changes which may take place during the biophysical changes.

Since vibrational spectroscopy is one of the very powerful tools to gain insight into the nature of chemical bonds and geometrical structure of molecules in solution, Raman spectra of metalloporphyrins have been extensively investigated.[4] Resonance Raman (RR) technique offers a means of selectively enhancing certain vibrational modes of the porphyrin chromophore only in a complex heme-protein which are sensitive probes of the changes in the oxidation, spin and coordination states of the central iron atom and reflect the structural and bonding changes as well. Therefore extensive RR studies on many heme-proteins and model complexes have been carried out in the recent past and have resulted in useful correlations between Raman frequencies and various stereochemical parameters.

This thesis describes systematic RR studies for understanding the mechanism of photoreduction of some iron-porphyrins in the presence of biologically relevant 2-methylimidazole (2-MeIm), 1,2-dimethylimidazole (1,2-Me_2Im) and imidazole (Im) as axial ligands and stereochemical aspects of axial ligation in these systems. We have measured action spectrum and have carried out systematic RR studies to explore the detailed mechanism of photoreduction process in iron porphyrins. We have performed similar studies at low temperatures upto $\sim$20K which have further substantiated our proposed mechanism on

photoreduction and also revealed temperature dependent changes in axial ligation. Solvent dependence on the yield of photoreduction of iron porphyrin has been initiated with the aim of understanding the specific role of environment on the photoreduction process. Our RR studies on the stereochemical aspects of axial ligation in the photoreduced iron-porphyrins have revealed the coexistence of both the upright and tilted configurations of axial ligand Fe-N_{Im} bond with respect to the normal to the porphyrin plane. The different aspects of these studies are given in individual chapters.

This thesis is divided into seven chapters.

In Chapter I, we review RR and other related studies on iron porphyrins. Some of the important stereochemical parameters of iron porphyrins have been discussed because of their direct influence on the reactivities of porphyrin complexes as a whole. The increasing importance of photoreduction technique employed here for obtaining reduction of iron porphyrin complexes and in situ monitoring by RR technique have been emphasized over other conventional methods.

We have presented relevant theoretical background to understand the electronic absorption and resonance Raman (RR) spectra of iron porphyrins in Chapter II.

Chapter III presents pertinent details of the different experimental techniques that have been used in this study. A

brief description of the method of sample preparation, lasers and laser Raman spectrometer have been incorporated, apart from details of other instruments and accessories used in this work.

In Chapter IV, we present our detailed RR studies on the mechanism of photoreduction of iron protoporphyrin-IX dimethyl ester chloride in the presence of biologically relevant axial ligands.[5] In this study, we have discovered the important catalytic role of trace amount of alcohol (primary or secondary) as "directing ligand", which facilitates the ligation of nitrogenous bases to the fifth coordination site by replacing the tightly bound halide ion from the coordination sphere of iron porphyrins. The dependence of photoreduction on excitation wavelength and coincidence of the maximum of quantum yield of photoreduced species with the Soret transition has been observed, indicating that photoreduction process is driven by absorption in the Soret region. From the action spectra of Fe^{III}PPDME(2-MeIm) complex obtained by irradiation with a white light source for different times in the presence of a short-cut filter L-38, we have obtained the rate constant for photoreduction as k_R^{-1}= 10 minute. We have identified ligand free, four coordinated, Fe^{II}PPDME as the transient species involved in the photoreduction of Fe^{III}PPDME(2-MeIm) complex from concentration dependent RR studies of photoreduction on axial ligand (2-MeIm). On the basis of these results, a mechanism for photoreduction of iron porphyrins has been proposed. Light irradiation in the Soret region excites the Fe^{III}PPDME(2-MeIm) complex to the $e_g(\pi^*)$ or to

the antibonding d_z2 orbital where ligated 2-MeIm dissociates donating its charge to the iron centre. The resulting 2-MeIm$^+$ then diffuses away from the coordination sphere of iron porphyrins. The ligand free, Fe^{II}PPDME, transient species is stabilized by coordination with another 2-MeIm molecule from solution giving five coordinated, high spin, reduced Fe^{II}PPDME(2-MeIm) complex as the final photoreduced species.

In Chapter V, we discuss our RR studies on Fe^{III}PPDME(1,2-Me_2Im) complex at low temperatures. In this temperature dependent RR study[6], we have observed photoreduction of this complex in soft dimethyl sulfoxide (DMSO) matrix at ~100K by excitation in the Soret absorption region and have characterized the photoreduced product as six coordinated, intermediate spin, $Fe^{II}PPDME(DMSO)_2$ complex. Non-photoreducibility in the hard glassy DMSO matrix at ~20K indicates that the long-range quantum-mechanical electron tunneling plays insignificant role while the short-range electron transfer is the primary process involved in the photoreduction of iron porphyrin complexes. Temperature dependent changes in the axial ligation have been observed where in cold solution at ~250K 1,2-Me_2Im coordinates at the fifth ligand position by replacing DMSO. The photoreduced species has been characterized as five coordinated, high spin, Fe^{II}PPDME(1,2-Me_2Im) complex at this temperature. We also report our preliminary RR studies on the solvent dependent yield of photoreduction where it appears that the yield of photoreduction depends on the polarity of the

solvent which facilitates the solvent-induced dissociation of ion-pairs created by electron transfer, although other solvent parameters also play important role.

In Chapter VI, we give the details of stereochemical aspects of axial ligation in the photoreduced iron-porphyrins.[7] During concentration dependent RR studies on axial ligands of FeOEP and FePPDME complexes, we have observed doublet structure in the Fe-N_{Im} stretching region in these complexes with 2-MeIm and 1,2-Me_2Im as axial ligands due to coexistence of the upright and tilted configurations of the Fe-N_{Im} bond with respect to the normal to the porphyrin plane. With 2-MeIm complexes of iron porphyrins, the upright configuration is the predominant species. The frequency of the Fe-N_{Im} stretching mode shows an upshift with increase in the concentration of 2-MeIm axial ligand due to H-bonding between the N_δ-proton of free 2-MeIm and ligated 2-MeIm. However, a larger frequency shift in the case of Fe^{II}PPDME(2-MeIm) complex is attributed to non-bonded interactions between the vinyl groups of Fe^{II}PPDME complex and methyl groups of ligated 2-MeIm. With more sterically hindered ligand 1,2-Me_2Im, we have once again observed that the non-bonded repulsive interaction is responsible for stabilizing the upright configuration of Fe-N_{Im} bond in the Fe^{II}PPDME(1,2-Me_2Im) complex, where as in the Fe^{II}OEP(1,2-Me_2Im) complex, it is the tilted configuration which is the predominant species.

Chapter VII presents summary and conclusions from our RR studies described in this thesis for understanding the mechanism of photoreduction of iron porphyrins and stereochemical aspects of axial ligation. Suggestions for extension of this work in future studies are also made which may help to confirm our proposed mechanism of photoreduction and other aspects discussed in this thesis.

References

1. Donhoe, R.J.; Atamian, M.; Bocian, D.F. *J. Am. Chem. Soc.* 109, 5593, **1987.**

2a. Seely, G.R.; Talmadge, K. *Photochem. Photobiol.* 3, 195, **1964.**

b. Kim, D.; Miller, L.A.; Rakhit, G.; Spiro, T.G. *J. Phys. Chem.* 90, 3320, **1986.**

c. Bottomely, L.A.; Kadish, K.M. *Inorg. Chem.* 20, 1348, **1981.**

3a. Bortocci, C.; Maldotti, A.; Traversso, O.; Bignozzi, C.A.; Carassitti, V. *Polyhedron*, 2, 97, **1983.**

b. Bizet, C.; Morliere, P.; Brault, D.; Delgado, O.; Bazin, M.; Santus, R. *Photochem. Photobiol.* 34, 315, **1981.**

4a. Spiro, T.G. in *"Iron Porphyrins"* Lever, A.B.P.; Gray, H.B. Eds., Adision-Wesley, Reading, M A Part II, p. 91, **1983.**

b. Kitagawa, T.; Ozaki, Y. *"Structure and Bonding"*, 64, 71, **1987.**

5a. Verma, A.L.; Chaudhury, N.K.; Saini, G.S.S. in *"Recent Trends in Raman Spectroscopy"* Banerjee, S.B.; Jha, S.S. Eds., World Scientific Publishing Co., Singapore, p. 192, **1989.**

b. Verma, A.L.; Chaudhury, N.K.; Saini, G.S.S. *"XIIth International Conference on Raman Spectroscopy"* Durig, J.R.; Sullivan, J.F. Eds., John Wiley and Sons, New York, p. 592, **1990.**

c. Verma, A.L.; Saini, G.S.S.; Chaudhury, N.K. *Proc. Ind. Acad. Sci. (Chem. Sci.)* 102, 291, **1990**.

5d. Verma, A.L.; Chaudhury, N.K. *J. Raman Spectrosc.* (Submitted).

6. Chaudhury, N.K.; Saini, G.S.S.; Verma, A.L. (Submitted).

7. Chaudhury, N.K.; Saini, G.S.S.; Verma, A.L. *Inorg. Chem.* (Submitted).

INTRODUCTION

Porphyrins and metalloporphyrins are important class of compounds from the point of view of physico-chemical studies as well as their importance in many biological processes. These compounds are macrocyclic tetrapyrrole systems with conjugated double bonds having various groups attached to the periphery. They also possess the ability to combine with many kinds of metals. Some of the porphyrin-related structures are shown in Fig. 1.1 with the types and positions of the side-chains indicated.

The porphyrins play most significant role in photosynthesis in green plants and electron transfer in respiratory chain. Chlorophyll, present in one form or another in green plants, is a magnesium complex containing a modified ring system called chlorin while vitamin B_{12} is a related cobalt complex of somewhat different tetrapyrrolic structure. Phthalocyanines and their metal derivatives possess interesting semiconducting and photoconducting properties. However, one of the most widely spread, both from the point of view of occurrence in a variety of organisms and their diverse functions, is heme, an iron complex of porphyrin. Heme related proteins are involved in three distinct biological functions: myoglobin and hemoglobin serve as reversible oxygen transport proteins; the cytochromes b's and c's function as reversible one electron transport agents; and the cytochrome-P450's and peroxidases are involved in

irreversible transformation of substrates.[1] In spite of these diverse functions, all heme-proteins have the unifying feature of a common active site or "prosthetic group" composed of an iron-porphyrin complex which is the centre of all the diverse functions of heme-proteins. The macrocycle acts as a reservoir of electrons and controls reactivity at the axial position of metal which usually serves as a catalytic site in heme-enzymes.[2]

The obvious variables found in these natural systems include porphyrin structure, axial ligands to the metal, its oxidation and spin states, and the medium provided by the protein and/or solvents at the active site. The oxygen which is reversibly transported binds directly to the iron atom of hemoglobin (Hb) in competition with other small molecules. The one-electron transfer in cytochromes occurs by reversible oxidation-reduction of iron between ferrous and ferric states. Oxidation of substrates by cytochrome-P450 most likely occurs by transfer of oxygen atom directly bound to the iron. The intermediates formed by peroxidases and catalases are also thought to involve an oxygen atom binding directly to the iron of heme group itself.[3] While the remainder of the protein obviously plays a significant role in modulating their biological activity, there is a great deal of evidence that the biological functions of the heme proteins are determined to a large extent by the conformational and electronic properties of the heme group. As a result, a wide variety of structure-function, structure-reactivity and structure-property relationships are expected in

heme- related systems.[4]

Apart from these, alterations in porphyrin metabolism have been associated with cancer, drug metabolism and even in the diagnosis and chemotheraphy of malignant tumors using hematoporphyrin derivatives in combination with laser irradiation.[5]

Most of the heme proteins like hemoglobin and myoglobin contain iron protoporphyrin IX (Figure 1.1) as prosthetic group. Central metal, iron, is covalently linked by axial ligands. In the ferrous state of myoglobin and hemoglobin, the fifth coordination position is occupied by the imidazole group of nearby histidine residue and the sixth coordination site is the one which reversibly binds an oxygen molecule as well as other active molecules like CO, CN and NO. On the other hand in the ferric state, it is attached to two endogeneous axial ligands, most often by an imidazole and a mercaptide moiety. The local heme environment in relation to the changes in axial ligands, spin and oxidation states are thus associated with the diverse biological functions. Iron porphyrins in both the oxidation states and in various spin and ligation states have been characterized by many workers[6-10] using a variety of experimental techniques. Ligand binding to even model complexes and to a single subunit protein such as myoglobin has been shown to be a multistep process involving the movement of the central iron above the porphyrin plane, and a change in its spin and oxidation states[11] followed by structural alterations.

It is thus obvious that during the reversible binding of oxygen and electron transfer processes in heme-proteins, the chromophore undergoes reversible oxidation and reduction reactions involving many intermediate steps. Therefore, in order to understand the functioning of heme-related proteins, it is of crucial importance to delineate the mechanism of oxido-reduction processes including the studies of intermediate complexes involved in the activation process, electron distribution and possible structural changes in the prosthetic group during various processes.

We have undertaken systematic resonance Raman (RR) studies on some model systems of iron-porphyrins with the aim of understanding some of the basic steps involved in the functioning of heme-proteins. This thesis describes detailed RR studies on photo-reduction of iron(III) proto-porphyrin-IX dimethylester chloride [(Cl)Fe^{III}(PPDME)] under selective laser irradiation in order to elucidate the mechanism of reduction process of iron-porphyrins in the presence of biologically relevant axial ligands like 2-methylimidazole [2-MeIm]; 1,2-dimethyl imidazole [1,2-Me_2Im] and imidazole [Im] etc. We have found that a degassed solution of (Cl)Fe^{III}(PPDME) in CH_2Cl_2 containing 2-MeIm or 1,2-Me_2Im in the presence of a trace amount of alcohol or other polar solvents undergoes photoreduction by excitation in the Soret absorption region converting it to Fe^{II}(PPDME)-2MeIm while porphyrin macrocycle remains unaffected. From the concentration dependence of photoreduction on 2-MeIm and

the action spectrum in the presence of short-cut filters, we have inferred that ligand-free, four coordinated, intermediate spin Fe^{II}(PPDME) is the transient intermediate species formed during photoreduction while the polar solvents help in charge separation by increasing the lifetime of redox pairs.[50] The low temperature RR studies indicate the short-range electron transfer mechanism as predominant process while quantum mechanical tunneling is insignificant during photo-reduction.[52]

The physico-chemical properties of heme-proteins are related to the coordination structure and stereochemistry of the axial ligands to the iron atom. We also describe in this thesis the nature of iron-axial ligand bonds and geometrical details in some iron-porphyrin model systems. We have found that the axial ligands coexist with bonding arrangements such that the $Fe-N_{Im}$ bond is tilted in one configuration while it attains upright configuration in another form with respect to normal to the heme-plane. From comparative study on Fe^{III}(PPDME) and Fe^{III}(OEP) in the presence of 2-MeIm and $1,2Me_2Im$ as axial ligands, we infer that the vinyl groups in the protoporphyrin complex play dominant role in non-bonded interactions with the sterically hindered axial ligands in stabilizing the specific configurations.[51]

Before discussing our work, we give here pertinent details of the stereochemical aspects of iron-porphyrins which are necessary to build-up the base for this study and to understand the structure function relationship. This is followed by a brief review of important studies on different

metalloporphyrins using resonance Raman and few other relevant techniques.

The stereochemistry of iron porphyrins depend upon the spin and oxidation states as well as their coordination states. The common oxidation states of the iron atom in hemes are +2 and +3. The porphinato ring itself is four coordinated and additional coordination can take place at the fifth and sixth coordination position (Fig. 1.1) of the metal. The diversity in coordination positions produces various possible spin states, depending upon the relative magnitudes of spin pairing energy (P) and the ligand field strength (Δ). Figure 1.2 illustrates the basic electronic arrangement in different d-orbitals of iron in the high and low spin systems. Thus, in an octahedral field as found in heme, the different d-orbitals split into two discrete groups of three low lying (t_{2g}) and two higher orbitals (e_g) separated by a ligand field energy Δ. When Δ is small relative to spin-pairing energy, P, all the five d orbitals populate with equal number of electrons giving rise to high spin iron (III) complex (d^5system). For the ferrous complex (d^6system), the sixth electron pairs up in the lowest d_{xy} orbital to give rise to a high spin system. The different electronic arrangements for the corresponding low spin systems are also shown in this Figure. A more detailed discussion is incorporated in theoretical section 2.4 of this thesis. Thus prediction of the details of the geometry and spin states requires information about the nature of axial ligands to be known simultaneously. The iron

protoporphyrin-IX is directly linked to the globin protein through an axial complexing bond between the iron atom and an imidazole nitrogen atom of the proximal histidine residue. Molecular oxygen occupies the sixth coordination position in the low spin oxyhemoglobin (oxy-Hb) and hence in the high spin deoxyhemoglobin, there is no oxygen at the vaccant sixth ligand position. It has been established[12] that the iron atom moves by $0.5A^{o}$ relative to the porphyrin charge-centre on oxygenation accompanying a change in the spin state[13] of iron.

The stereochemistry of high spin iron(III) porphyrins (d^5 systems) is the most well studied class of porphyrins. Table 1 shows some of the iron complexes with various stereochemical parameters. The effective radius of the high spin iron(III) is too large to fit into the central hole and an out of plane displacement of $\sim 0.48\ A^{o}$ and a resulting doming of the porphyrin core is thus frequently observed. The average Fe-N(porphyrin) distance (pyrrole nitrogen to the centre of the porphyrin) of $2.07\ A^{o}$ is observed, although it shortens by $\sim 0.13\ A^{o}$ when iron is coordinated to amine type nitrogen atoms implying its strong complexing ability. Salient stereochemical parameters of the high-spin iron(III) porphyrins include specific orientation of the axial ligands. e.g., the methoxy ligand in (CH_3O)FeMPDME[13] is required to have most favorable orientation where FeOC angle is 125.9^{o}. In general the effective radius of the high-spin iron(II) ion is higher than that of the high-spin iron(III), and the stereochemistry of the high-spin iron(II)

porphyrins (d^6 systems) is expected to be similar to that of the high-spin iron(III) porphyrins (d^5 systems). Hence an appropriate choice of the two axial ligands can influence both the iron(II) and iron(III) porphyrins to form low spin species. In this spin state, the iron atom is expected to be nearly centred in the porphyrin plane. Consequently one observes shorter $Fe-N_\epsilon$ (pyrrole nitrogens of porphyrins) bond distances; e.g., in the $[(Im)_2Fe(TPP)]^+Cl^-$ complex, the iron ion is ~ 0.009 A^o displaced from porphyrin mean plane.[14] It has also been found that the two ligated imidazole units are nonequivalent with respect to bond distances, $Fe-N_\epsilon$ (imidazole), as well as the orientations of the imidazoles also differ slightly. In the case of centro-symmetric complexes, as in $(Pip)_2Fe(TPP)$[15], the iron(II) atom is exactly centred. The $Fe-N_\epsilon$ (Pip) bonds are relatively longer compared to those with imidazole complexes. Among other low spin iron(II) complexes the important axial ligands are dioxygen and carbonmonoxide. The iron(II) dioxygen complex of "picket fence" porphyrin, with 1-methyl imidazole as axial ligand[16] is a model compound of oxygen carrying heme-proteins. The dioxygen ligand is coordinated in two unique orientations[17] when the imidazole is coordinated at the fifth ligand position. There are even examples of intermediate spin states in iron-porphyrins. $Fe(TPP)^6$ has unusual spin state, S=1, which results from the removal of an electron from the $d_{x^2-y^2}$ orbital.

Apart from these stereochemical studies, many spectroscopic measurements on various iron porphyrins have been

performed. NMR studies on iron porphyrins were performed with regard to their coordination[18], and thermodynamical properties[19] alongwith other features.[20] Other techniques like EPR[21], Mossbauer[22], Magnetic susceptibility[23], Mass Spectroscopy[24], Electronic absorption Spectroscopy[25], Infrared[26] and Raman spectroscopy[27] etc.,have been applied to illustrate the different aspects of iron porphyrin's stereochemistry.

The spectacular development of molecular biology in the recent past has widened the prospects of understanding of biological functions in terms of stereochemistry of iron porphyrins. With the basic structural knowledge available from X-ray diffraction methods, a large variety of other experimental techniques have been introduced to monitor the dynamical aspects and structure-function relationship during various biochemical processes. The study of vibrational frequencies available from Raman and infrared spectra, play significant role in structural investigations. Vibrational frequencies are sensitive to geometrical and bonding arrangements, intermolecular interactions, etc. Thus, the structural information content of Raman and infrared spectra is very high, although in a complex system like porphyrins the spectral features are often very complicated. With the advent of tunable lasers, it has been possible to make systematic exploration of the resonance Raman effect. It also provides a means of selectively observing RR scattering from specific chemical groups by tuning the laser wavelengths to match its electronic transitions and thus

simplifying the spectral complexity.

The fundamental process involved in Raman scattering process arises as a result of interaction between electromagnetic radiation with matter resulting in inelastic scattering of light from different excitations of the medium. With the availability of intense, monochromatic, polarized light from lasers, it has become possible to monitor various parameters like intensity, half-width, polarization properties of Raman bands more conveniently and precisely. Also Raman bands can be monitored as a function of external parameters like temperature, pressure, concentration etc. Availability of continuously tunable lasers have helped in systematic exploration of various vibrational modes in the resonance Raman effect. When the energy of the exciting radiation matches with the electronic transition of the system, selective enhancement of those vibrations occurs which involve mainly the motion of the atoms in that part of the chromophore where the electronic transition is localized. Under resonance conditions the intensity enhancement of vibrations coupled to that particular electronic transition is of the order of 10^3 - 10^6 compared to normal Raman scattering, where the excitation wavelength is far away from any of the electronic transitions. As a result, very dilute solutions with concentrations between 10^{-4} - 10^{-6} M can provide a good quality spectra. The positions of Raman bands are characteristics of the properties of the electronic ground state while their intensities are strongly dependent on the properties of the excited as well

as ground electronic states. This effect is of much intrinsic interest and novel experimental findings have rather stimulated a great deal of activity due to its practical importance in the study of biological systems.[28] Metalloporphyrins absorb strongly in the U.V. and visible regions. Thus when the exciting frequency falls within an electronic absorption band, enhancement of the vibrational modes coupled to it might occur. The selective and specific enhancement of vibrations in the RR spectra due to excitation in different spectral regions allows the bands to be classified according to their origin.

The biological and chemical properties of metalloporphyrins depend on the porphyrin macrocycle substituents and the metal as well.[29a-d] The macrocycle is a π-conjugated electronic system and functions as a reservoir of electrons to control reactivity at the axial ligand position of the metal. The prominent bands in the resonance Raman spectrum arise mainly from those vibrations which affect the π-conjugation in the macrocycle. Any alterations in this π-conjugation due to substituents are depicted in the RR spectra. The early RR spectra of hemoglobin (Hb)[29e,f] showed markedly different spectra for different chemical states, and attention was focused on oxidation and spin state marker bands of the central iron.[30] The oxidation state sensitive bands were attributed[30a,31] to the backbonding between the iron atom and the porphyrin ring. Any alteration in the $d\pi$ electrons greatly alters the extent of backbonding and hence the oxidation state marker bands (ν_4). The

spin-state marker bands were first thought to be affected due to doming of the porphyrin ring.[30a] *Spaulding et al*[32] later on suggested that one of the spin state marker bands, the anomalously polarized band in the 1580 cm^{-1} region (ν_{19}) was more sensitive to the porphyrin core size in iron porphyrin. This was further confirmed by crystallographic[33] and Raman[34] studies on iron porphyrins. A negative linear correlation with core-size was also observed for the Raman bands associated with the ν_{19} and two other spin state marker bands ν_3 and ν_{10}.[34a,b] Systematic deviations have been observed for domed porphyrins which were thought to arise from loss in porphyrin π-conjugation due to tilting of pyrrole rings.

Asymmetric disposition of the peripheral groups, e.g., in protoporphyrin-IX, which forms the prosthetic groups in Hb, Mb, peroxidase, catalase, cytochrome-P450, etc., has two vinyl groups (Figure 1.1), which are capable of conjugation with the porphyrin π-system. As a result, the electronic absorption spectrum shows a 10 nm red shift of Soret and Q bands relative to the octaethylporphyrin (OEP) complexes. The internal modes of vinyl groups are also expected to show enhanced resonance vibration, alongwith some porphyrin skeletal modes. Further, the presence of vinyl groups on the adjacent pyrrole rings destroys the inversion center of the chromophore and induces Raman activity for the infrared active modes (E_u in D_{4h} symmetry).[35]

Apart from the above mentioned (1300 - 1675 cm^{-1}) finger print spectral region, the region below 500 cm^{-1} is also

important from the very fact that the axial ligand modes, out of plane and in plane deformation modes are expected in the low frequency region. The importance of axial coordination site in iron porphyrins is obvious from the fact that it is the catalytic site for the chemical as well as biological transformations.

The assignment of the axial ligand modes in relation to the strain model for hemoglobin(Hb) cooperativity has attracted much attention. *Hori and Kitagawa*[36] first reported the Fe-N_ϵ (2-MeIm) stretching mode for the five coordinate (2-MeIm)Fe(T_{piv}PP) and (2-MeIm)Fe(PP) systems and associated it to a Raman band at $\sim 206cm^{-1}$. Later studies by *Nagai et al*[36d] revealed the existence of strain in the Fe-His bond in the low affinity Hb. The ν_{Fe-N_ϵ} (Imidazole) mode is also found to be solvent sensitive. Moreover, the central iron atom is bound to an imidazole group in most hemoproteins, the importance of the Fe-Im stretching frequency is of particular significance to understand the nature of iron-ligand interactions. It was also surprisingly observed at the same frequency for the $[(Im)_2Fe^{III}(PP)]^+$ complex although an increase in oxidation state might have expected to increase the bond strength. It is suggested that the extra electron in $[(Im)_2Fe^{II}(PP)]^+$ is completely delocalized in the porphyrin ring as reflected in the lowering of different skeletal mode frequencies in the high frequency region, and thereby the bond strength of $Fe-N_{Im}$ bond is left unaltered. A variation in the position of the ν_{Fe-N_ϵ} (2-MeIm) stretching mode has also been observed for five-coordinated, high spin iron(II)porphyrins with

sterically hindered ligand like 2-MeIm. The ν_{Fe-N_ϵ} (2-MeIm) has been observed at 220 cm^{-1} [36b] in aqueous solution but appreciably lowered to 205 cm^{-1} when the complex was dispersed in a detergent medium or dissolved in a benzene solution.[36c] This decrease in frequency has been attributed to the absence of hydrogen bonding between the N_δ -proton of the imidazole and hydrogen acceptor molecule, which would otherwise have increased this frequency. Examples of such hydrogen bonding have also been found in deoxyhemoglobin and deoxymyoglobin[36c,d] as well as in reduced horseradishperoxidases(HRP)[36e], where this mode was observed at higher frequency position at 244 cm^{-1}.

Thus extensive studies on iron porphyrins have been performed by different techniques to explore the various aspects of these systems. In the process of RR studies on some heme proteins, a very special effect of laser irradiation, "Photo-reduction" of the central metal atom has been observed at selected wavelengths[37], but its mechanism is yet to be ascertained. Only recently the first RR study on photo-reduction of (2-MeIm)Fe^{III}(OEP) complex has been reported by *Ozaki et al*[38a], where a preliminary mechanism has been proposed. Simultaneously, *Verma et al*[38b-d] from RR studies on (2-MeIm)Fe^{III}(PPDME) have proposed, that the light induced charge-transfer from axial ligand to the iron ion is the primary process involved in photo-reduction. In a different RR study on the photo-reduction aspects of cytochrome-C (Cyt-C), *Verma and Kitagawa*[38e] have also proposed a mechanism for photo-reduction of Cyt-C which is

consistent with the inhibition of this process in the presence of oxygen. It was also concluded that ligated histidine acts as an electron donor for photo-reduction. Apart from these, few other studies on photo-reduction on metalloporphyrins were also performed from the point of photochemical interest.

The importance of photochemistry of porphyrins and metalloporphyrins has attracted much attention since its relation with pigments of plants and animals became known. The fundamental reaction is "Photosynthesis" in which light energy is converted to chemical energy by an electron transfer process. As for The photochemical reactivity, porphyrins with low oxidation potential are found to be easily oxidized and those with high oxidation potential are easily photoreduced. The central iron atom distributes its two negative charges mostly within the porphyrin macrocycle. Thus an electron can be easily removed, but is added with more difficulty.[39a] The situation is, however, different in case of free base porphyrins where addition of electron is easier. *Mauzerall*[39b] in a photo-reduction study of free base porphyrin in protic solvents reported that it resulted in generation of phlorin with mild reducing agents like tertiary amines, thiols as electron donors. In the redox reactions of porphyrins, an understanding of the distribution of electrons is extremely necessary. An useful model in this respect is due to *Woodward*.[40] In this model, each pyrrole unit (Figure 1.3a) of the porphyrin macrocycle contains five π-electrons and is expected to achieve an aromatic sextet on removing electron

density from methine bridge C_m positions of the porphyrin macrocycle. Figure 1.3b shows an extreme case. When no electron transfer takes place between the metal and porphyrin, i.e., for no redox reactions, the methine bridges carry a partial positive charge and nucleophylic type additions should occur. Alternatively, when electrons are introduced from the central metal ion or from axial ligand, they will have pronounced effect on the electron density at the methine bridge positions. However, the reactivities of methine bridges in porphyrin complexes with different metals reflect great diversity, according to the variable redox behaviour of the central metal ion.[41]

Amongst various metalloporphyrins, *Seely and Talmadge*[42] reported photoreduction of zinc porphyrins by ascorbic acid in a degassed solution, resulting into the generation of the corresponding chlorin complexes. Significant differences between photochemically generated chlorin and neutral chlorin derivatives were observed. This was due to selective cis-photohydrogenation. Only a few studies have been reported where photoreduction of central metals had occurred. Examples are cited by manganese etioporphyrins in pyridine solution in the presence of Sunlight[42], molybdenum alkoxo tetraphenyl porphyrins in benzene in visible light.[43] *Imamura et al*[44] had reported photoreduction of manganese (III), iron (III), cobalt (III), oxomolybdenum (V) tetraphenylporphyrin with axial ligands like halogen in 2-methyltetrahydrofuran, and concluded from electronic absorption and electron spin resonance studies that

photoreduction of metal occured via cleavage of the M-X (halogen) bond followed by the reaction of the radical X$^{\bullet}$ with the solvent.

Recently *Bartocci et al*[45a] reported a study on the photochemical reduction of iron(III)protoporphyrin-IX chloride (chlorohemin) in pyridine containing aqueous alcoholic solutions. It was concluded that iron(III) was reduced to iron(II) and a bis-pyridine iron(II)protoporhyrin complex was formed. The use of mixed solvents in aqueous medium introduced some problems in establishing the photo-reduction mechanism, since the plausible complex coordination equilibrium interrupted a clear identification of the photoreactive species. In subsequent studies[45c] on the photo-reduction of ferrideuteroporphyrins in benzene, water or micelle solutions containing primary or secondary alcohols, the authors proposed an intra molecular electron transfer process from alcoholate to iron(III), responsible for the primary photo-reduction. However, these results could not be correlated due to the different nature of both the solvents and substrates used. In view of this, *Bartocci et al*[45a] carried out photo-reduction of chlorohemin in pyridine. The result suggested that a charge transfer from pyridine to iron(III) was involved in photo-reduction of hemin and a band due to charge transfer should have been present in the absorption spectrum, which probably was encompassed by a strong Soret band at 400 nm. The only resonance Raman studies on photo-reduction of iron porphyrins were performed by *Ozaki et al*[38a], where a preliminary photo-reduction mechanism was proposed for

iron(III) octaethyl porphyrin complex, with axial ligands like 2-MeIm.

There have been some photochemical studies on the oxidation aspects of porphyrins as well. An ESR and ENDOR study[48a] has been carried out on the photoinduced electron transfer from magnesium and zinc tetrakis(4-sulfonato phenyl)porphyrins(Mg/ZnTPPS) to $K_3Fe(CN)_6$ in H_2O-DMSO glass. ESR signals from the porphyrin photo-excited triplet state and π-cation radical were used to monitor the yield of the photo-oxidation reaction. The viscosity effect was attributed to the fact that during the excited-state life time of the donor molecules, donor-acceptor pairs can attain a configuration favouring electron transfer. Photochemical oxidation of tetraphenyl porphine(TPP) and corresponding metal derivatives (M = Mg, Zn) has been investigated at low temperature[48b] by optical absorption and EPR technique using external electron acceptors. Both the accumulation of the porphyrin π-cation radical species and the quenching of the porphyrin luminescence were due to one-electron photo-oxidation reaction that was interpreted in terms of a long-range electron transfer mechanism. There have been few other works in this direction reported so far.[48c,d] The first RRS of photo-oxidation of TPP has been initiated by *Saini et al*[48e] in order to explore the mechanism and electron transfer processes under selective laser excitation in the presence of external electron acceptors like CCl_4.

Few studies were also performed by electrochemical

methods, mostly cationic species were achieved in metallo-porphyrins (M = Zn, Mg, Ni, Cu).[46] The RR characterization of different skeletal modes have suggested that either a_{1u} or a_{2u} type radicals were generated depending upon whether addition of electron took place either into a_{1u} or a_{2u} orbitals of porphyrin π-system. The electrochemical studies on iron porphyrins in different solvents[42] indicated that the reduction potential of iron(III) $\longrightarrow$ iron(II) shifts in a positive (anodic) direction in strongly coordinating solvents while strongly coordinating anions shift the potential in a negative (cathodic) direction. In 1981, the first systematic study[47c] of the interacting effects of solvents and axially coordinated monovalent anions on the electro-reduction mechanism and redox potential of iron porphyrins was presented. Five different anions were coordinated to $[Fe^{III}_{TPP}]^{+}$ and their respective redox reactions were investigated in twelve organic solvents. Potential shifts with changes in solvent were directly related to solvent donicity. No other structural information was revealed in these studies so far, and in many cases the reduction process involved contaminations from intermediate products which inhibit the actual reaction process.

There are also some studies on the reduction of iron-porphyrins by chemical methods probed by optical absorption, EPR, and RR techniques.[49] The RR and EPR data demonstrated that the reduction process resulted in a low-spin configuration of the iron(II) species and the extra unpaired electron primarily

localized on the porphyrin ring, although a small amount of unpaired electron density was available to be shared with the central metal ion through π-orbital interactions.

Thus studies of iron-porphyrin complexes under conditions approaching the physiological state appear very useful for a thorough understanding of their physico-chemical properties which play dominant role in the functioning of related biological systems. The redox processes involving the central iron atom are of particular interest due to their role in cytochromes, heme proteins etc., in the transfer of electrons in the respiratory chain. Most of the biological reactions require the reduced state of iron and thus characterization of reduced iron porphyrins in relation to their structural properties through vibrational studies by RR technique is gaining significant importance.

In this thesis, we discuss our systematic resonance Raman studies on iron porphyrins to elucidate the mechanism involved in the photoreduction process in the presence of biologically relevant axial ligands in organic solvents and to reveal structural implications in the photoreduced iron porphyrins by monitoring the iron-axial ligand stretching modes. In order to get insight into the mechanism of electron transfer process involved during photo-reduction, we have performed RR studies on synthetically prepared model complexes, iron(III) protoporphyrin-IX-dimethyl ester chloride and iron(III)

octaethylporphyrin iodide in the presence of axial ligands like 2-methylimidazole and 1,2-dimethylimidazole. We also report the simultaneous presence of two types of iron-ligand stretching modes $\nu_{Fe-N_{Im}}$ in the concentration dependent RR studies of iron(III) porphyrins with axial ligands. A preliminary study at low temperatures on the photoreduction process is also presented alongwith effects of solvents on the yield of photo-reduction.

References

1. Dickerson, R.E.; Timkovich, R. in"*The Enzymes*" Boyler, P.D. Ed., Vol. XI, Part A, p. 397, Academic Press, New York,1975.

2. Loew, H.G. in "*Iron Porphyrin*" Lever, A.B.P.; Gray, H.B. Eds., Addison-Wesley, Reading, Part I, p. 1, 1983.

3a. Groves, J.T. in "*Cytochrome P-450: Structure, Mechanism and Biochemistry*", Ortiz deMontellano, P., Ed., Plenum, New York, Chap. 1, 1985.

b. Hewson, W.D.; Hager, L.P. in "*The Porphyrins*", Dolphin, D.,Ed., Academic Press, New york, Vol. III, p. 295, 1978.

4. Felton, R.H.; Yu, N.T., in " *The Porphyrins*", Dolphin, D. Ed., Academic Press, New York, Vol. III, p. 376,1978.

5a. *"Lasers and Hematoporphyrin Derivatives in Cancer"*, Hayato,Y.; Dougherty, T.J. Eds.; Ikaku-Shoin; Tokyo, 1983.

b. Anderson-Engels, S.; Johansson, J.; Svanberg, S. *Anal. Chem.* 61, 1367, 1989.

6. Collman, J.P.; Hoard, J.L.; Kim, N.; Lang, G.; Reed, C.A. *J. Am. Chem. Soc.* 97, 2676, 1976.

7. Chang, C.K.; Dolphin, D. *J. Am. Chem. Soc.* 98, 1604, 1976.

8. Collman, J.P.; Sorrel, T.N.; Hoffmann, B.M. *J. Am. Chem. Soc.* 97, 913, 1975.

9. Caron, C.; Mitscher, A.: Riviere, L.R.; Schappacher, M.; Weiss.R. *J. Am. Chem. Soc.* 101, 1401, 1979.

10. Jamesson, G. B.; Molinaro, F.S.; Ibers, J.H.; Collman, J.P.; Brauman, J.L.; Rose. E.; Suslick, K.S. *J. Am. Chem. Soc.* 102, 3224,1980.

11. Austin, R.H.; Beeson, K.W.; Eisenstein, L.; Frauenfelda, H.; Gunsalas, I.C. *Biochemistry*, 14, 5355, 1975.

12. Hoard, J.L. in "*Hemes and Hemoproteins*" Chance, B.; Esterbrook, R.W.; Yonetani, T. Eds., Academic Press, New York, p. 9, 1966.

13. Hoard, J.L.; Hamor, M.J.; Hamor, T.A.; Caughey, W.S. *J. Am. Chem. Soc.* 87, 2312, 1965.

14. Collins, D.M.; Countryman, R.; Hoard, J.L. *J. Am. Chem. Soc.* 94, 2066, 1972.

15. Rodonovich, L.J.; Bloom, A.; Hoard, J.L. *J. Am. Chem. Soc.* 94, 2073, 1972.

16. Collman, J.P.; Gagne, R.R.; Reed, C.A.; Robinson, W.T.; Rodly, G.A. *Proc. Natl. Acad. Sci. U.S.A.* 71, 1326, 1974.

17. Hoard, J.L. in "*Structural Chemistry and Molecular Biology*" Rich, A.; Davidson, N. Eds., Freeman, SanFrancisco, Califorinia, p. 573, 1968.

18a. LaMar, G.N.; Budd, D.L.; Goff, H. *Biochem. Biophys. Res. Commn.* 77, 104, 1977.

b. Goff, H. *J. Am. Chem. Soc.* 102, 3252, 1980.

c. Walker, F.A. *J. Am. Chem. Soc.* 102, 3254, 1980.

19a. Satterlee, J.D.; LaMar, G.N.; Frye, J.S. *J. Am. Chem. Soc.* 78, 7275, 1976.

b. Wang, J.T.; Yeh, H.J.C.; Johnson, D.F. *J. Am. Chem. Soc.* 100, 2400, 1978.

20a. Abraham, R. J.; Bedford, G. R.; McNeillie, D.; Wright, B. *Org. Magn. Res.* 14, 418, 1980.

20b. Perkins, S.J. *J. Magn. Res.* 38, 297, 1980.

21a. Scheidt, W.R.; Cohen, I.A.; Kastner, M.E. *Biochemistry*, 18, 3546, 1979.

b. Simplicio, J.; Schwenzer, K.; Maenpa, F. *J. Am. Chem. Soc.* 97, 7319, 1975.

c. Schultz, C.E.; Devaney, P.W.; Winkler, H.; Debrunner, P.G.; Doan, N.; Chiang, R.; Rutler, R.; Hager, L.P. *FEBS Letts.* 103, 102, 1980.

d. Mazumder, S.; Medhi, O.K.; Mitra, S. *Inorg. Chem.* 27, 2541, 1988.

22a. Scheidt, W.R.; Geiger, D.K.; Haynes, R.G.; Lang, G. *J. Am. Chem. Soc.* 105, 2625,1983.

b. Gans, P.; Buisson, G.; Duee, E.; Regnard, J.R.; Marchon, J.C. *J.C.S. Chem. Commn.* 393, 1979.

23a. Boyd, P.D.W.; Buckingham, D.A.; McMeeking, R.F.; Mitra, S. *Inorg. Chem.* 18, 3585, 1979.

b. Casey, A.T.; Mitra, S. in "*Theory and Applications of Molecular Paramagnetism*", Boudreaux, E.A.; Mulay, L.N. Eds., Wiley, New York, 1976.

c. Collman, J.P.; Reed, C.A. *J. Am. Chem. Soc.* 95, 2048, 1973

24a. Jackson, A.H.; Kenner, G.W.; Smith, K.M.; Aplin, R.T.; Budzikiewicz, H.; Djerassi, C. *Tetrahedron*, 21, 2913, 1965.

b. Murphy, M.J.; Sieyel, L.M.; Kamin, H.; Rosenthal, D. *J. Biol. Chem.* 248, 2801, 1975.

25a. Zerner, M.; Gouterman, M.; Kobayashi, H. *Theoret. Chim. Acta. (Berlin)* 6, 363, 1966.

b. Gouterman, M. in "*The Porphyrins*", Dolphin, D. Ed. Academic Press, New York, Vol.III, p. 109, 1978.

c. Gouterman, M. *J. Mol. Spectrsc.* 6, 138, 1961.

26a. McCoy, S.; Caughy, W.S. *Biochemistry*, 9, 2387, 1970.

b. Alben, J.O. in "*The Porphyrins*", Dolphin, D. Ed., Academic Press, New York, Vol.III, p. 323, 1978.

27a. Spiro, T.G. in "*Iron Porphyrins*", Lever, A.B.P.; Gray, H.B. Eds., Addison-Wesley, Reading, M.A., Part II, p. 91, 1983.

b. Felton, R.H.; Yu, N.T. in "*The Porphyrins*",Dolphin, D. Ed., Academic Press, New York, Vol. III, p. 347, 1978.

c. Kitagawa, T.; Ozaki, Y. "*Structure and Bonding*", 64, 71, 1987.

28a. Spiro, T.G.; Loher, T.M. in "*Advances in Infrared and Ràman Spectroscopy*", Clark, R.J.H.; Hester, R.E., Eds., Heyden, London, Vol.I, Chap. 3., 1975.

b. Strekas, T.C.; Spiro, T.G. *Biochim. Biophys. Acta.* 263, 830, 1972.

c. Spiro, T.G.; Strekas, T.C. *Proc. Natl. Acad. Sci. U.S.A.* 69, 2622, 1972.

d. Warshell, A. *Ann. Rev. Biophys. and Bioeng.* 6, 273, 1977.

e. Kitagawa, T.; Ozaki, Y.; Kyogoku, Y. *Advances in Biophysics*, 11, 153, 1978.

29a. Verma, A.L.; Bernstein, H.J. *Biochem. Biophys. Res. Commn.* 57, 1, 1974.

29b. Verma, A.L.; Bernstein, H.J. *J. Chem. Phys.* 61, 2560, 1974.

c. Verma, A.L.; Mendelsohn, R.; Bernstein, H.J. *J. Chem. Phys.* 61, 383,1974.

d. Mendelsohn, R.; Sunder, S.; Verma, A.L.; Bernstein, H.J. *J. Chem. Phys.* 62, 37, 1975.

e. Brunner, H.; Mayer, A.; Sussner, H. *J. Mol. Biol.* 70, 153, 1972.

f. Verma, A.L.; Bernstein, H.J. *J. Raman. Spectrsc.* 2, 163, 1973.

30a. Spiro, T.G.; Strekas, T.C. *J. Am. Chem. Soc.* 96, 338, 1974.

b. Yamamoto, T.; Palmer, G.; Gill, D.; Salmeen, I.T.; Remai,L. *J. Biol. Chem.* 248, 5211, 1973.

31a. Kitagawa, T.; Iizuka, T.; Saito, M.; Kyogoku, Y. *Chem. Lett.* 849, 1975.

b. Spiro, T.G.; Burke, J.M. *J. Am. Chem. Soc.* 98, 5482, 1976.

32. Spaulding, L.D.; Chang, C.C.; Yu, N.T.; Felton, R.H. *J. Am. Chem. Soc.* 97, 2517, 1975.

33a. Mashiko, T.; Kastner, N.E.; Spartalian, K.; Scheidt, W.R.; Reed, C.A. *J. Am. Chem. Soc.* 100, 6354, 1978.

b. Reed, C.A.; Mashiko, T.; Scheidt, W.R.; Spartalian, K.; Lang, G. *J. Am. Chem. Soc.* 102, 2302, 1980.

34a. Spiro, T.G.; Stong, J.D.; Stein, P. *J. Am. Chem. Soc.* 101, 2648, 1979.

b. Huong, P.V.; Pommier, J.C. *C. R. Acad. Sci. Ser. C.*285 519, 1977.

34c. Scholler, D.M.; Hoffman, B.M. *J. Am. Chem. Soc.* 101, 1655, 1979.

d. Choi, S.; Spiro, T.G.; Langry, K.C.; Smith, K.M.; Budd, D.L.; LaMar, G.N. *J. Am. Chem. Soc.* 104, 4345, 1982.

35a. Choi, S.; Spiro, T.G.; Langry, K.C.; Smith, K.M. *J. Am. Chem. Soc.* 104, 4337, 1982.

b. Sarkar, M.; Verma, A.L. *J. Raman Spectrsc.* 17, 407, 1986.

36a. Hori, H.; Kitagawa, T. *J. Am. Chem. Soc.* 102, 3608, 1980.

b. Kincaid, J.R; Stein, P.; Spiro, T.G. *Proc. Natl. Acad. Sci. U.S.A* 76, 549, 4156.

c. Stein, P.; Mitchell, M.; Spiro, T.G. *J. Am. Chem. Soc.* 102, 7797, 1980.

d. Kitagawa, T.; Nagai, K.; Tsubaki, M. *FEBS Lett.* 104, 376, 1978.

e. Teroaka, J.; Kitagawa, T. *J. Biol Chem.* 256, 3969, 1981.

37a. Kitagawa, T.; Orii, Y. *J. Biochem. (Tokyo)* 84, 1245, 1978.

b. Salmeen, I.T; Remai, L.; Babcock, G.T. *Biochemistry* 17, 800, 1978.

c. Ogura, T.; Sone, N.; Tagawa, K.; Kitagawa, T. *Biochemistry*, 23, 2826, 1984.

d. Kitagawa, T.; Nagai, K. *Nature*, 281, 503, 1979.

e. Yoshikawa, S.; Mochizuki, H.; Chihara, S.; Hagihara, B.; Kitagawa, T. *Biochim. Biophys. Acta.* 786, 267, 1984.

38a. Ozaki, Y.; Iriyama, K.; Ogoshi, H.; Kitagawa, T. *J. Am. Chem. Soc.* 109, 5583, 1987.

b. Verma, A.L.; Chaudhury, N.K.; Saini, G.S.S. in "*In Recent*

Trends In Raman Spectroscopy", Banerjee, S.B.; Jha, S.S. Eds., World Scientific Publishing Co., Singapore, p. 192, 1989.

38c. Verma, A.L.; Chaudhury, N.K.; Saini, G.S.S. *XIIth International Conferenece on Raman Spectroscopy*, Durig, J.R.; Sullivan, J.F. Eds., John Wiley and Sons, New York, p. 592, 1990.

d. Verma, A.L.; Saini, G.S.S.; Chaudhury, N.K. *Proc. Ind. Acad. Sci. (Chem. Sci.)* 102, 291, 1990.

e. Verma A.L.; Kitagawa, T. *Biochemistry*,(In Press).

39a. Fuhrhop, J.H.; Mauzerall, D. *J. Am. Chem. Soc.* 91, 4174, 1969.

b. Mauzerall, D. *J. Am. Chem. Soc.* 84, 2437, 1962.

40. Woodward, R.B.S. *Ind. Chim. Belge.* 2, 1293, 1962.

41a. Fuhrhop, J.H.; Kadish, K.; Davis, D.G. *J. Am. Chem. Soc.* 95, 5140, 1973.

b. Fuhrhop, J.H. *Structure and Bonding*, 18, 1, 1974.

42. Seely, G.R.; Talmadge, K. *Photochem. Photobiol.* 3, 195, 1964.

43. Engelsma, G.; Yamamoto, A.; Markham, E.; Calvin, M. *J. Phys. Chem.* 66, 2517, 1962.

44. Imamura, T.; Jin, T.; Suzuki, T.; Fujimoto, M. *Chem Lett.* 847, 1985.

45a. Bartocci, C.; Maldotti, A.; Traversso, O.; Bignozzi, C.A.; Carassitti, V. *Polyhedron*, 2, 97, 1983.

b. Bartocci, C.; Scandola, F.; Ferri, A.; Carassitti, V. *J. Am.*

Chem. Soc. 102, 7067, 1980.

45c. Bizet, C.; Morliere, P.; Brault, D.; Delgado, O.; Bazin, M.; Santus, R. *Photochem. Photobiol.* 34, 315, 1981.

46. Kim, D.; Miller, L.A.; Rakhit, G.; Spiro, T.G. *J. Phys. Chem.* 90, 3320, 1986.

47a. Lexa, D.; Momenteau, M.; Mispelter, J. *Biochim. Biophys. Acta.* 338, 151, 1974.

b. Wolberg, A. *Isr. J. Chem.* 12, 1031, 1974.

c. Bottomely, L.A.; Kadish, K.M. *Inorg. Chem.* 20, 1348, 1981.

48a. Willigen, H.V.; Ebersole, M.H. *J. Am. Chem. Soc.* 109, 2299, 1987.

b. Gasyna, Z.; Browett, W.R.; Stillman, M.J. *Inorg. Chem.* 24, 2440, 1985.

c. Godziela, G.M.; Goff, H.M. *J. Am. Chem. Soc.* 108, 2237, 1986.

d. Harriman, A.; Porter, G. *J. C. S. Faraday Trans.* 75, 1532, 1979.

e. Saini, G.S.S.; Chaudhury, N.K.; Verma A.L. *Photochem. Photobiol.* (Submitted).

49. Donhoe, R.J.; Atamian, M.; Bocian, D.F. *J. Am. Chem. Soc.* 109, 5593, 1987.

50. Verma, A.L.; Chaudhury, N.K. *J. Raman Spectrosc.* (In Press).

51. Chaudhury, N.K.; Saini, G.S.S.; Verma, A.L. *Inorg. Chem.* (Submitted)

52. Chaudhury, N.K.; Saini, G.S.S.; Verma, A.L. *Chem. Phys. Lett.* (Submitted)

Table 1

Parameters of the Square-Pyramidal Coordination Group in Several High-Spin Iron(III) Porphyrins

Derivatives	$(Fe-N)_{av}$	Distance(A^{o})		
		Ct-N	Ct-Fe	Fe-X
FeProtoDME(Cl)	2.062(10)	2.008	0.475	2.218(6)
FeMesoPDME(CH_3O)	2.073(6)	2.022	0.455	1.842(4)
FeTPP(Cl)	2.049(9)	2.012	0.38	2.192(12)
$(FeTPP)_2O$	2.087(5)	2.027	0.50	1.763(1)
FeTPP(SCN)	2.065(5)	2.007	0.485	1.957(5)
FeTPP(N_3)	2.055	2.027	0.34	1.909
$(FeProtoDME)_2O$	2.08	-	-	1.73
$(FeODM)_2O$	2.065(8)	2.002	0.53	1.752(1)

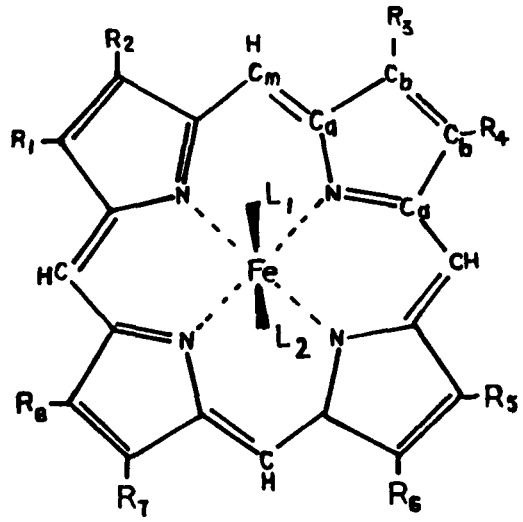

	R_1	R_2	R_3	R_4	R_5	R_6	R_7	R_8
Protoporphyrin-IX	Me	V	Me	V	Me	P	P	Me
Deuteroporphyrin-IX	Me	H	Me	H	Me	P	P	Me
Hematoporphyrin-IX	Me	CHMe OH	Me	CHMe OH	Me	P	P	Me
Octaethylporphyrin	Et	Et	Et	Et	Et	Et	Et	Et

Me $-CH_3$, Et $-CH_2CH_3$, V $-CH=CH_2$, P $-C_2H_4COOH$

L_1, L_2 = Axial coordination sites.

Fig. 1.1 Structural diagram of the porphyrin ring with different substituents at the peripherial positions.

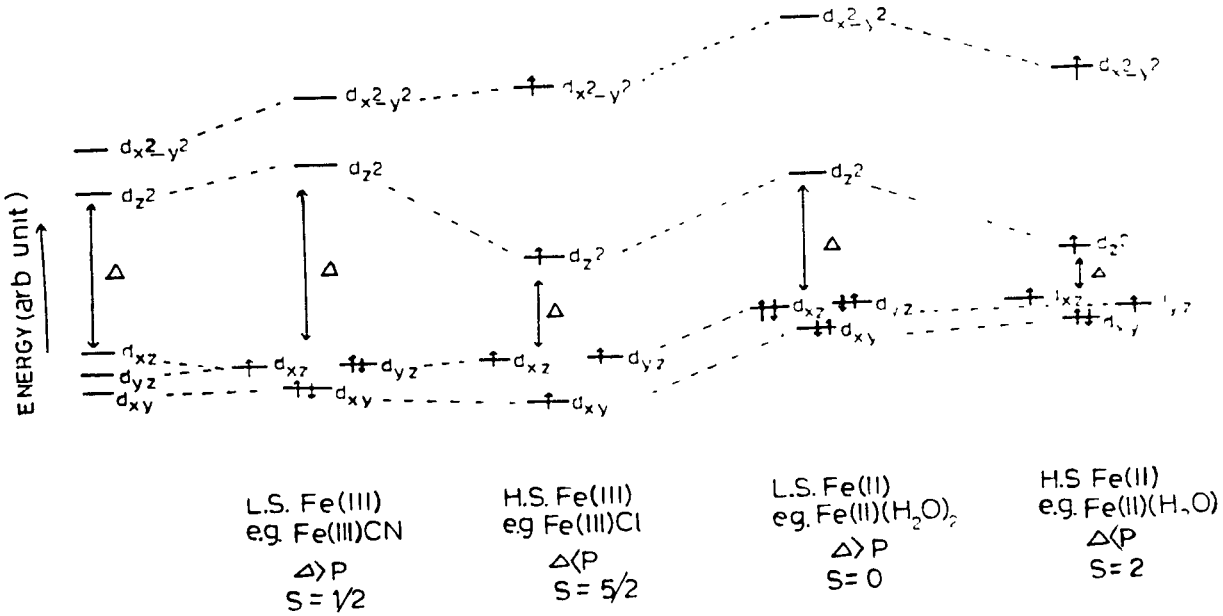

Fig. 1.2 Schematic energy level diagrams of different d orbitals of iron in octahedral field in the presence of various types of axial ligands.

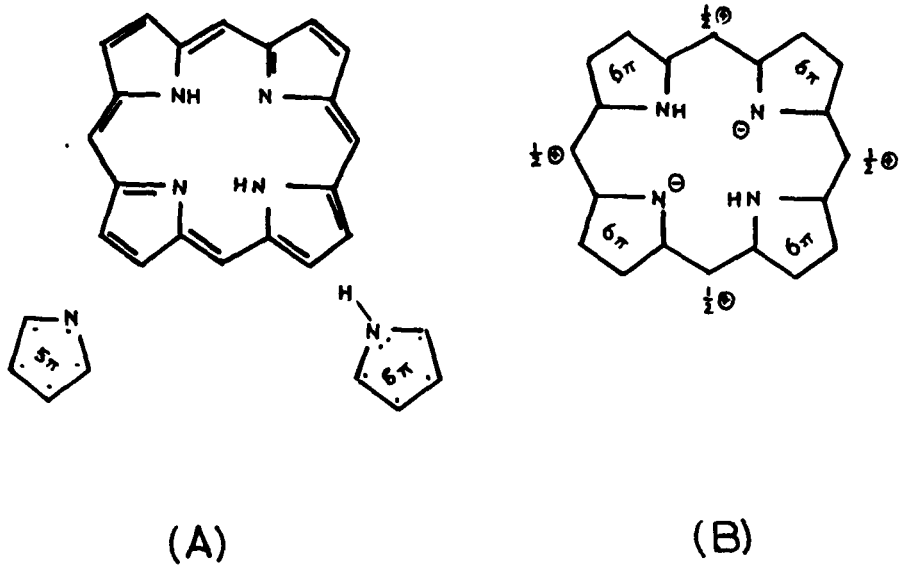

(A) (B)

Fig. 1.3 Model for porphyrin electron distribution as proposed by Woodward.

THEORETICAL DESCRIPTION OF ELECTRONIC ABSORPTION AND RESONANCE RAMAN SPECTRA

This chapter describes detailed theoretical aspects of electronic absorption spectra of iron porphyrins and relevant resonance Raman spectra.

2.1 Structure and Nomenclature of Iron Porphyrins

The porphyrins are a class of molecules which are derived from the basic skeleton of carbon and nitrogen atoms as shown in Figure 2.1. The skeleton consists of four pyrrole rings linked by methine bridges. The outer ring system may be substituted at any of the peripheral positions from 1 to 8 and/or at the meso α , β , γ and δ positions. The central core may be occupied by two hydrogen atoms or by any metal. The compound of first type is known as free base; and the second type are the metalloporphyrin complexes. Depending upon the type of substituents at different positions, the compounds are designated by specific nomenclature.

2.2 Absorption Spectra

Spectroscopically, all metalloporphyrins have one feature in common: the absorption spectrum shows a very intense band at 400 nm with molar extinction coefficient $\varepsilon \simeq 2$ to $4X10^5$ $M^{-1}cm^{-1}$ known as Soret, B or band, and a much weaker band with $\varepsilon \simeq 10^4$ $M^{-1}cm^{-1}$ in the 550 nm region and is called the Q_{00} or the α band. Another weaker band on the higher energy side and

separated by ~1200 cm^{-1} from the Q_{00} band arises due to vibronic coupling and is called as the Q_{01} or β band. On the higher energy side of the Soret band, metalloporphyrins generally show a weaker N band at ~325 nm and an M band at ~215 nm. These compounds often show a weaker L band between the N and M bands. All these bands are interpreted as (π, π^*) in origin. Figure 2.2 shows all these transitions in a typical metalloporphyrin.

In general, the electronic absorption spectra of iron-porphyrins and model complexes and intact heme-proteins have as their common and dominant characteristic intense Soret band in the 400-420 nm region, and another pair of weak Q_{00} and Q_{01} bands in the visible region, 550-600 nm range. These characterstic transitions are polarized in the plane of the porphyrin skeleton. In addition to these, some iron-porphyrins show additional weak features, which may arise due to charge-transfer transitions, metal d-d transitions or some other type of transitions. Figure 2.3 gives the electronic absorption spectrum for a typical iron(III)porphyrin.

The electronic absorption spectra of metalloporphyrins vary with the nature of chromophoric system and various substituents at the macrocyclic periphery. For example, electrophilic substituents such as vinyl or formyl groups cause a red-shift of the absorption bands due to increase in the π-electron density at the periphery of porphyrin macrocycle, which in turn decrease the porphyrin basicity. The correlation between

the nature of the substituents and absorption spectra have been described by *Stern et al*[1] and other workers.[2]

2.3 Theoretical Description of Absorption Spectra

The first successful theoretical treatment for understanding the electronic absorption of porphyrins was given by Simpson in 1949[3] in his free electron model which predicted that the long-wavelength transitions would be forbidden while the short-wavelength transitions would be allowed. Figure 2.4 shows the π-system for free-base porphin. Simpson assumed that the electrons were allowed to move in close conjugated paths consisting of 18 lattice points. In analogy with benzene, electrons occupy orbitals of increasing angular momentum, two in the lowest level(l=0) and four each in the l=1,2,3,4 levels. The lowest excited states are formed by promoting an electron from an orbital with angular momentum $l = \pm 4$ to an orbital with $l = \pm 5$. Since the change of orbital angular momentum will then be either ± 1 or ± 9, the pairs of transitions will be respectively allowed or forbidden. Hund's rules predict the lower energy state to correspond to $\Delta l = \pm 9$. This predicts, as observed, that the longer wavelength transitions are much weaker than the UV transitions. Simpson also suggested that the two sets of visible bands observed in metal free porphyrins were due to two forms of tautomers. However, in reality the free-base porphin occurs only with protons on opposite nitrogens and the extra spectral features are due to the large distortions from the square symmetry of the porphin skeleton.[4] Replacement of the imine

protons by a metal results to a large extent in four fold axial symmetry. *Platt*[2a] was first to realize that the four visible bands of free-base porphyrins collapse to two bands in the metal complexes.

In spite of early success, Simpson model was unable to explain many quantitative features, as the porphyrin was assumed to have cylindrical symmetry $D_{\infty h}$, while in reality, metalloporphyrins have approximately D_{4h} symmetry. In the subsequent theoretical work in the electron systems, the molecular orbitals are expressed as linear combinations of atomic orbitals and the orbital coefficients are determined by a variational procedure. Later on *Longuet-Higgins et al*[5] made the first Huckel calculations on porphyrins and showed that the $3a_{2u}(\pi)$ and $1a_{1u}(\pi)$ were the top filled orbitals and lowest empty degenerate orbital was $4e_g(\pi^*)$. The orbital coefficients for these orbitals are shown in Figure 2.5. According to this, the transition $3a_{2u} \rightarrow 4e_g$ at lower energy was identified with the $Q_{0,0}$ band and the transition $1a_{1u} \rightarrow 4e_g$ at higher energy as Soret-band. This model predicts equal absorption intensities which is, however, not the case.

In order to account for the observed electronic absorption spectra, *Gouterman* [4,6] has developed the "four orbital model", which is a combination of free electron model[3] and LCAO-MO description.[5] *Gouterman* considered only two lowest empty orbitals and two highest-filled orbitals of the molecule in the

ground state. Because of the four fold symmetry, the two empty orbitals are degenerate and carry the D_{4h}-level as e_g. The two highest occupied molecular orbitals are designated as a_{1u} and a_{2u}. Figure 2.5 shows these four orbitals, depicting the electronic wave function amplitude on the molecular frame. The top filled orbitals are not symmetry degenerate but are assumed to be accidentally degenerate. These a_{1u}, a_{2u} and e_g orbitals are analogous to the free-electron orbitals with $l=\pm4$ and $l=\pm5$ respectively in the Simpson's model.[7] The one electron transitions arise due to excitation of electrons from either the a_{2u} or a_{1u} to the e_g orbital. These excited states or configurations are denoted by (a_{2u}, e_g) and (a_{1u}, e_g). As they have the same symmetry, their overlap due to Coulomb repulsion energy is finite and the states mix together. Thus the singly excited configurations are not adequate descriptions of the excited states. If H_{eff} be the Hamiltonion of the pure configuration, and if they interact via coulomb repulsion between electrons represented by $H' = e^2/r_{ij}$, then the total Hamiltonion of the system may be written as

$$H = H_{eff} + H' \qquad \text{------2.3.1}$$

The coefficients for the mixed states can be calculated by defining the parameters as follows:

$$A'_{1g} = 1/2[E(a_{1u}e_{gx}) + E(a_{2u}e_{gy})] \qquad \text{------2.3.2}$$

$$A_{1g} = 1/2[E(a_{2u}e_{gy}) - E(a_{1u}e_{gx})] \qquad \text{------2.3.3}$$

$$A''_{1g} = \int (a_{2u}e_{gx}) H (a_{1u}e_{gy}) dv \qquad \text{------2.3.4}$$

$$R_{1y} = \int (a_{1u}e_{gx}) y \, \Psi_0 \, dv \qquad \text{------2.3.5}$$

$$R_{2y} = \int (a_{2u} e_{gx})_y \ \Psi_0 dv \qquad \text{------2.3.6}$$

Since $R_1 \simeq R_2$

$$R = 1/\sqrt{2}\ (R_1 \pm R_2) \qquad \text{------2.3.7}$$

Where A'_{1g} is the centre of gravity of the two configurations before their interaction, A_{1g} is the splitting between them, A''_{1g} is the configurational interaction and R's are the transition dipole moments. Because of X-Y degeneracy, the matrix describing only the Y-polarized mixed states is given in Table 2.1. The rows of the table represent approximate mixtures for the case in which the configuration interaction is much larger then the splitting between the pure states. This case predicts weak Q band, a minimum in the energy difference E (Soret)-E(Q) which is observed in the absorption spectra of metalloporphyrins. Moreover, it is expected that,

$$E_B - E_Q \simeq 2A'_{1g} = \text{Constant} \qquad \text{------2.3.8}$$

and

$$q_B^2 \simeq R^2 = \text{Constant} \qquad \text{------2.3.9}$$

Where the oscillator strength f_B of the Soret band is related to q_B by an expression

$$f_B \simeq E_B q_B^2 \qquad \text{------2.3.10}$$

The major conclusion of this calculation is the removal of the degeneracy of the Soret and Q states by configuration interaction.

The lower energy transition α, borrows back some intensity of the higher energy transition (Soret) (about 10%)

through vibronic coupling with the formation of a vibronic side band called β or Q_{01} band on the higher energy side of the - band, such that

$$\nu_{\beta}^{max} = \nu_{\alpha}^{max} + \nu_{vib} \qquad \text{------2.3.11}$$

Where $_{vib}$ is the frequency of vibrational modes in the excited electronic state.

Because of the degeneracy of the electronic states of metalloporphyrins, it is necessary to apply degenerate perturbation theory to linear combinations of the degenerate components. For the symmetry group (D_{4h}), only the b_{1g}, b_{2g} and a_{2g} modes are vibronically active. Since both the excited states responsible for the Q and Soret bands have E_u symmetry, vibronic coupling between the states can take place by those vibrations having symmetry species given by :

$$\Gamma_{vib} \subset E_u X E_u = A_{1g} + A_{2g} + B_{1g} + B_{2g} \qquad \text{------2.3.12}$$

It is argued that if the cyclic polyene model is truly relevant to metalloporphyrin, A_{1g} modes will not be vibronically active.[8]

While vibrational structure that can be resolved in the Soret region of the porphyrin spectra can probably be assigned to Frank-Condon activity of symmetric vibrations, the vibrational transitions in the Q_{01} or β band have been attributed to vibronic borrowing from the Soret state.[7-9] However, additional strong experimental evidence from resonance Raman studies[10] substantiates

this model, as the experimental evidence is that when exciting Raman spectra in resonance with the Q states, the A_{2g}, B_{1g} and B_{2g} vibrational modes, which are clearly identifiable by their polarization ratios, are strongly enhanced. Further details of vibronic coupling shall be given in the theoretical section on resonance Raman scattering.

2.4 Theoretical Description of Iron Porphyrins

In general, porphyrins can form complexes with various transition metals. Because of the proximity of the energy levels and favourable symmetry of the electronic orbitals, the metals and porphyrins will interact strongly and the resulting molecular orbitals will contain mixtures of metal and porphyrin orbitals. In addition, transition metals can complex with other ligands along the axial directions which may affect the energy levels of metal porphyrins. All the five d levels of a transition metal are degenerate in unperturbed state. They split when the metal is complexed to a porphyrin and thereby perturbing the metal d levels, with the result that different d orbitals will interact differently with the porphyrin depending upon the geometry of the electronic orbitals relative to the porphyrin orbitals.

If the metal is complexed to additional axial direction with strong field nitrogeneous ligands, then in the relevant octahedral field, the five degenerate d levels split into two groups, (d_{xy}, d_{xz}, d_{yz}) and ($d_{x^2-y^2}$, d_{z^2}). Depending upon the relative magnitudes of the ligand field strength and the electron

spin pairing energy, these groups are separated by ligand field strength and electrons occupy different orbitals starting from lowest energy orbitals. For iron-porphyrins, Figures 2.6 and 2.7 show the formation of low or high spin, oxidized or reduced complexes. Because the X-Y axes in metalloporphyrins are defined with respect to the iron-nitrogen directions, the d_{xy} orbital (b_{2g} in D_{4h} symmetry) will interact much less with the porphyrin than the $d_{x^2-y^2}$ (b_{1g}) orbital; electronic repulsion places the $d_{x^2-y^2}$ orbital at much higher energy than the d_{xy} orbital. Similar arguments indicate that the d_{z^2} (a_{1g}) orbital will be relatively high in energy if axial ligands are present. Moreover, the energy of this orbital will be most sensitive to axial ligation. Since the interaction of the metal with the porphyrin nitrogen orbital is different than with the ligand orbitals, the d_{xy} (b_{2g}) orbital is split from the d_{xz}, d_{yz} {e_g (d_π)} orbitals in tetragonal field.

Iron porphyrins exhibit a number of different type of absorption spectra including hypso(blue shifted, spectra of transition metal porphyrins which have $e_g(d_\pi)$ orbitals filled) and hyper (extra absorption in the region $\lambda > 320$ nm) spectra. They also occur in various spin states in the valence states +2 and +3. However, they may also occur in unusual valence states of +1 and +4. Figure 2.6 shows energy level diagrams of several ferrous porphyrins with H_2O ligands. In the absence of any ligands and iron in the porphyrin plane, the four metal orbitals d_{xy}, d_{yz}, d_{xz}, d_{z^2} are quite close in energy which implies for

the d^6 configuration an intermediate spin state with S = 1. When iron is raised out of plane, the $d_x2_{-y}2$ metal orbital drops in energy sufficiently to lead to a high spin state. Addition of water as a fifth ligand to non-planar ferrous iron causes d_z2 orbital to rise in energy. Since water is a weak ligand, this increase in energy is not very large. For strong ligands, such as CO, imidazole (Im), d_z2 orbital is raised further high in energy and low spin state for iron is favoured. Once the system goes to low spin, S=0 state, the iron probably moves back into the plane of the porphyrins and assume a lower energy configuration.

Figure 2.7 shows similar energy level diagram for a ferric complex. In this case the iron is out of plane the of porphyrin and five coordinated. For example, the cyanide (CN) ion gives low spin configuration, while the chloride (Cl) and fluoride (F) ions lead to a high spin configuration. The hydroxide (OH) ion results in a mixed spin state determined by the position of the d_z2 orbital.

Thus it is evident that except for ferrous, low spin complexes, all other complexes have vacancies in the metal e_g ($d\pi$) orbitals. Thus, the charge transfer (CT) transitions from the $a_{2u}(\pi)$ orbital to the $e_g(d\pi)$ orbital are allowed and will be polarized in the porphyrin plane which can interact with porphyrin transitions and borrow intensity from them. Another possible charge-transfer transition $a_{1u}(\pi) \longrightarrow e_g(d\pi)$ is also allowed but is expected to be weak as the $a_{1u}(\pi)$ orbital has no

charge density on the nitrogen atoms. In the ferric high-spin state complexes, these CT, transitions are responsible for strong visible bands. For example, a band at 640 nm in $Fe^{III}(PP)Cl$ is a CT band. In the ferric low spin complexes these CT transitions have been identified at low energy around $\sim 6500\ cm^{-1}$. In the ferrous high spin case they are expected at higher energy.

2.5 Raman Scattering

When an electromagnetic radiation interacts with matter, molecule or atom, the molecule or the atom is then polarized, i.e., a dipole is induced, usually oscillating in phase with the incident electromagnetic wave. When the exciting frequency of e.m. radiation does not match with any dipole allowed transition frequencies of the system, the oscillating dipole instantaneously generates a secondary wave of the same frequency and it is the interaction or interference of secondary waves with the incident radiation which is the basis of the phenomena such as refraction (transmission), reflection and scattering. If the exciting frequency of the e.m. radiation is in the visible or UV range, molecules sometimes fall to a different excited vibrational or rotational energy level of the electronic ground state giving rise to secondary emission of different wavelength - this phenomenon is called **"Raman effect"**.

Raman scattering is one class of a wide varieties of light scattering phenomenon. During the process of Raman

scattering, photons of the exciting radiation interact with the molecules of the medium being irradiated. The energies of the inelastically scattered photons may either be increased or decreased relative to the exciting photon energy by quantized increments corresponding to the vibrational or rotational energy levels.[11] The molecule in the ground state may be momentarily raised to a higher unstable state due to interaction with the incident photon, which in turn comes back to the ground vibrational state or to an excited vibrational state which correspond to Rayleigh and Stokes Raman scattering respectively. On the other hand, if the exciting photon interacts with a molecule in the excited vibrational state, it may return to the ground vibrational state via a higher unstable state giving rise to anti-Stokes Raman scattering.

The fraction of incident photons scattered during Raman process is always very small, and thereby Raman lines or shifts are of extremely weak intensity as $I_{Rayleigh} \sim 10^{-3}$ of the intensity of the incident light and $I_{Raman} \sim 10^{-3}\ I_{Rayleigh}$. Because of this, intense monochromatic laser is used as excitation source to obtain good quality Raman spectra. In normal Raman scattering the excitation frequency of radiation is far away from the stationary energy states of the system, i.e., the intermediate state is not associated with any particular molecular eigen state as such and is considered to be a statistical superposition/summation of a large number of excited electronic states of the system. When the incident light

approaches an electronic absorption band, the intermediate state assumes more importance and summation term is dominated by this electronic state. Thereby one obtains pre-resonance and resonance Raman scattering by tuning the exciting frequency through the electronic absorption band (Figure 2.8). In resonance Raman scattering, the intermediate state is dominated by a few vibronic levels in the vicinity of the incident light frequency. Finally, the resonance fluorescence limit is reached when the incident light coincides with a single sharp level of the electronic state. Though both resonance Raman and resonance fluorescence involve excitation and emission in the electronic absorption band, however, there is a very precise demarcation between these two processes. In case of resonant scattering, the process depends not only on the energy difference between the molecule and the photon state, but also on the line shapes associated with them. In the resonant fluorescence case, the molecular state is much sharper than the photon state and is thus completely in resonance with the incident beam. The scattering may then be described as a rapid population of the excited state followed by a slow decay characteristic of the life time of this state. In the resonance Raman limit, the photon state is much sharper than the molecular state and in resonance with only a small part of it. In this case, the two emission processes are involved; a fast one with lifetime of the incident photon state and a slower one with the excited state lifetime. The former part represents the resonant contribution, while the later represents

the non-resonant part of the scattering. Thus the re-emission lifetime is characteristic of either the excited state or of the incident radiation, whichever has the narrower linewidth. The resonance fluorescence is attributed to the later situation and resonance Raman scattering to the former.[12] Inspite of this distinction between the two phenomena, the physical process remains the same.

2.6 Theory of Resonance Raman Scattering

The charge distribution of a molecule is perturbed periodically by electric and magnetic components of the interacting field. The induced alternating dipole moment resulting from the interaction acts as a source of secondary radiation and forms a basis of light scattering phenomena. This treatment fairly demonstrates how polarizability fluctuations give rise to frequency shifts in the scattered radiation. However, this simple classical treatment offers no clues to the inherent nature of the interaction of radiation with matter, nor it explains important phenomenon like resonance and stimulated Raman scattering. A quantum mechanical electrodyanamical approach in this direction was first given by *Jacon*[13] for RR scattering. However, the correct results for RR scattering may be obtained by using semi-classical treatment of *Kramers and Heisenberg*[14] which correlates the scattering tensor to the wave functions and the energy levels of the scatterer. The radiation is treated classical and is regarded as a source of perturbation of the

energy levels of the scattering system while quantum mechanical techniques are used to investigate transitions between the energy levels of the perturbed system. This approach has been extended by many workers in later studies.[15]

If the molecule is considered at the origin of a space fixed coordinate system which interacts with an incident plane wave of light with electric vector represented as

$$\bar{E}_\sigma = \bar{E}^o_\sigma \exp(i\bar{k}.r - i\omega t) \qquad \text{------2.6.1}$$

propagating along $\bar{k}$ with angular frequency ω, the oscillating electric dipole moment induced in the molecule is given by

$$(\bar{\mu}_\rho)_{mn} = (\tilde{\tilde{\alpha}}_{\rho\sigma})_{mn} \bar{E}_\sigma \qquad \text{------2.6.2}$$

where $(\bar{\mu}_\rho)_{mn} = \langle \Psi_m | e\bar{\rho} | \Psi_n \rangle$ is the amplitude of the transition moment and Ψ_m and Ψ_n are the time dependent wavefunctions of the initial and final states respectively, $(\tilde{\tilde{\alpha}}_{\rho\sigma})_{mn}$ is the polarizability tensor for the transitions from m to n and $\bar{\rho}$ and $\bar{\sigma}$ are molecular cartesian axes of the scattering tensor $(\tilde{\tilde{\alpha}}_{\rho\sigma})$.

Let us consider a molecule, initially in a vibronic state $|m\rangle$, which is perturbed by plane polarized incident light of frequency ν_o and intensity I_o causing a transition to a vibronic state $|n\rangle$ and scattering light of frequency $(\nu_o \pm \nu_{mn})$. The intensity of scattered light I_{mn} in terms of photons per molecule per second in 4π solid angle, after averaging over all orientations of the molecule is given by[16],

$$I_{mn} = 128\pi^5/9c^4(\nu_o \pm \nu_{mn})^4 I_o \sum_{\rho,\sigma} |(\alpha_{\rho\sigma})_{mn}|^2 \quad \text{-----2.6.3}$$

where c is the velocity of light and the sum goes over $\rho, \sigma = x,y,z$

Thus the intensity of the scattered radiation depends upon the frequency of the incident radiation, and more critically it depends on $|(\alpha_{\rho\sigma})_{mn}|^2$ when the exciting radiation approaches an electronic absorption band in the resonance Raman effect. Consequently the main effort in the development of Raman theory is to provide a theoretical frame work for calculating $(\alpha_{\rho\sigma})_{mn}$ in terms of molecular parameters.

In order to determine the polarizability, the distortion of the wave functions due to periodic perturbation by the incident e.m. wave has to be known or calculated and then to evaluate the electric dipole transition moment with the new wave functions using time dependent perturbation theory. The molecular wave functions are obtained from time dependent Schrodinger equation

$$i\hbar \frac{\partial}{\partial t} |\Psi\rangle = (H_o + V)|\Psi\rangle \quad \text{------2.6.4}$$

Where H_o is the unperturbed hamiltonian

and

$$|\Psi\rangle = \sum_k a_k(t)|\Psi_k^o(t)\rangle \quad \text{------2.6.5}$$

Where

$$|\Psi_k^o(t)\rangle = |\psi_k^o\rangle e^{-iH_o t/h} \quad \text{------2.6.6}$$

is the solution for V=0

$$V = -1/2[\bar{\mu}_\rho\{\bar{E}^o_\rho \exp(-i\omega t) + \bar{E}^o_\rho \exp(i\omega t)\}] \text{ ------2.6.7}$$

describes the major part of the interaction of the molecule with light wave.

The $(\rho\sigma)^{th}$ component of the matrix element of the polarizability tensor for the transition from vibronic state $|m\rangle$ to a vibronic state $|n\rangle$ is given by the second order perturbation theory as calculated by *Kramer-Heisenberg-Dirac.*[17]

$$(\alpha_{\rho\sigma})_{mn} = \frac{1}{h}\sum_e \left[\frac{\langle n|\mu_\sigma|e\rangle\langle e|\mu_\rho|m\rangle}{\nu_{em} - \nu_o + i\Gamma_e} + \frac{\langle n|\mu_\sigma|e\rangle\langle e|\mu_\rho|m\rangle}{\nu_{en} + \nu_o + i\Gamma_e} \right] \quad \text{---2.6.8}$$

and the sum goes over the excited vibronic states, e, of the molecule.

When $\langle e|\mu|m\rangle$ is finite for a real state $|e\rangle$, the transition from $|m\rangle$ to $|e\rangle$ is accompanied by light absorption which would have the center of frequency at ν_{em} and full width at half maximum of $2\Gamma e$, and the absorption intensity would be proportional to $|\langle e|\mu|m\rangle|^2$. If the photon energy of Raman excitation ($= h\nu_o$) were close to the energy of the electronic transition, the first term of $(\alpha_{\rho\sigma})_{mn}$ and thus I_{mn} would be remarkably large. This is called resonance Raman scattering. The vibrational modes which gain resonance enhancement in intensity are limited to the vibrations involved in the chromophore

responsible for the absorption band.

The equation 2.6.8 is made more meaningful by incorporating Born-Oppenheimer adiabatic approximation[18] for all wave functions involved and then expanding of the electronic wave functions in a Taylor's series around the ground state equilibrium configuration of the nuclei. Thus, a given vibronic state must now be identified according to electronic and vibrational levels, as $|m\rangle=|g,i\rangle$, $|n\rangle=|g,j\rangle$ and $|e\rangle=|r,v\rangle$

Where $|g\rangle$ and $|r\rangle$ are the electronic wave functions for the ground and excited states, respectively, $|i\rangle$, $|j\rangle$ and $|v\rangle$ are the vibrational wave functions with the quantum numbers of i, j and v, respectively. Here it is postulated that the vibrational wave functions in the electronic excited state are the same as those in the electronic ground state except for the origin of the coordinates, i.e., the equilibrium structure of molecules, which differs between the two states. The change of the electronic wave function due to the origin shift is incorporated with Herzberg-Teller expansion. Then the main terms contributing to the polarizability tensor of equation 2.6.8 under resonance with a particular electronic state, $|r\rangle$, are the following two terms

$$(\alpha_{\rho\sigma})^{\pi}_{ij} = (A_{\rho\sigma})^{\pi}_{ij} + (B_{\rho\sigma})^{\pi}_{ij} \qquad \text{---- 2.6.9}$$

where

$$(A_{\rho\sigma})^{\pi}_{ij} = \frac{M^{g\pi}_{\sigma}\, M^{g\pi}_{\rho}}{h} \sum_{v} \frac{\langle j|v\rangle\langle v|i\rangle}{\nu_{\pi g} + (v-i)\Delta\nu_a - \nu_0 + i\Gamma_{\pi}} \qquad \text{-- 2.6.10}$$

and

$$(B_{\rho\sigma})^{\pi}_{ij} = \frac{M^{g\pi}_{\sigma}\, h^{\pi s}_{a}\, M^{sg}_{\rho}}{h^2(\nu_\pi - \nu_s)} \sum_{v} \frac{\langle j|\, Q_a|v\rangle\langle v|i\rangle}{\nu_{\pi g} + (v-i)\Delta\nu_a - \nu_0 + i\Gamma_\pi} +$$

$$\frac{M^{gs}_{\sigma}\, h^{s\pi}_{a}\, M^{\pi g}_{\rho}}{h^2(\nu_\pi - \nu_s)} \sum_{v} \frac{\langle j|v\rangle\langle v|\, Q_a|i\rangle}{\nu_{\pi g} + (v-i)\Delta\nu_a - \nu_0 + i\Gamma_\pi} \quad --2.6.11$$

Where $M^{gr}_{\sigma} = \langle g^o|\, \mu_\sigma\, |r^o\rangle$, $h\nu_{rg}$ is the energy separation between $|r\rangle$ and $|g\rangle$, $\Delta\nu_a$ is the frequency of the normal mode with coordinates q_a and h_a is a vibronic coupling operator $\left(\frac{\partial H}{\partial q_a}\right)$ for a normal mode q_a.

The above results can be summarized as follows: when Raman spectra are obtained with excitation in the region of an electronic absorption band, the vibrational modes which are expected to show enhancement are the ones which contribute intensity to the electronic spectrum, i.e., they are vibronically active modes, which are of two types: (i) modes which connect the ground state to the excited state involved in resonance through the Franck-Condon (FC) overlap (A-term); (ii) modes which mix the resonant electronic state to another one of higher energy (B-term). In FC effect, the potential energy curve of the excited electronic state is shifted so that the vibrational wave functions are not orthogonal. Raman scattering from modes due to FC effect can arise only when the orthogonality is removed between a ground state and an excited state vibrational wave function. Since A-term is the leading term, it is generally the

dominant contribution to RR intensity. A-term enhancement varies directly with the strength of the electronic transition and inversely with its band width and it also depends on the magnitude of the product $\langle j|v\rangle\langle v|i\rangle$. These increase with the increase in displacement of the excited state potential well along the normal coordinate (origin shift). Hence, the extent of excited state distortion determines the degree of enhancement of a given mode. As for nontotally symmetric modes, there is no origin shift, the Franck-Condon product $\langle j|v\rangle\langle v|i\rangle$ is zero and thereby no enhancement of these modes via the FC term.

Non-totally symmetric modes, however, can gain intensity via the B-term because of Q-dependent vibrational integrals. The contributions of $\langle 1|Q|0\rangle\langle 0|0\rangle$ and $\langle 1|1\rangle\langle 1|Q|0\rangle$ terms are significant to the B-term for vibrational modes differing by one quantum. Therefore, the B-term becomes important in situations where a forbidden or weakly allowed transition gains intensity from vibronic mixing with a strongly allowed transition. The mixing modes are then prominent in the RR spectrum when excited at the weak transition. The enhancement depends on the magnitude of the mixing integral and on the proximity of the electronic states. A limiting case is the Jahn-Teller effect, in which the mixing states are degenerate.

2.7 The Polarizability Tensor and Depolarization Ratios

The polarizability tensor α_{ij} is given by:

$$\alpha_{ij} = \begin{bmatrix} \alpha_{xx} & \alpha_{xy} & \alpha_{xz} \\ \alpha_{yx} & \alpha_{yy} & \alpha_{yz} \\ \alpha_{zx} & \alpha_{zy} & \alpha_{zz} \end{bmatrix} \qquad \text{------2.7.1}$$

The elements α_{ij}'s generally depend on the frequency of the excitation.

The scattering geometry, for incident light propagating along Y-axis is shown in Figure 2.9. Scattered radiation is detected along the Z-axis. Then for this scattering geometry, the depolarization ratio for randomly oriented molecules in fluid state in 90^{o} scattering geometry is defined as follows:

$$\rho_1(\theta=90^{o}) = I_{\perp} / I_{\parallel} \qquad \text{------2.7.2}$$

The subscript on ρ_1 indicates linearly polarized incident radiation. In terms of polarizability components,

$$\rho_1 = \frac{3\gamma_s^2 + 5\gamma_a^2}{45(\bar{\alpha})^2 + 4\gamma_s^2} \qquad \text{------2.7.3}$$

Where

$$45(\bar{\alpha})^2 = 5(\alpha_{xx} + \alpha_{xy} + \alpha_{xz})^2$$

$$\gamma_s^2 = \frac{1}{2}[(\alpha_{xx} - \alpha_{yy})^2 + (\alpha_{xx} - \alpha_{zz})^2 + (\alpha_{yy} - \alpha_{zz})^2]$$

$$+ \frac{3}{4}[(\alpha_{xy} + \alpha_{yx})^2 + (\alpha_{xz} + \alpha_{zx})^2 + (\alpha_{yz} + \alpha_{zy})^2]$$

------2.7.4

and,

$$\gamma_a^2 = \frac{3}{4}[(\alpha_{xy}-\alpha_{yx})^2 + (\alpha_{xz}-\alpha_{zx})^2 + (\alpha_{yz}-\alpha_{zy})^2]$$

------2.7.5

$\bar{\alpha}$, γ_s , γ_a represent the isotropic, symmetric anisotropic (quadrupolar) and antisymmetric anisotropic (magnetic dipolar) tensor invariants respectively.

For normal Raman effect, the tensor is symmetric and $\alpha_{ij} = \alpha_{ji}$. Hence $\gamma_a^2 = 0$ and ρ_l has its well known form for non-resonant Raman scattering given by

$$\rho_l = \frac{3\gamma_s^2}{45(\bar{\alpha})^2 + 4\gamma_s^2}$$ ------2.7.6

and reduces equation 2.7.4 to

$$\gamma_s^2 = \frac{1}{2}[(\alpha_{xx}-\alpha_{yy})^2 + (\alpha_{xx}-\alpha_{zz})^2 + (\alpha_{yy}-\alpha_{zz})^2]$$

$$+3[\alpha_{xy}^2 + \alpha_{xz}^2 + \alpha_{yz}^2]$$ -----2.7.7

For Raman scattering from non-totally symmetric modes.

$(\bar{\alpha})^2 = 0$ and $\rho_l = \frac{3}{4} + \frac{5}{4} \cdot \frac{\gamma_a^2}{\gamma_s^2}$

If $\gamma_a^2 = 0$, we have normal polarization with $\rho_l = 3/4$. Under RR scattering, the tensor need not remain symmetric i.e., $\alpha_{i,j} \neq \alpha_{j,i}$

If $\gamma_a^2 \neq 0$, then $\rho_l > 3/4$, provided $\gamma_s^2 \neq 0$; if $\gamma_s^2 = 0$

then $\rho_1 = \infty$ (inverse polarization).

For totally symmetric modes, where $(\bar{\alpha})^2 \neq 0$; and $\gamma_a^2 = 0$;

$$\rho_1 = \frac{3}{\left\{45\frac{(\bar{\alpha})^2}{\gamma_s^2} + 4\right\}}$$ and so $0 < \rho_1 < 3/4$ according as $\infty > \frac{45(\bar{\alpha})^2}{\gamma_s^2} > 0$

Group thereotical considerations can provide information about the invariants which are non-zero for particular vibrational modes in molecules of a given symmetry, and thus about the symmetry properties of the general polarizability tensor. The symmetries of the scattering tensor in different molecular point groups have been given by *McClain*.[19] This helps in evaluating the contributions from any of the invariants for a Raman process transforming under any irreducible representations of a point group pertinent to the molecule.

Experimentally the evaluation of all three tensor invariants requires three independent intensity measurements. The measurement of the total scattering at 90^o, ($I_\perp + I_{||}$), and the depolarization ratio ρ_1, may be supplemented by a measurement involving circularly polarized light. It is usual to measure the reversal coefficient I_{contra}/I_{co}, which is the ratio of the intensity of contra-rotating to that of co-rotating light for the back scattering of pure circularly polarized incident radiation. This is however, not sufficient to determine the point group symmetry of the molecule having modes which show a dispersion of

ρ_l. In addition to the measurement at a particular exciting frequency, one requires measurements at various values of ν_o and if $I_\perp$ and $I_\parallel$ are measured at various exciting frequencies.

2.8 Antisymmetric Tensor Contributions

The first experimental evidence of inverse polarization in resonance Raman studies of porphyrins[20a] and heme proteins[20b] was provided by *Verma and Bernstein*[20a] and *Spiro and Strekas*[20b] respectively. The modes which are responsible for this value of ρ_l are of A_{2g} symmetry. Since A_{2g} modes are associated with antisymmetric scattering tensor i.e., $\alpha_{i,j} = -\alpha_{j,i}$ and therefore are inactive in normal Raman scattering. *Warshel*[21] has explicitly demonstrated the scattering tensor of A_{2g} mode in D_{4h} symmetry, and has shown that such a situation can exist in the presence of a doubly degenerate electronic level and a rotational type vibrational mode which leads to equal rotation of the two orthogonal transition moments. The A_{2g} vibrations have rotational symmetry about the four fold axis. From the form of porphyrin molecular orbitals, as shown in Figure 2.9A and the nature of A_{2g} mode (Figure 2.9B), it is clear that the two electronic transitions and their intensity will be accordingly enhanced. Inverse polarization may be observed with proper exciting line, i.e., the plane of polarization of the incident light is rotated through 90^o on scattering and $\rho_l = \infty$. Some of the Raman bands in different systems have been observed for which $\rho_l \neq \infty$ but $\rho_l > 3/4$ are called anomalously polarized bands. There are two

possible explanations for anomalous polarization. The effective symmetry of the molecule may be less than D_{4h} in which case the A_{2g} mode may acquire symmetric and antisymmetric contributions from scattering tensors. Alternatively, there may be accidental degeneracies between A_{2g} modes and the modes of other symmetries, which are polarized (A_{1g}) or depolarized (B_{1g} or B_{2g}), giving an overall depolarization ratio which is anomalous.

References

1a. Stern, A.; Wenderlein, H. *Z. Physik. Chem.* A177, 165, 1936.

b. Stern, A.; Molvig, H. *Z. Physik. Chem.* A178, 161, 1937.

c. Stern, A.; Pruckner, F. *Z. Physik. Chem.* A180, 321, 1937.

2a. Falk, J. E. in *"Porphyrins and Metalloporphyrins"*, Smith, K.M. Ed.; Elsevier, Amsterdam, 1964.

b. Platt, J.R. in *"Radiation Biology"*, Hollaender, A. Ed.; McGraw-Hill, New York, Vol. III, Ch. 2, 1956.

3. Simpson, W.T. *J. Chem. Phys.* 17, 1218, 1949.

4. Gouterman, M. in *"Excited States of Matter"*, Shoppee, C.W. Ed.; Graduate Studies Tech. Univ., 2, p. 1, 1973.

5. Longuet-Higgins, H.C.; Rector, C.W.; Platt, J.R. *J. Chem. Phys.* 18, 1174, 1950.

6. Gouterman, M. *J. Mol. Spectrosc.* 6, 138, 1961.

7. Eaton, W.E.; Hochstrasser, R.M. *J. Chem. Phys.* 46, 2533, 1967.

8. Perrin, M.H.; Gouterman, M.; Perrin, C.L. *J. Chem. Phys.* 50, 4137, 1969.

9a. Sulovev, K.N. *Opt. Spectrsc.* 10, 389, 1961.

b. Eaton, W.E.; Hochstrasser, R.M. *J. Chem. Phys.* 49, 985,1968.

10a. Spiro, T.G.; Strekas, T.C. *Proc. Natl. Acad. Sci.* U.S.A. 69, 2622, 1972.

b. Friedman, J.M.; Hochstrasser, R.M. *Chem. Phys.* 1, 457, 1973.

10c. Friedman, J.M.; Hochstrasser, R.M. *J. Am. Chem. Soc.* 98, 4043, 1976.

11. Herzberg, G. in *"Infrared and Raman spectra of Polyatomic Molecules"*, Van Nostrond Reinhold Co: N.Y., Vol. 2, 1945.

12. Friedman, J.M.; Hochstrasser, R.M. *Chem. Phys.* 6, 155, 1974.

13. Jacon, M. in *"Advances in Raman Spectroscopy"* Mathein, J.P., Ed., Vol. I, 1973.

14. Kramers, H.A.; Heisenberg, W. *Z. Physik* 31, 681, 1925.

15a. Dirac, P.A.M. *Proc. Roy. Soc.* London, 114, 710, 1927.

b. Albrecht, A.C. *J. Chem. Phys.* 34, 1476, 1961.

c. Krushinskie, L.L.; Shorygin, P.P. *Opt. Spectrosc.* USSR, 19, 312, 1965.

d. Savin, F.A. *Opt. Spectrosc.* USSR, 19, 308, 1965.

e. Verlan, E.M. *Opt. Spectrosc.* 20, 341, 1966.

f. Verlan, E.M. *Opt. Spectrosc.* 20, 447, 1966.

g. Verma, A.L. *Indian J. Phys.* 54B, 54, 1980.

16. Tang, J.; Albrecht, A.C. in *"Raman Spectroscopy"*, Szymanski, H.A., Ed., Plenum, N.Y., Vol. 2, 33, 1970.

17. Kramers, H.A.; Heisenberg, W. *Z. Physik*, 31, 681, 1925.

18. Herzberg, G. in *"Electronic Spectra of Polyatomic Molecules"* Van Nostrand Reinhold Co., N.Y., 1960.

19. McClain, W.M. *J. Chem. Phys.* 55, 2789, 1971.

20a. Verma, A.L.; Bernstein, H.J. *J. Raman Spectrosc.* 2, 163, 1974.

20b. Spiro, T.G.; Strekas, T.C. *Proc. Natl. Acad. Sci.*, U.S.A., 69, 2622, 1972.

21. Warshel, A. *Chem. Phys. Lett.* 43, 273, 1976.

TABLE 2.1

Hamiltonians for y Polarized State

	$(a_{2u}e_{gy})$	$(a_{1u}e_{gx})$	Dipole strength (q^2)
(a)			
$(a_{2u}e_{gy})$	$A'_{1g} + A_{1g}$	A''_{1g}	R_2^2
$(a_{1u}e_{gx})$	A''_{1g}	$A'_{1g} - A_{1g}$	R_1^2
	B_y^o	Q_y^o	
(a')			
$B_y^o \equiv (2)^{-1/2}[(a_{2u}e_{gy})+(a_{1u}e_{gx})]$	$A'_{1g} + A''_{1g}$	A_{1g}	$R^2 \equiv 1/2(R_1+R_2)^2$
$Q_y^o \equiv (2)^{-1/2}[(a_{2u}e_{gy})-(a_{1u}e_{gx})]$	A_{1g}	$A'_{1g} - A''_{1g}$	$r^2 \equiv 1/2(R_2-R_1)^2$
	B_y	Q_y	
(b) $[\tan 2\nu \equiv A_{1g}/A''_{1g}]$			
$B_y \equiv \cos\nu B_y^o + \sin\nu Q_y^o$	$A'_{1g} + A''_{1g}/\cos 2\nu$	0	$1/2(1+\cos 2\nu)R^2 + R r \sin 2\nu + 1/2(1-\cos 2\nu)r^2$
$Q_y \equiv -\sin\nu B_y^o + \cos\nu Q_y^o$	0	$A'_{1g} - A''_{1g}/\cos 2\nu$	$1/2(1-\cos 2\nu)R^2 - R r \sin 2\nu + 1/2(1+\cos 2\nu)r^2$
(c) $[2\nu = A_{1g}/A''_{1g} \ll 1]$			
$B_y = B_y^o + \nu Q_y^o$	$A'_{1g} + A''_{1g}(1+2\nu^2)$	0	$R^2 - \nu^2 R^2 + 2\nu R r$
$Q_y = Q_y^o - \nu B_y^o$	0	$A'_{1g} - A''_{1g}(1+2\nu^2)$	$(\nu R - r)^2$

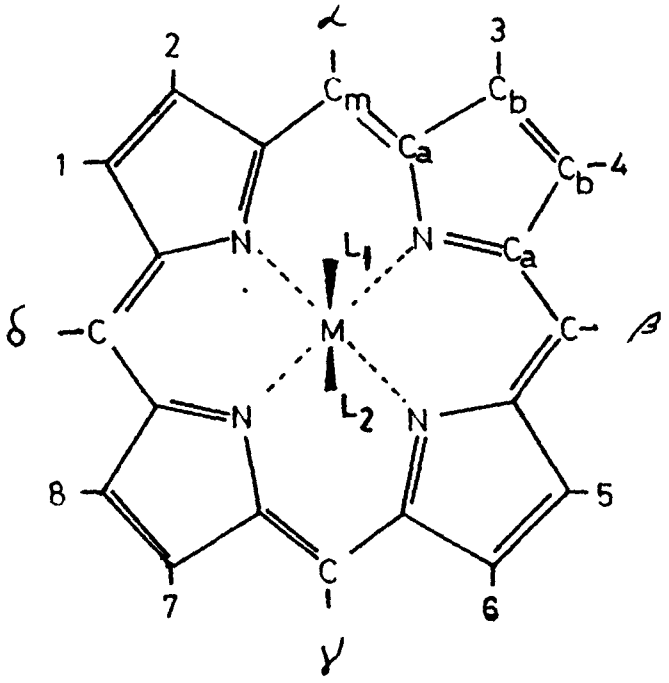

	1	2	3	4	5	6	7	8	α	β	γ	δ
Protoporphyrin-IX dimethylester	Me	V	Me	V	Me	Es	Es	Me	H	H	H	H
Hematoporphyrin-IX	Me	H	Me	H	Me	P	P	Me	H	H	H	H
Mesoporphyrin-IX	Me	Et	Me	Et	Me	P	P	Me	H	H	H	H
Octaethylporphyrin	Et	Et	Et	Et	Et	Et	Et	Et	H	H	H	H
Tetraphenylporphine	H	H	H	H	H	H	H	H	Ph	Ph	Ph	Ph

Me $-CH_3$, Et $-CH_2CH_3$, V $-CH=CH_2$, P $-C_2H_4COOH$, Es $-C_2H_4COOCH_3$, Ph $-C_6H_5$, L_1, L_2 are the axial coordination sites.

Fig. 2.1 Structural diagram of the porphyrin ring with different substituents at the macrocycle for several physiological-type porphyrins.

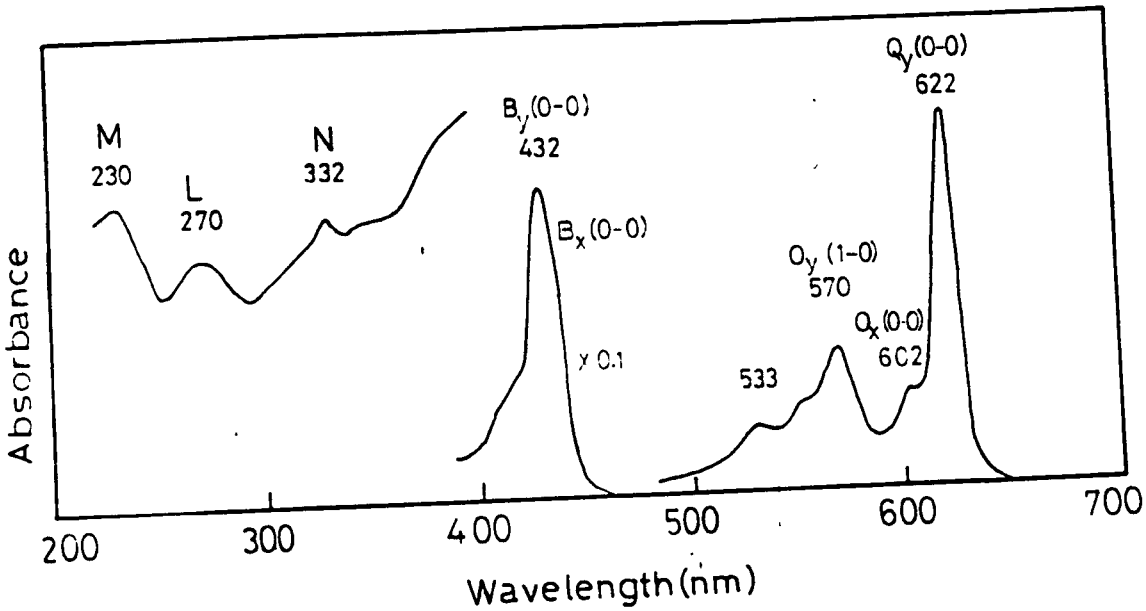

Fig. 2.2 Absorption spectrum of Protochlorophyll in ether.

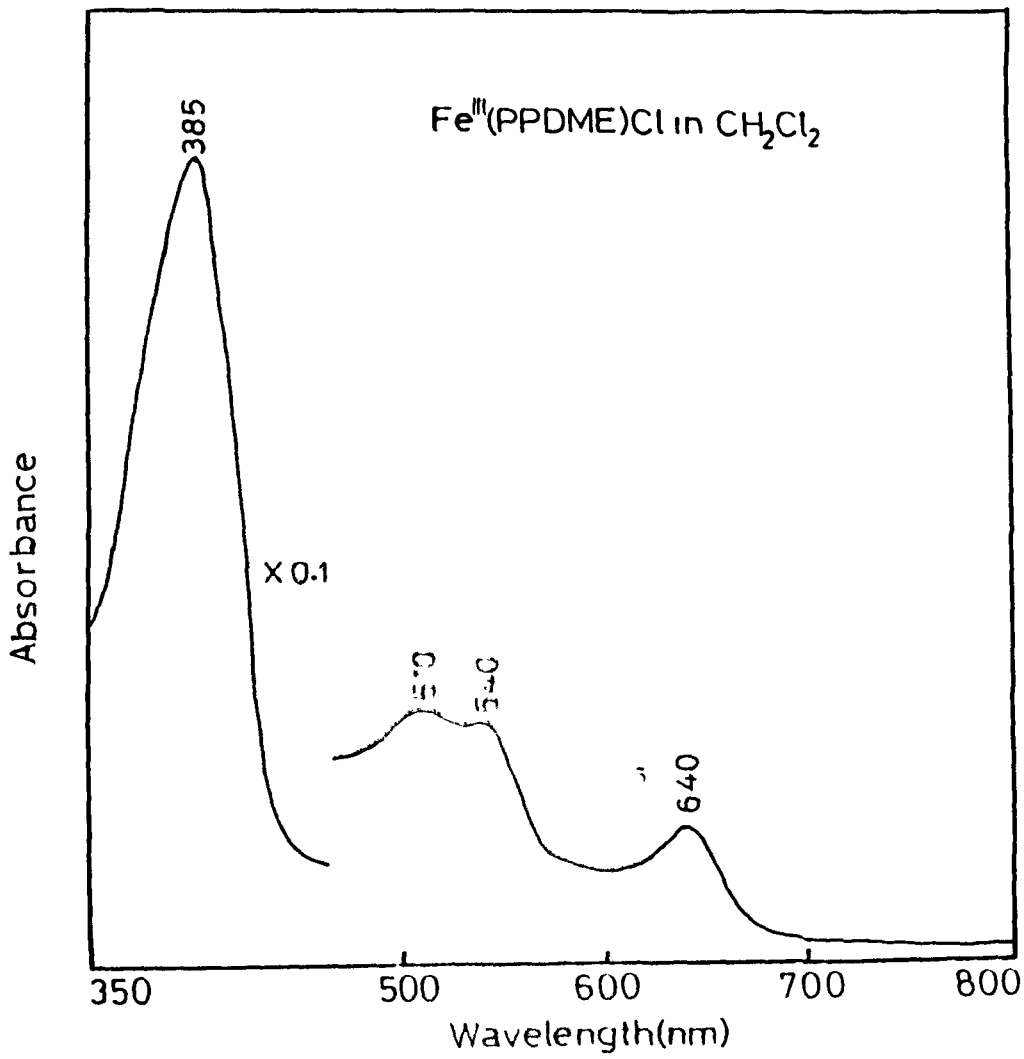

Fig. 2.3 Absorption spectrum of Iron(III)protoporphyrin-IX dimethylester chloride in CH_2Cl_2.

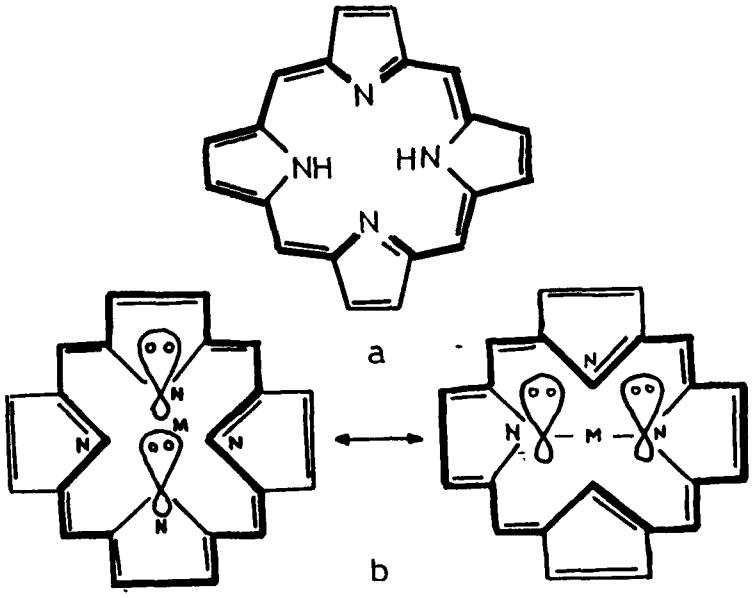

Fig. 2.4 (a) Resonance structure for free base porphyrin. The heavy bonds indicate the 18-membered cyclic polyene.
(b) Resonance structure for metalloporphyrin.

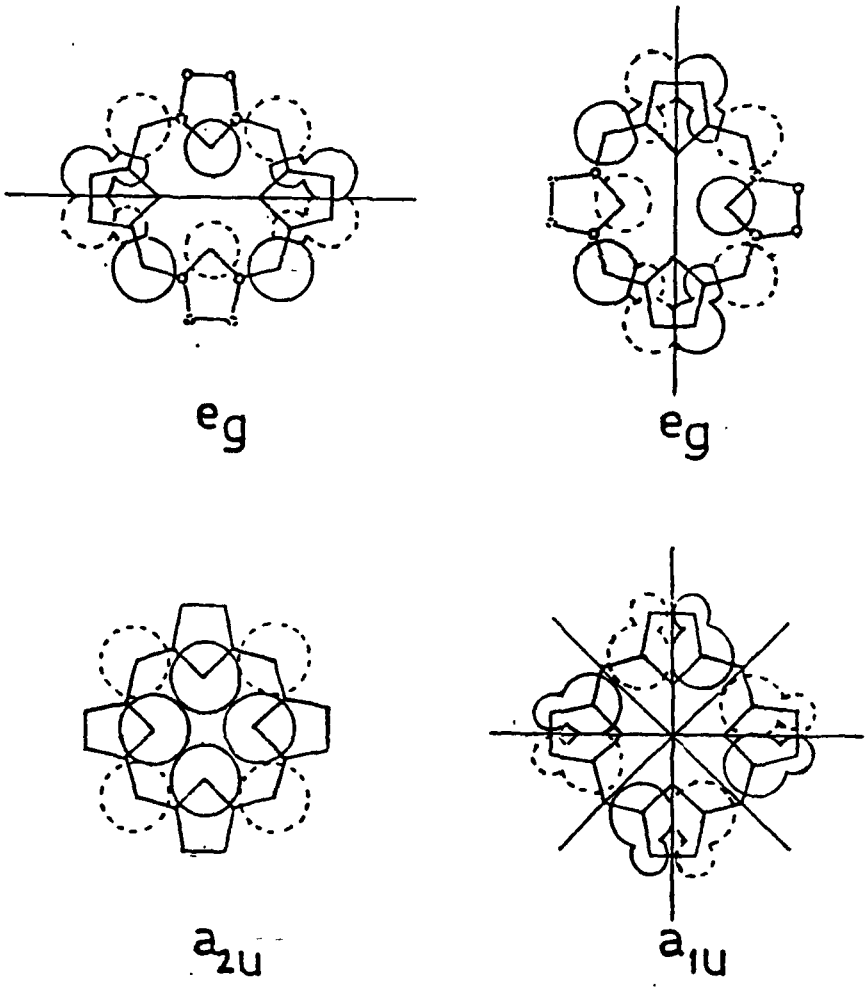

Fig. 2.5 Porphyrin top filled molecular orbitals e_g and lowest empty molecular orbitals a_{2u} and a_{1u}. The orbital coefficients are proportional to the size of the circles. Solid or dashed circles indicate sign of the orbitals. Lines indicate the symmetry nodes.

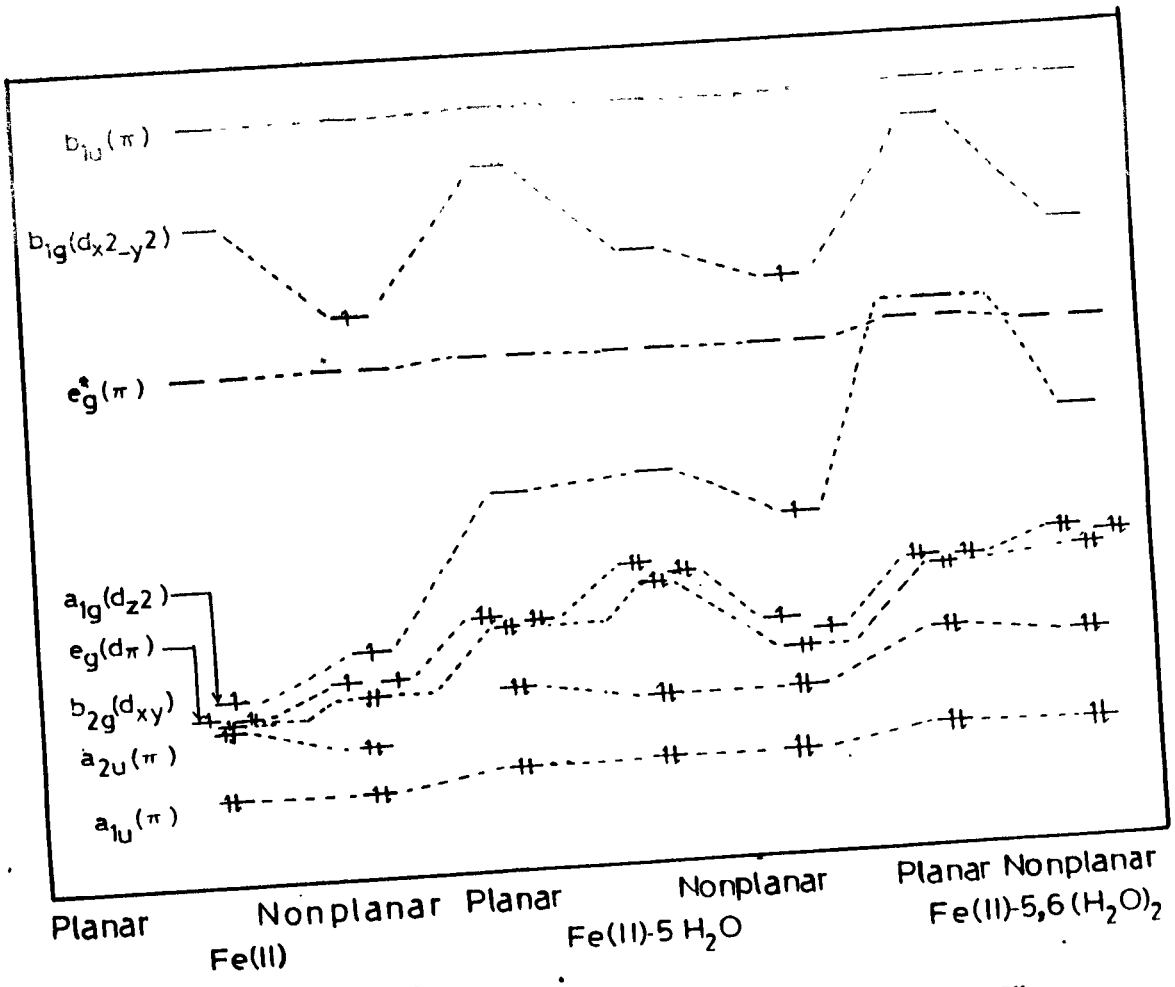

Fig. 2.6 Top-filled and lowest-empty orbital energies by EHH model for iron(II) porphyrin complexes with none, one or two waters as axial ligand(s).

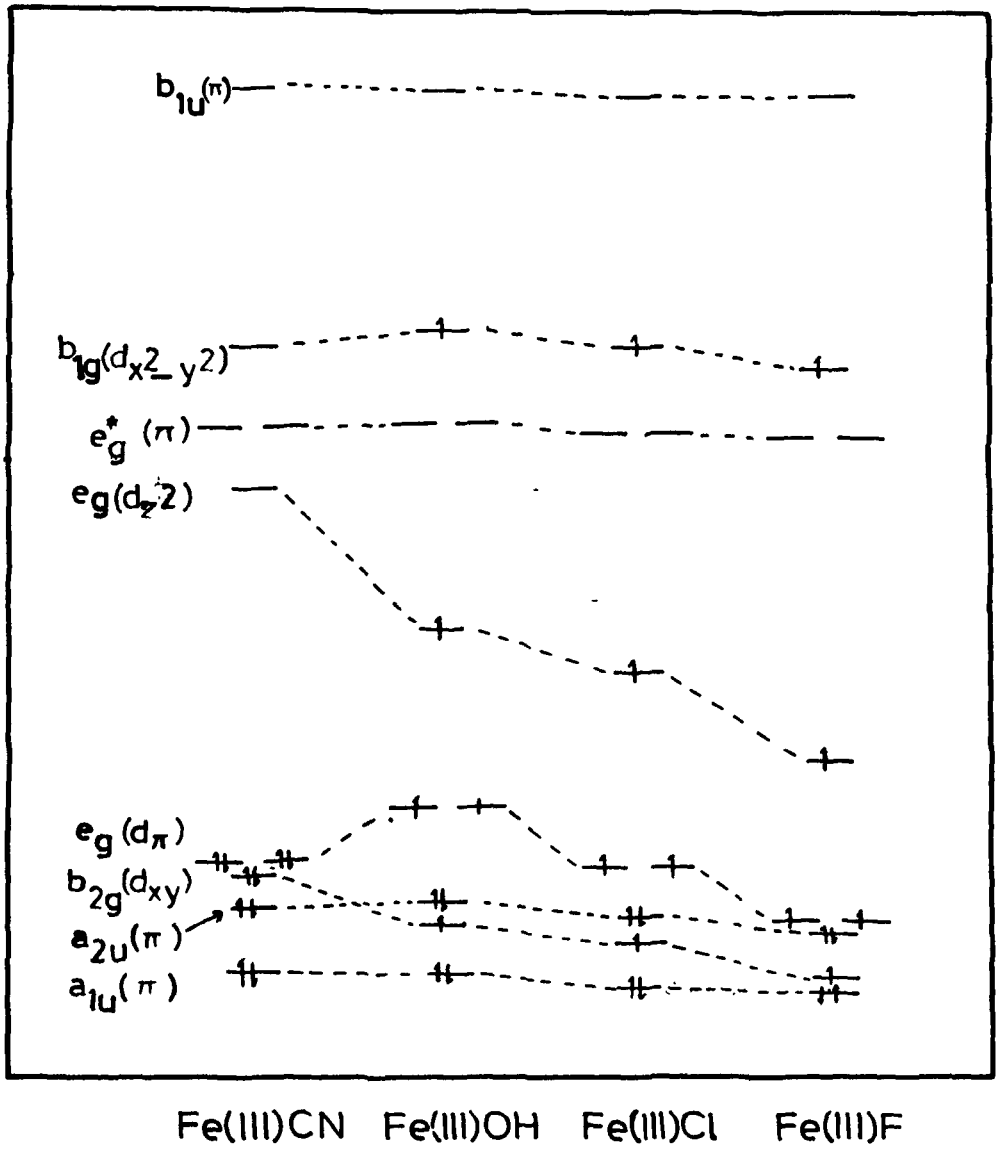

Fig. 2.7 Top-filled and lowest-empty orbital energies by IEH model for five coordinated iron(III) porphyrin complexes.

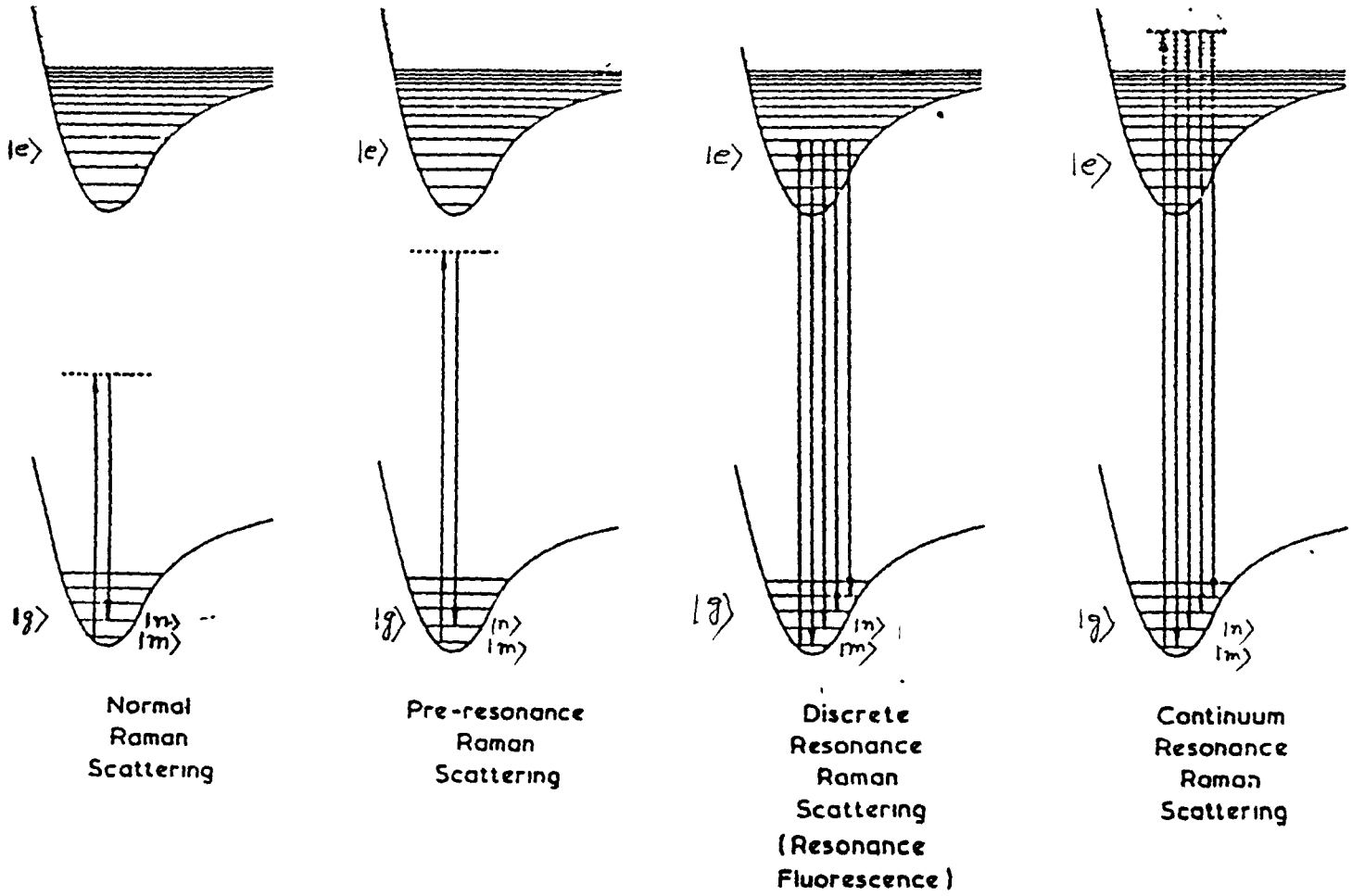

Fig. 2.8 Illustration of various light scattering processes.

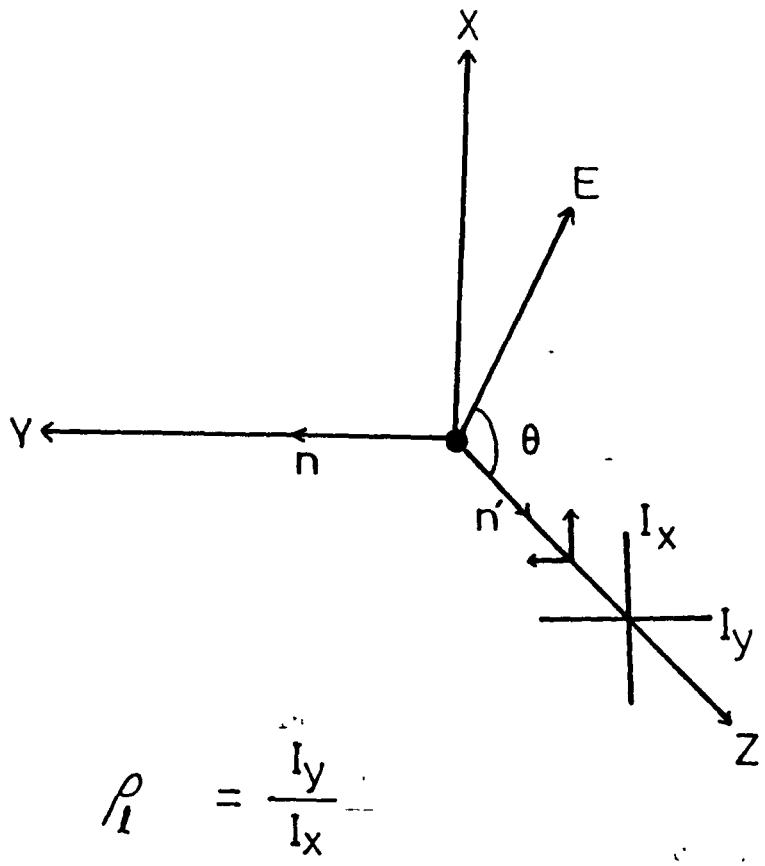

Fig. 2.9 Raman scattering geometry. Light propagating along the Y direction is characterized by an electric vector E lying in the XZ plane. Scattered radiation is detected along the Z direction. Conventional scattering experiment has $\theta = 90^{\circ}$.

EXPERIMENTAL DETAILS

This chapter presents a brief discussion of the methods of sample preparation, the experimental techniques and the instruments used to obtain the vibrational and electronic absorption spectra.

3.1 Preparation of Samples

3.1.1 Iron Protoporphyrin-IX Dimethyl Ester Chloride

The synthesis of iron(III) protoporphyrin-IX dimethyl-ester chloride, Fe^{III}(PPDME)Cl, was carried out by the following procedure.[1] Free base protoporphyrin-IX dimethyl ester purchased from Sigma Chemicals Co., U.S.A., was added (500 mg) to a refluxing (50 ml) dimethylformamide (Analytic Reagent Grade, BDH). Formation of a homogeneous solution was achieved after about 5 minutes of refluxing. A large excess, (5 g) ferrous chloride ($FeCl_2$) was added to this solution in order to complete metallation of all the free base porphyrin used. The refluxing was continued for another one and half hours. The completion of the reaction was checked by recording the electronic absorption spectra, where the absorption bands corresponding to the free-base porphyrin disappeared. The reaction vessel was then allowed to cool down to room temperature by keeping it in a cold water bath. Chloroform was added to the reaction mixture and the resulting solution was washed with triply distilled water in a separating funnel to remove unreacted $FeCl_2$. The chloroform layer which contained the Fe^{III}(PPDME)Cl was then dried over anhydrous Sodium Sulfite. The chloroform solution was then

filtered to obtain crude Fe^{III}(PPDME)Cl. This crude iron complex was then further purified by column chromatographic method.

3.1.2 Iron Octaethyl Porphyrin Iodide

The method of synthesis for iron(III) octaethyl porphyrin iodide was almost identical to that of iron(III) protoporphyrin-IX dimethyl ester chloride, as described in the section 3.1.1, except that, in place of ferrous chloride, a mixture of ferrous acetate and sodium iodide was added to the refluxing dimethylformamide solution of free base octaethylporphyrin, purchased from Sigma Chemical Co. U.S.A. Other steps for purification were identical to that used in the case of Fe^{III}(PPDME)Cl.

3.1.3 Degassing of Solutions

By this process, free and dissolved air contained in the solution is removed by freeze and thaw cycles. The solution for Raman studies is then transfered to a evacuating cell. This cell is then dipped into liquid nitrogen container to freeze the solution, which is then connected to a high vacuum pump having fore pressure of $\sim 10^{-4}$ Torr through a stop cock. After sufficient evacuation, the cell is disconnected from the pump and is warmed up to room temperature. In this solution, again nitrogen gas is purged for few minutes and the above cycle is repeated. The entire cycle is repeated atleast thrice to ensure

proper degassing and removal of dissolved oxygen from the solution. The degassed solution is then transfered to Raman cell (connected with vacuum tight joint) and the unit is mounted properly with a stand for laser excitation and hence Raman spectral measurements under anaerobic conditions.

3.2 Liconix Model 4240 Helium-Cadmium Laser

This laser consists of two units: a laser head and a power supply.

The optical section of laser head is formed by two mirrors mounted on adjustable plates and held at a precise separation by three invar rods that run along the length of the laser tube made of pyrex glass. The mirrors are adjusted to reflect the laser light down the bore of the pyrex glass laser tube and to allow the emission of a precise amount of light as an out put beam. Functionaly the helium-cadmium laser is a helium filled plasma discharge tube terminated in vertically polarized brewster windows of the resonating cavity and coherent laser emission occurs by way of a mechanism similar to that of the helium neon laser. This laser head is a air cooled system and requires no external cooling. The out put power at 441.6 nm is about 40 mW.

The power supply Model 4240 PS utilizes AC power from the primary source and converts it into different DC levels for maintaining constant out put power by controlling gas pressure (both helium pressure and cadmium vapor pressure) and associated

current regulations in different electronic circuits.

3.3 Spectra-Physics Model 165-09 Argon Ion Laser

The MOdel 165 Argon ion laser is a CW laser and consists of the laser head and Model 265 Exciter.

The laser head consists of a beryllium oxide (BeO) plasma tube terminated at each end by fused-silica Brewster's angle windows, a solenoid for providing necessary magnetic field and an optical resonator. The plasma tube is mounted in an optical cavity resonator formed by a spherical reflector at the out put and a prism and flat mirror assembly at the high reflector end. The whole assembly of the resonator is held solidly against quartz rods with springs to minimize microphonic frequency shifts. The plasma tube is supported on a kinematically adjustable mount and is adjusted in such a way that the plasma tube is exactly centered. Wavelength selections are achieved by rotating a thumbwheel control on the rear side of the laser head.

The Spectra-Physics Model 265 Exciter is fully equipped with the necessary electric and electronic circuits to achieve regulated ion discharge current in the plasma tube and then by control the out put power from the laser by simultaneously regulating the solenoid current. The 265 Exciter is feeded with stabilized three phase 203 V (Phase to phase) power line. This unit requires cooling of the transistor pass bank in the exciter, the solenoid and BeO plasma tube which is achieved by circulating distilled and deionized water at $15^{o}C$ at 40 PSI from water

chiller plant from Neslab Model HX 500.

3.4 Measurement of Raman Spectra

Raman spectra of different iron porphyrins were recorded in a 90^{o} scattering geometry with a SPEX Ramalog 1403 triple monochromator equipped with a thermoelectrically cooled RCA 31034 photomultiplier and photon counting arrangement. The spectrometer control and data processing were achieved with the help of a microprocessor based SPEX "Datamate". Excitation lines were obtained from Liconix Model 4240 HeCd Laser and Spectra-Physics Model 165-09 Argon ion laser. AIR products close-cycle Helium cryocooler, Model Displex CSA 202E, was used to achieve low temperatures upto 10K, for measurement of low temperature Raman spectra. We shall give some details of various instruments used in this study.

3.5 SPEX Model Ramalog 1403 Laser Raman Spectrophotometer

The Raman spectra were measured with the help of a SPEX Model Ramalog 1403 double monochromator alongwith a third monochromator coupled with a thermoelectrically cooled photomultiplier tube, Model RCA 31034. The relevant optical diagram is shown in Figure 3.1

This spectrophotometer (SPEX 1403 double monochromator) is a f/7.8, instrument with spectral coverage from 31000 cm^{-1} to 11000 cm^{-1} with an accuracy of ± 1 cm^{-1} in the 10000 cm^{-1} range. The spectral repeatability is ± 0.2 cm^{-1} and the resolution is

0.15 cm^{-1} at 5791 A^{o} (Hg line, FWHM). The gratings used in this instrument are holographic type having rulings with 1800 grooves/mm and blazed at 5000 A^{o}. The gratings are mounted on a modified Czerny-Turner mount using the following fundamental grating equation

$$m\lambda = d(\sin\alpha + \sin\beta) \qquad \text{------ 3.5.1}$$

Where m = Spectral order

λ = Wavelength

d = grating spacing

α = angle of incidence

β = angle of diffraction

For simplicity

Let $\alpha = \theta + \phi$

and $\beta = \theta - \phi$

Where θ is the angle of grating rotation measured from zero as shown in Figure 3.2, and is the constant angle, dependent on the instrument's design. This equation 3.5.1 can be rewritten as

$$m\lambda = 2d\sin\theta\cos\phi \qquad \text{------- 3.5.2}$$

In the SPEX Model 1403 Ramalog spectrophotometer, the Raman peaks are measured in terms of frequency shift in cm^{-1} on a linear X-axis, by utilizing a cosecant drive for grating rotation with a $\phi = 10^{o}$ and thus $\cos\phi = 0.984$ (manufacturer's supplied value).

For recording the Raman spectra, the laser beam is passed through the SPEX Model 1459 UVISIR, illumination after being filtered from "Lasermate" SPEX Model 1460, a small unit

consists of a grating having 1200 lines/mm blazed at 5000 A^{o} and a mirror assembly to isolate the spurious plasma lines. The filtered laser beam from the lasermate is then deflected upward (90^{o}) by a mirror and focused on to the sample to a spot of diameter 10 m by the fused silica condensing lens. Scattered radiations from the sample then passes through a polarization analyzer (optional). Use of polarization analyser provides direct information about the state of polarization of the observed Raman bands. The scattered radiation is then collected by an elliptical mirror (f/1.4) and focused onto the entrance slit (S_3), (Figure 3.1) of spectrometer after deflecting from the mirror (M_7) and passing through a polarization scrambler. The polarization scrambler converts plane-polarized scattered radiation to circularly polarized radiation before it reaches the spectrometer and thus cancels variations in spectrometer response that result from polarization-dependent efficiencies. The polychromatic scattered radiation focused onto the entrance slit gets dispersed by the 1800 lines/mm holographic gratings(G_2 and G_3). Thus finally a nearly monochromatic light signal of frequency (cm^{-1}) selected by spectrometer control reaches the exit slit (S_7) of the double monochromator. This exit slit is coupled to the third monochromator Model SPEX 1442.

3.6 The Third Monochromator Model SPEX 1442

This device is used for reducing stray light in Raman scattering where the weak spectral features are not clearly

resolved in the vicinity of the intense Rayleigh line. This device functions as a variable band pass, variable frequency filter. The third monochromator is a modified Czerny-Turner spectrograph attached to the exit slit of the double monochromator. The light entering the third monochromator is nearly monochromatic at the particular tuned frequency of the double monochromator plus some stray light of the excitation frequency. This light is further dispersed and finally made to fall onto the exit slit of the third monochromator to which the photomultiplier tube is connected. This final dispersion and adjustment of the exit slit is such that only the desired components of the incoming monochromatic light pass between the slit blades of the exit slit of the third monochromator and the stray radiation at other frequencies are obstructed by the slit blades. The third monochromator can operate, in the fixed mirror mode, in the scanning grating mode or in the stationary grating mode. The fixed mirror mode essentially converts the system to a double monochromator and so maximizes the signal level. It is ideal for work at high resolution when the signal level is poor. The scanning grating mode is suggested for substances plagued by scattered light over the complete Raman spectrum. The stationary grating mode is especially valuable for identifying Raman lines close to the excitation frequency (Rayleigh line).

In all the Raman measurement, the third monochromator was used in the fixed mirror mode.

3.7 Spectrometer Control and Data Processing

The spectrometer control (frequency scanning) and data data processing were carried out through a 8-bit dedicated micro computer SPEX 'DATAMATE' with the help of the inbuilt software, it is possible to manipulate the spectral data by back ground subtraction, integration, addition, division, frequency range and intensity range expansion/reduction, differentiation etc., whenever necessary. The incoming spectral data as well as the manipulated data array could be stored in the 4K data point storage in any of the eight variable length files. The stored data could be plotted on a stripchart recorder or transfered to external peripherals, e.g., floppy discs or to a PC through the standard RS 232 port for further manipulation of data. The unavoidable wavelength dependent distortions to the spectral data from the spectrometer optics could be erased by applying the radiometric corrections from the inbuilt 1K EAROM. Using the programming option, the entire spectrometer control as well as data collection and manipulation could be completely automated. The data storing facility could be bypassed and real time spectra could be recorded in the stripchart recorder.

The raw data is obtained from the out put of the pre-amplifier (PC Dam). The anode of the photomultiplier tube is the input of the PC Dam. The preamplifier gain is 400. The high voltage (-1750 volts) required for operating the photomultiplier tube is also supplied by the Datamate with a stability of $\pm 0.002\%$ after half an hour warm up.

The photomultiplier tube Model RCA 31034 is used with the instrument, is a 2 diameter, head-on, 11-stage QUANTACON photomultiplier having a gallium arsenide chip as its photo cathode, an ultraviolet transmitting glass window and an in-line copper beryllium dynode structure. This tube is cooled to $-30^{o}C$ by a thermoelectric cooling device and has a almost linear absolute response in the 3000 A^{o} to 8500 A^{o} wavelength range and operated for current gain of 10^{6} with a maximum dark pulse summation of 12CPS (count per second).

3.8 Scanning of the Raman Spectra

There are a number of difficulties associated with recording the Raman spectra of coloured samples under resonance conditions. The most prominents include (a) the optimization of the concentration of the scattering species in the solution to minimize reabsorption of the scattered light by the sample and at the same time allowing the scattering to be maximum, (b) the local heating of the sample due to absorption of exciting line which may give rise to thermal lens effect and also lead to thermal decomposition of the sample , (c) the strong background due to fluorescence from impurities in the compound or in the solvents or intrinsic fluorescence from the sample itself.

The first one can be taken care by using samples of different concentrations until a good quality spectrum is obtained. To avoid local heating effect *Kiefer and Bernstein*[2,3] had developed a technique which involve continuous rotation of

the sample with respect to the laser beam. In this case, as the sample rotates continuously, the small portion of the sample from which light scattering takes place due to laser irradiation remains in the laser beam only for a short period of time and a fresh sample replaces this due to continuous movement of solution, and thereby reducing the local heating and thermal decomposition. To reduce the fluorescence background, Raman spectra can be measured in the solid form in KBr pellet. However, to obtain vibrational informations from solution, it always better to get rid of impurities from compounds and solvents that are in use by usual purification methods.

To record the Raman spectrum of liquid solution, 2-3 ml solution of respective porphyrin at an appropriate concentration is taken in a cylindrical cell and positioned in a proper mount. The laser beam at a selected wavelength is then made to strike the bottom edge of the cell. In this way, the self absorption of the scattered light is minimized. The spectra were routinely calibrated with known CCl_4 lines in the lower region (100-500 cm^{-1}) and with Indene in the higher frequency region (1300-1675 cm^{-1}) and some times with known Raman lines of solvents that are being used. Other spectral parameters such as laser power, integrating time, wavenumber increment, slit width etc. are adjusted time to time in order to optimize signal to noise ratio. For weak Raman signals, 3-4 spectra were averaged with the help of Datamate.

3.9 Measurement of Raman Spectra at Low Temperatures

The Raman spectra of samples at low temperatures were obtained with the help of an AIR products Helium cryocooler (Model Displex CSA 202E). This unit can cool the sample upto 10K and the temperature control was achieved by a controller Model APD-E upto a precision on $\pm$ 0.5K. Temperature sensing was achieved through a precalibrated Gold/Chromel thermo-couple.

3.9.1 AIR Products Model CSA 202E Closed-cycle Helium Cryocooler

The closed-cycle Helium cryocooler from AIR products, Displex Model CSA 202E mainly consists of a compressor unit module 202 and the expander module DE 202.

This is an air cooled compressor unit and operates with a stabilized power supply (single phase 230V), supplies helium gas at a pressure of 260 psig to the expander module. This compressed gas at high pressure is then allowed to expand in the expander assembly. In the process of expansion, the heat station temperature decreases because of Joule-Thompson effect, and the helium gas at 110 psig pressure returns to the compressor unit. Through repetition of this cycle for several times, cryogenic temperature of 10K is achieved at the heat station. The refrigeration capacity of this machine is 1.8 watts at 20K. The temperature at any other higher values can be obtained by using temperature controller Model APD-E unit.

The iron porphyrin solution was sealed in a quartz capillary and mounted with the help of a conductive glue on the sample holder made of copper which is mechanically connected to the second stage heat station. Vacuum shroud Model DMX 1E is connected at the vacuum shroud mount and the system is thoroughly evacuated ($\sim 10^{-5}$ Torr) by a Hind Hivac oil diffusion pump to obtain necessary thermal insulation. In addition to this, to obtain good thermal stability "radiation shield" is connected to the final stage heat station. DMX-1X interface extension is used to obtain Raman spectra.

To support the expander module, a home made stand equipped with necessary arrangements for measurements and adjustments along all the three axes was used.

3.10 Electronic Absorption Spectra

The electronic absorption spectra were recorded a Beckman UV visible Model 26 and Hitachi Model 330 spectrophotometers.

3.10.1 Beckman Model 26 U.V. VIS. Spectrophotometer

The Beckman Model 26 spectrophotometer is a double-beam, digital reading and recording instrument for measuring light levels at specified wavelengths. This Model is capable of measuring light from 190 to 900 nm range and employ a tungsten light source in the visible range of the spectrum (340 to 900 nm) and a deuterium source in the ultraviolet region of the spectrum

(190 to 360 nm). Light from either source is directed through a band pass or long pass filter to the single grating monochromator (1200 lines/mm, blazed at 250 nm). Light transmission through the sample/reference cell is detected by side-on photomultiplier tube. The current pulses generated by the sample and reference light levels to the photomultiplier tube are then amplified, displayed and recorded either in transmission or absorbance mode. In the absorbance mode, the amplified signal is analyzed by log converter, which transforms the light transmission current values into optical density values, and absorbance is equal to the logarithm (1/transmission). The resolution of this spectrophotometer is 0.2 nm and has wavelength repeatability better than 0.2 nm.

3.10.2 Hitachi Model 330 U.V. VIS. Spectrophotometer

The Model 330 is used for measuring transmittance and absorbance of liquid, solid and gaseous samples, in the visible, ultraviolet and near infrared regions.

Principle of Operation and Function

The light emitted from the light source passes through two grating monochromators for preparing a monochromatic beam and is then split into two beams. After passing through the sample compartment, the monochromatic beams are converged and converted into an electrical signal by detector, photomultiplier PbS cell. The electric signal provided from the detector is amplified by a

preamplifier and immediately converted into a digital variable by 16 bit A/D converter. At all the subsequent stages, the signal is processed by a CPU and the computational result is displayed directly on the CPU or output to the recorder.

The Model 330 adopts the differential feedback system in which reference or sample signal, whichever is at the higher level is kept constant by the CPU. The instrument is therefore capable of measuring negative absorbance. When the detector is irradiated with intense external light while sample compartment cover is open, a safety device is automatically actuated to protect the detector, by an inter locking arrangement at the door of sample compartment.

Specification

Wavelength accuracy $\pm$0.02 nm for UV-Vis. region.

Wavelength repeatability 0.1 nm for UV-Vis. region.

3.11 Corrections of Spectral Response to Calculate Quantum Yield of Photoreduced Iron Porphyrins

The degassed (10^{-4} Torr) solution of Fe^{III}(PPDME)(2-MeIm) in CH_2Cl_2 containing 1% MeOH was placed in a water bath at a temperature of 20°C and illuminated by a 150 W projector lamp for 5 minutes in the presence of short-cut filters Y-48, Y-46, Y-44, L-42, L-40 and L-38 using fresh sample for each measurement. The difference in the absorption spectrum designated by $S(\lambda_1 - \lambda_2)$ observed in the presence of filters with cut-off wavelengths

λ_1 and λ_2 represents the effect of illumination of light with wavelengths between λ_1 and λ_2. As e.g. Y-48 means it will allow light of wavelength $\lambda > 480$ nm to pass. The relative intensity of the illuminating projector light after the short-cut filter was measured by dispersing it with a 10 cm monochromator and detecting with a pin photodiode Model Hamamatsu S172202. After measuring the transmission spectra of individual filters, the difference spectra $D(\lambda_1 - \lambda_2)$, between the two spectra obtained in the presence of short-cut filters with cut-off wavelengths as λ_1 and λ_2 were calculated and corrected for the inherent wavelength dependences of the monochromator and detector sensitivities. The transmitted light intensity is converted to relative number of photons by the method of partial integration. Where the area of $D(\lambda_1 - \lambda_2)$ vs λ curve obtained by dividing the region between λ_1 and λ_2 into ten segments.

We have analyzed the action spectral data and the details are given in Chap. IV.

References

1a. Adler, A.D.; Longo, F.R.; Kampas, F.; Kim, J. *J. Inorg. Nucl. Chem.* 32, 2443, 1970.

b. Fuhrhof, J.H.; Smith, K.M. in "*Porphyrins and Metalloporphyrins*", Smith, K.M. Ed., Elsevier, Amsterdam, 803, 1975.

c. Ogoshi, H.; Sugimoto, H.; Yoshida, Z. *Bull. Chem. Soc. Jpn.* 54, 3414, 1981.

2. Kiefer, W.; Bernstein, H.J. *J. Appl. Spectrsc.* 25, 500, 1971.

3. Kiefer, W.; Bernstein, H.J. *J. Appl. Spectrsc.* 25, 609, 1971.

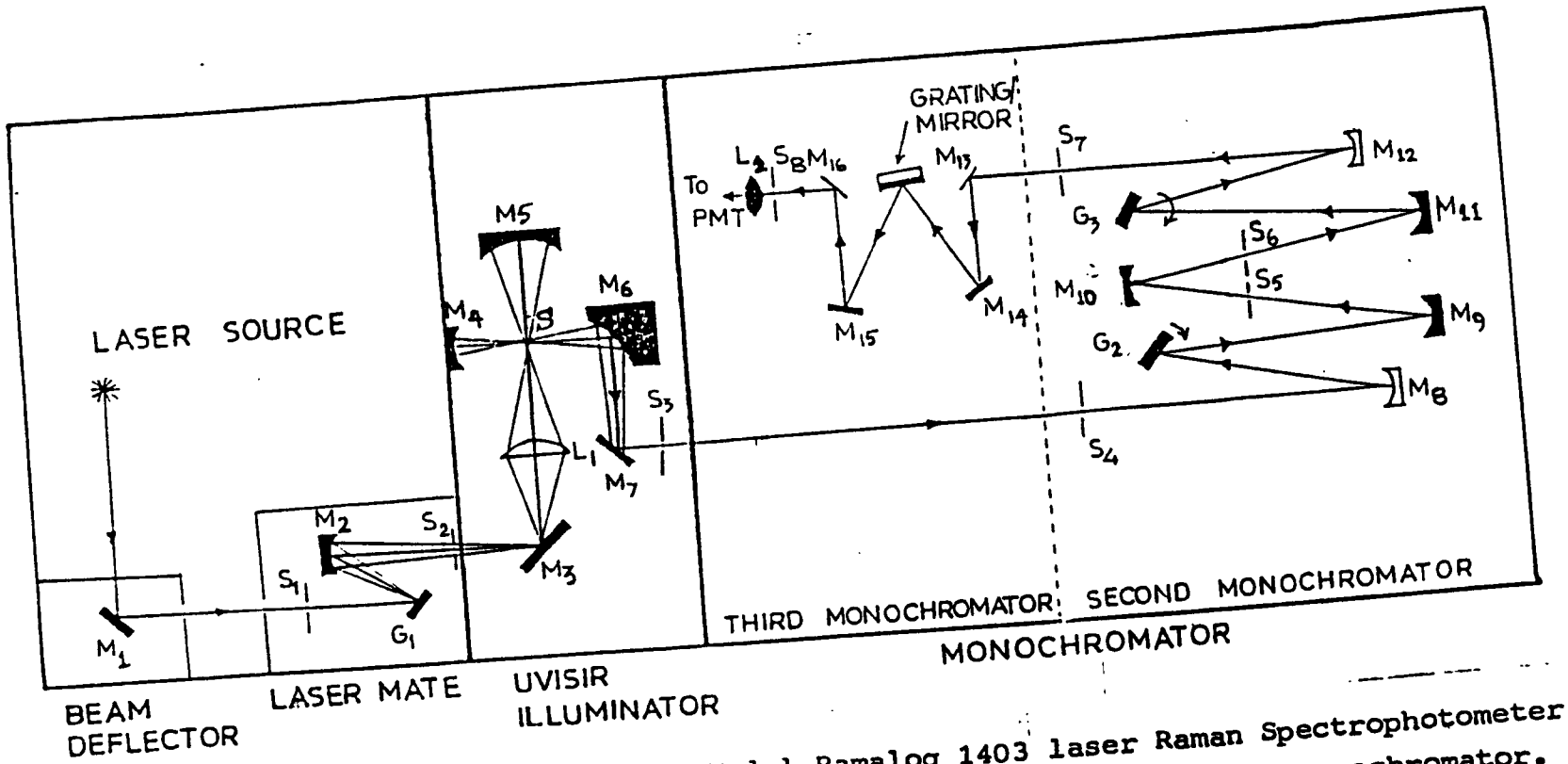

Fig. 3.1. Optical diagram of a SPEX Model Ramalog 1403 laser Raman Spectrophotometer, including the laser mate, UVISIR illuminator and the third monochromator. (M_1, M_3, M_7, M_{13}-M_{16} are the plane mirrors: M_2, M_4, M_5, M_8, M_9-M_{12} are concave mirrors, M_6 is elliptical mirror, S_1-S_8 are slits: L_1 is fused silica condenser lens: L_2- field lens: S - sample: G_1-G_3 are the gratings and PMT is the photomultiplier tube).

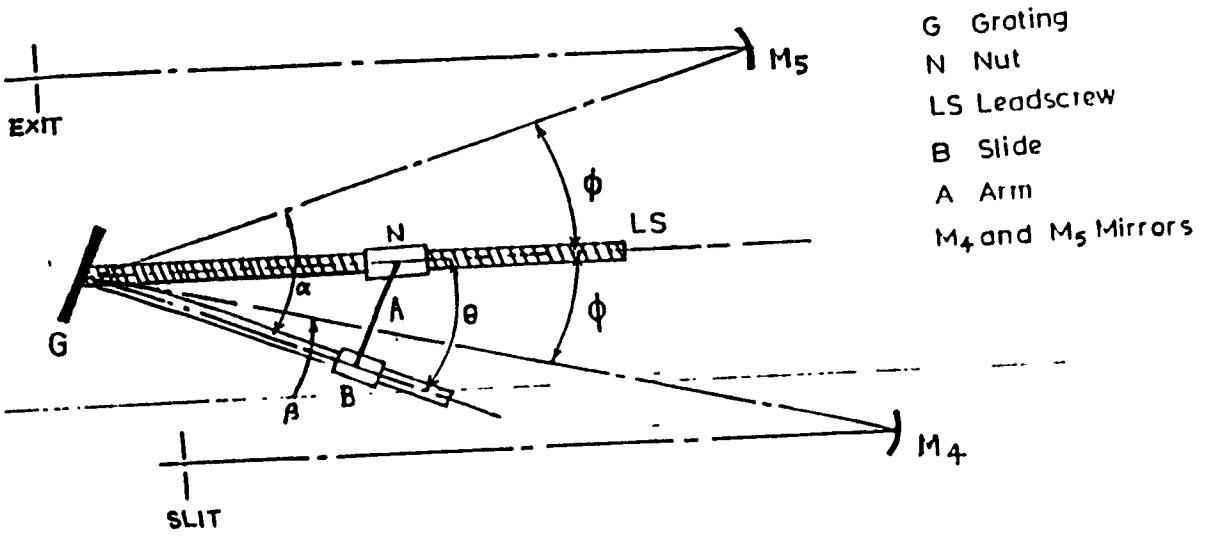

Fig.-3.2 Mechanical cosecant drive mechanism for the Czerny-Turner mount of gratings for the SPEX Model 1403 Ramalog. The nut N moves along lead screw LS while the slide B moves along a bar held at right angles to the grating G. The grating rotates as the arm A moves along the bar.

RESONANCE RAMAN STUDIES OF THE MECHANISM OF PHOTOREDUCTION OF IRON-PROTOPORPHYRIN-IX DIMETHYLESTER IN THE PRESENCE OF AXIAL LIGANDS*

ABSTRACT

Resonance Raman studies of Iron protoporphyrin-IX dimethylester chloride [Fe^{III}(PPDME)Cl] in the presence of biologically relevant axial ligands like 2-methylimidazole [2-MeIm] and 1,2-dimethylimidazole [1,2-Me_2Im] have revealed the occurrence of photo-reduction even under aerobic conditions by excitation near the Soret absorption band. A comparison of the vibrational modes sensitive to the oxidation, spin and coordination states of the photoreduced and chemically reduced forms of Fe^{III}(PPDME)Cl has confirmed that the reduction of the central iron atom in the high spin state takes place without any reduction of the porphyrin ring. No photoreduction is observed in pure CH_2Cl_2 solvent but a trace amount of alcohols and also some other polar solvents, which facilitate the separation of ion pairs, catalyse the process of photo-reduction. From the exponential dependence of the fraction of sample reduced upon rate of photo-reduction and illumination time, the rate constant

---

* Based on these studies, following papers have been published.
(a). Verma, A.L.; Saini, G.S.S.; Chaudhury, N.K. *Proc. Ind. Acad. Sci. (Chem. Sci.)* 102, 291, 1990
(b) Verma, A.L.; Chaudhury, N.K. (Submitted in *J. Raman Spectrosc.*)

for photo-reduction, k_R^{-1} = 10 min. is obtained and the action spectrum of photo-reduction shows a maximum coinciding with the Soret absorption band. The electron transfer from the axially ligated 2-MeIm to iron appears to be a primary step in photo-reduction. From the dependence of photo-reduction on the concentration of 2-MeIm, we have identified the ligand-free, intermediate spin Fe^{II}(PPDME) as the intermediate species formed during photo-reduction.

(c) Verma, A.L.; Chaudhury, N.K.; Saini, G.S.S.in *"Recent Trends in Raman Spectroscopy"* Banerjee, S.B.; Jha, S.S. Eds. World Scientific publishing Co. Singapore, p. 192 **1989**

(d) Verma, A.L.; Chaudhury, N.K.; Saini, G.S.S. *"XIIth International Conference on Raman Spectroscopy"* Durig, J.R.; Sullivan, J.F. Eds., John Wiley and Sons, New York, p.591 **1990**

4.1 INTRODUCTION

Many iron porphyrins take part in catalytic functions in oxygen carriers (hemoglobin, myoglobin), peroxidases, cytochrome-C etc. The study of electron transfer reactions between metals and hemeproteins has an extensive history[1-3] but the role of iron in the biological redox processes was recognized rather recently.[4] Under aerobic conditions the iron exists predominantly in the oxidized state. However, the essential biochemical functions require the reduced state of iron. Apart from usual chemical and other classical methods for obtaining reduced species, occurrence of photo-reduction has been noticed during resonance Raman (RR) studies of some heme-proteins[5] by irradiation at selected wavelengths. Many studies of photo-reduction of metalloporphyrins[6] have also been reported from the point of view of their photochemistry. However the first RR study of the photo-reduction of iron-porphyrin[7] was reported only very recently and preliminary attempts to understand the mechanism of photo-reduction, nature of electron donors etc. have been made. Recently, Ogura et al[15b] have explored the effect of primary alcohols on photoreduction of [Fe^{III}(OEP)(2-MeIm)]. They found that, at higher concentration ($\sim$3.5% v/v), alcohol binds to the sixth coordination position of [Fe^{III}(OEP)(2-MeIm)]. Non photoreducibility by laser irradiation within the charge transfer band from alcohol to Fe^{III} ion near 585 nm indicates that the charge transfer excited state does not participate in the

electron transfer process. Therefore the mechanism of photoreduction is still far from clear. We have therefore undertaken further studies in this area employing RR technique which holds great promise for elucidating the role of excited electronic states, axial ligation, core size, state of aggregation etc. on the mechanism of photoreduction of metalloporphyrins.

We report here a systematic RR study of biologically relevant iron protoporphyrin-IX dimethylester chloride in the presence of axial ligands like 2-methylimidazole [2-MeIm] and 1,2-dimethylimidazole [1,2-Me_2Im] using excitation wavelengths in different spectral regions. From a comparison of the position of different vibrational modes, ν_2, ν_3, ν_4, ν_{10} and ν_{11} with the chemically reduced [Fe^{II}(PPDME)(2-MeIm)] complex, we have found that a substantial fraction of this system undergoes photo-reduction even under aerobic conditions with excitation in the Soret region in the presence of primary alcohols as catalyst. The coincidence of maximum in the action spectrum with the Soret absorption band suggests that the photo-reduction process is driven by absorption in the Soret band region with a rate constant K_R^{-1} = 10 minutes. From concentration dependent studies of photo-reduction of Fe^{III}(PPDME) on (2-MeIm), it has been possible to disentangle the contribution of vinyl group modes on the RR spectra of Fe^{III}(PPDME)Cl.

4.2 EXPERIMENTAL PROCEDURE

Fe^{III}(PPDME)X (X=Cl,I) were synthesized in accordance with the procedure described elsewhere.[8] The 2-MeIm was recrystallized before use and all solvents were of spectroscopic grade and were used without further purification. Samples of Fe^{III}(PPDME)Cl with different concentrations of 2-MeIm were obtained by adding a known quantity of 0.1M solution of 2-MeIm in CH_2Cl_2 in a 1mM solution of Fe^{III}(PPDME)Cl in CH_2Cl_2 containing a trace amount ($\sim$0.1% v/v) of methanol (MeOH). To prepare chemically reduced [Fe^{II}(PPDME)(2-MeIm)], a few drops of an aqueous solution of sodium dithionite and 2-MeIm in phosphate buffer (0.1M, pH 6.9) were overlaid on the CH_2Cl_2 solution of Fe^{III}(PPDME)Cl under anaerobic conditions and the cell was vigorously shaken. All solutions were degassed with a fore pressure of 10^{-4} Torr using freeze and thaw cycles before Raman measurements unless otherwise stated.

Raman spectra were recorded with the help of a JEOL 400D and SPEX 1403 Ramalog spectrometers equipped with cooled RCA-31034A *photomultiplier and photon counting electronics. The* excitation lines were obtained from Krypton (Spectra-Physics, Model 164), He-Cd (Liconix, Model 4240) and Argon (Spectra-Physics Model 165) lasers. Raman shifts were calibrated with known lines of Indene. Absorption spectra were measured with a conventional Hitachi 124S spectrometer.

The dependence of photo-reduction on wavelength (action spectrum of photo-reduction) was measured in the presence of short-cut filters in a similar manner as reported by *Ozaki et al.*[7] The degassed solution of [Fe^{III}(PPDME)(2-MeIm)] in CH_2Cl_2 containing a trace amount of methanol was placed in a water bath at 20° C and illuminated by a projector lamp for 5 minutes in the presence of short-cut filters Y-48, Y-46, Y-44, L-42, L-40 and L-38 using fresh sample for each measurement. The difference in the absorption spectrum designated by $S(\lambda_1 - \lambda_2)$ observed in the presence of filters with cut-off wavelengths λ_1 and λ_2 represents the effect of illumination of light with wavelengths between λ_1 and λ_2. The relative intensity of the illuminating projector light after the short-cut filter was measured by dispersing it with a 10 cm monochromator and detecting with a pin photodiode (Hamamatsu, S172202). After measuring the transmission spectra of individual filters, difference spectra, $D(\lambda_1 - \lambda_2)$, between the two spectra obtained in the presence of short cut-filters with cut-off wavelengths as λ_1 and λ_2 were calculated and corrected for the inherent wavelength dependences of the monochromator and detector sensitivities. For converting the transmitted light intensity to the relative number of photons, the area of the $D(\lambda_1 - \lambda_2)$ vs λ curve was obtained with the help of partial integration method by dividing the region between λ_1 and λ_2 into ten segments. In order to determine the dependence of photo-reduction on illumination time, the fresh and degassed

solutions were illuminated for different times in the presence of short-cut filter L-38 which allows light of wavelengths greater than 380 nm to pass. All the solutions contained a trace amount of methanol in CH_2Cl_2.

4.3 RESULTS AND DISCUSSION

Since most of the structure and oxidation state sensitive bands appear in the higher frequency region, we concentrated our study on vibrational modes in the 1300-1700 cm^{-1} region. The RR spectra of Fe^{III}(PPDME) with excitation at the 441.6 nm under different experimental conditions are shown in Figure 4.1. Figure 4.1A gives the RR spectrum of Fe^{III}(PPDME)Cl in CH_2Cl_2. The vibrational assignment and mode numbering are followed on the basis of previous studies on Fe(OEP) and protoheme complexes.[9,10] The RR spectral pattern corresponds to a five coordinate, high spin species.[11,13] The highest frequency mode ν_{10}, appears at 1630 cm^{-1} with a shoulder at 1622 cm^{-1} which is associated with a vinyl $\nu_{C=C}$ stretching mode (see below). The totally symmetric ν_4 and ν_3 modes appear at 1372 and 1492 cm^{-1} respectively.

On addition of 2-MeIm upto 100 mM, the 640 nm optical absorption band of Fe^{III}(PPDME)Cl originating from charge transfer transitions from Cl^- to Iron decreases in intensity and distinct changes occur in the α-β absorption region where the broad band around 505 nm shifts to 525 nm. However the RR spectra in the higher frequency region under aerobic and anaerobic

conditions in pure CH_2Cl_2 are similar for both the systems as shown in Figure 4.1A. It is clear that there is no evidence of photo-reduction in pure CH_2Cl_2 with 2-MeIm. Addition of a trace amount of methanol, ethanol or 2-propanol to the solution affects the RR spectrum dramatically as shown in Figure 4.1B under aerobic conditions. Addition of even 0.01% (v/v) methanol or ethanol produces a small fraction of photoreduced species which keeps on increasing and complete photo-reduction occurs at 0.1% concentration of these alcohols with 441.6 nm (30 mW) excitation under anaerobic conditions. The oxidation state marker band ν_4 (P) shifts to 1355 cm^{-1}, while additional bands appear at 1471, 1562 and 1605 cm^{-1}. Figure 4.1C shows the RR spectrum of a degassed solution used for measurements in Figure 4.1B. The bands at 1471, 1562 and 1605 cm^{-1} gain intensity and corresponding bands at 1492, 1572 and 1628 cm^{-1} disappear altogether in anaerobic solution. Moreover, a band appears at 206 cm^{-1} corresponding to the ν_{Fe-N} stretching mode of an axially ligated 2-MeIm and Fe-atom in the reduced species.[13,29,30] In earlier reported RR studies,[7,14] photo-reduction of iron-porphyrins in CH_2Cl_2 in the presence of electron donors has been observed and confirmed recently[15] presumably due to the presence of alcoholic impurities in CH_2Cl_2 used as stabilizer. We have investigated the effect of some other protic and aprotic solvents on the process of photo-reduction. The yield of photo-reduction has been found to vary considerably in different solvents which does not correlate with any single physical

parameter of the solvents. The RR spectrum of chemically reduced [Fe^{II}(PPDME)][2-MeIm] is shown in Figure 4.1D whose spectral pattern is exactly identical to that shown in Figure 4.1C. A comparison of the spectral features in Figure 4.1B and Figure 4.1C with the known oxidation state marker bands suggests that even under aerobic conditions, a major fraction of [Fe^{III}(PPDME)](2-MeIm) complex is reduced by irradiation in the Soret absorption region with 441.6 or 406.7 nm excitations. A close inspection of Figure 4.1A in ref.7 on photo-reduction of [Fe^{III}(OEP)][2-MeIm] indicates a shoulder at 1361 cm^{-1} and a weak feature around 1475 cm^{-1} due to photoreduced species in the photo-steady state under aerobic conditions. This implies that only a small fraction of [Fe^{III}(OEP)][2-MeIm] is photoreduced under aerobic conditions. As the reduction process appears to be coupled to the Soret optical transition (see below), the concentration of the reduced species in the photo-steady state should be proportional to the product of the incident laser flux and the absorption cross-section for the transition. The power used in the experiments here and in the ref.7 was 30 mW at 441.6 nm using similar focusing arrangement while the concentration of sample was three times higher in ref.7 compared to our experiments. One would have expected larger photo-reduction in Fe(OEP) compared to Fe(PPDME) complex contrary to observations implying that the rates of aerobic photo-reduction are different in the two cases. This is one of the differences in the photo-reduction of the [Fe^{III}(PPDME)][2-MeIm] and

[Fe^{III}(OEP)][2-MeIm] complexes. The presence of the 1622 cm^{-1} band associated with the vinyl $\nu_{C=C}$ stretching mode in the RR spectra of the photoreduced species indicates that condensation of the vinyl groups has not taken place due to photo-irradiation in the presence of oxygen. Moreover, the coincidence of the RR spectrum of the photoreduced [Fe^{II}(PPDME)][2-MeIm] and its chemically reduced form rules out a possibility of reduction of the porphyrin ring to an anion radical or chlorin form as these systems have distinct RR features.[11a,13] There was hardly any evidence of photo-reduction in the degassed solution of [Fe^{III}(PPDME)]-[2-MeIm] by excitation with the 488.0 or 514.5 nm lines, while partial photo-reduction was observed for [Fe^{III}(OEP)][2-MeIm] system with these excitation lines. This is probably due to relatively much weaker absorption in the PP complex compared to the OEP complex at the positions of 488.0 and 514.5 nm excitation lines giving negligible photo-reduction in the former case. Since the RR scattering cross-section is different for the ferric and ferrous complexes, the relative intensity of the Raman bands due to these species can not serve as a quantitative measure for photo-reduction.

As the process of photoreduction is strongly dependent on the nature of axial ligands, we investigated the effect of 2-MeIm or 1,2-Me_2Im and alcohols on the absorption spectra of Fe^{III}(OEP)I more carefully as shown in Fig.4.2. The absorption spectra of Fe^{III}(OEP)I in pure CH_2Cl_2 and after addition of methanol, ethanol or propanol upto 0.1% v/v are found exactly

identical (Fig. 4.2A) without indicating any coordination of alcohol in place of I^- ion or at the vacant sixth ligand position. With 1% methanol, the 505 nm band splits into two components at 510 and 530 nm. When the concentration of methanol is increased beyond 5%, the 640 nm CT band keeps on diminishing and a pair of new bands around 585 and 475 nm grow in intensity with concomittant decrease in the intensity of the 510 and 530 nm bands (Fig. 4.2B) indicating that the halide ion is replaced by the methoxy radical. This solution containing 10% v/v or more methanol is ~30% photoreduced under anaerobic conditions without 2-MeIm. At the 50% v/v concentration of methanol, addition of 2-MeIm upto 100 mM does not affect absorption spectrum but a medium intense feature at 1481 cm^{-1} alongwith a dominant band at 1491 cm^{-1} in the RR spectrum indicate that the six and five-coordinated Fe^{III}(OEP) species coexist in solution where CH_3OH is attached as a sixth ligand.

Addition of 2-MeIm upto 100 mM to a 1 mM solution of Fe^{III}(OEP)I in CH_2Cl_2 without methanol affects the absorption spectrum as shown in Fig. 4.2C where the 640 nm CT band almost disappears, the broad 505 nm and the Soret band at 380 nm shift to 525 and 395 nm respectively. This solution is not photoreducible. When methanol upto 0.1% v/v is added to this solution, the alcohol acts as a directing ligand[16a], where it first replaces halide ion and then 2-MeIm is attached in its place as per the following scheme:

$$Fe^{III}(OEP)I + CH_3OH \rightleftharpoons Fe^{III}(OEP)(CH_3OH)$$

$$Fe^{III}(OEP)(CH_3OH) + 2\text{-MeIm} \rightleftharpoons Fe^{III}(OEP)\text{-}2MeIm + CH_3OH$$

The disappearance of the 640 nm CT band and the presence of the 525 and 395 nm bands in the absorption spectra and certain characteristic features in the RR spectra indicate five-coordinate $[Fe^{III}(OEP)](2\text{-MeIm})$ species in the solution. However, when the concentration of alcohol is increased to 1% v/v or higher, the 640 and 525 nm bands are replaced by another pair of bands at 585 and 480 nm (Fig. 4.2D) indicating formation of a six-coordinated species with 2-MeIm and methanol as axial ligands. Therefore it is evident that the 525 nm or 580 and 480 nm absorption bands are dignostic of five or six-coordinated species in these systems under the above discussed conditions.

In order to determine the fraction of the sample reduced as a function of illumination time t, we measured the action spectrum in the UV-visible region of anaerobic solutions of $[Fe^{III}(PPDME)][2\text{-MeIm}]$ in CH_2Cl_2 containing a trace amount of alcohol by irradiation with a white light source for different times in the presence of a short-cut filter L-38 which allows light with $\lambda > 380$ nm to pass. Since the experiments were conducted under anaerobic conditions, the fraction of photoreduced species by irradiation in a particular wavelength range may be expected to vary as $(1-e^{-k_R t})$ with time t where k_R is the rate constant for photo-reduction. The light driven conversion from the oxidized to the reduced form can be represented by a simple

kinetic equilibrium expression :

$$Fe^{III}(PP) + h\nu \xrightarrow{k_R} Fe^{II}(PP) \qquad \text{---- 4.1}$$

where $Fe^{III}(PP)$ represents the oxidized $Fe^{III}(PPDME)(2\text{-}MeIm)$ species at any instant, $Fe^{II}(PP)$ is the reduced species in the sample at any instant of time t due to irradiation. The fraction of the reduced species upon illumination for time t is given by

$$\phi = (1 - e^{-k_R t}) = \frac{[Fe^{II}(PP)]}{[Fe^{Tot}(PP)]} \qquad \text{----- 4.2}$$

$$\text{therefore } (1 - \phi) = e^{-k_R t} = \frac{[Fe^{III}(PP)]}{[Fe^{Tot}(PP)]} \qquad \text{----- 4.3}$$

where $Fe^{Tot}(PP) = Fe^{II}(PP) + Fe^{III}(PP)$

$= Fe^{III}(PP)_{\text{totally oxd.}} = Fe^{II}(PP)_{\text{totally red.}}$

From eqn. 4.3 , one obtains $\ln(1 - \phi) = -k_R t$ ------ 4.4

A plot of $-\ln(1-\phi)$ vs time t of irradiation would yield the value of k_R . Since The absorption bands due to the oxidized and reduced forms overlap in the Soret absorption region, we have used the following procedure[16b] for determining the fraction of photoreduced species . At any wavelength λ ,

$$\phi = \frac{[Fe^{II}(PP)]}{[Fe^{Tot}(PP)]} = \frac{[A_\lambda - A_{O\lambda}]}{[A_{R\lambda} - A_{O\lambda}]} \qquad \text{----- 4.5}$$

where A_λ is the absorbance of the reduced species at a given

wavelength (429 nm) at a specific concentration of $Fe^{II}(PP)$, $A_{O\lambda}$ and $A_{R\lambda}$ are the absorbances of the fully oxidized and fully reduced species at λ . We obtained the fraction of the photoreduced species by irradiation for different times in the presence of L-38 cut-off filter using expression 4.5. From a plot of $-\ln(1-\Phi)$ vs t in Figure 4.3, we obtained a value for k_R^{-1} =10 minutes.

The dependence of photo-reduction on wavelength of irradiation was also ascertained by monitoring the changes in the UV-visible absorption spectra after irradiation of a degassed solution of $[Fe^{III}(PPDME)][2\text{-MeIm}]$ in CH_2Cl_2 having a trace amount of methanol by a white light source in the presence of the short-cut filters. Figure 4.4 shows the absorption spectra of the anaerobic samples in the presence of short-cut filters where the absorption peaks for the ferric and photoreduced complexes arise at 403 and 429 nm, respectively. The insert in this figure shows the transmitted intensity of light after the indicated cut-off filters.

We analyzed the action spectral data using the following procedure. If the rate constants for photo-reduction in the presence of short-cut filters with cut-off wavelengths as λ_1 and λ_2 are represented by $k_{R\lambda_1}$ and $k_{R\lambda_2}$ respectively, then from expression 4.4

$$k_{R\lambda_1} = -\frac{1}{t} \ln(1- \phi)$$

and ------ 4.6

$$k_{R\lambda_2} = -\frac{1}{t} \ln(1- \phi)$$

$$\text{Therefore } (k_{R\lambda_1} - k_{R\lambda_2})t = \ln \left[\frac{[Fe^{III}_{\lambda_2}(PP)]}{[Fe^{III}_{\lambda_1}(PP)]} \right]$$

$$= \ln \left[\frac{(1 - [Fe^{II}_{\lambda_2}(PP)]/[Fe^{Tot}(PP)])}{(1 - [Fe^{II}_{\lambda_1}(PP)]/[Fe^{Tot}(PP)])} \right] \quad -- 4.7$$

Using expression 4.5 to obtain the fraction of photoreduced species in terms of absorbances, we obtain

$$(k_{R\lambda_1} - k_{R\lambda_2})t = \ln \left[\frac{[A_{R\lambda} - A_{\lambda_2}]}{[A_{R\lambda} - A_{\lambda_1}]} \right] \quad ------4.8$$

where A_{λ_2} and A_{λ_1} are the absorbances at 429 nm due to irradiation for time t in the presence of filters with cut off wavelengths as λ_2 and λ_1 respectively and $A_{R\lambda}$ is the absorbance due to the fully reduced form at 429 nm.

$$\text{Since } (k_{R\lambda_1} - k_{R\lambda_2})t \propto \int D(\lambda_1 - \lambda_2) \cdot A(\lambda) \, d\lambda$$
$$= A(\lambda_1 + \lambda_2/2) \int D(\lambda_1 - \lambda_2) d\lambda \quad --4.9$$

Therefore the action spectrum or relative quantum yield for photo-

reduction $A\left(\frac{\lambda_1+\lambda_2}{2}\right)$ is given by

$$A\left(\frac{\lambda_1+\lambda_2}{2}\right) = \ln\left[\frac{[A_{R\lambda} - A_{\lambda_2}]}{[A_{R\lambda} - A_{\lambda_1}]}\right] \Big/ \int D(\lambda_1 - \lambda_2)\, d\lambda \quad \text{--4.10}$$

The logarithm of the ratio of the absorbances $[A_{R\lambda} - A_{\lambda_2}]/[A_{R\lambda} - A_{\lambda_1}]$ due to irradiation for 5 min. from Figure 4.4 are plotted against the illumination wavelength where data for the absorbances in the presence of filters having cut-off wavelength as λ_1 and λ_2 are located at $(\lambda_1 + \lambda_2)/2$ of the abscissa (raw data). The data represented by the triangles in Figure 4.5 is obtained after dividing the raw data by the relative number of photons between λ_1 and λ_2 corrected for the spectral response of the monochromator and detection system. This plot shows a maximum coinciding with the Soret absorption band implying that the photo-reduction process is coupled to the Soret optical transition.

The effect of different axial ligands on photo-reduction of Fe^{III}(PPDME) was studied in the presence of other ligands such as 1,2-Me_2Im, imidazole, 1-MeIm etc. and our conclusions are similar to those of *Ozaki et al.*[7] We observed photo-reduction with 1,2-Me_2Im as axial ligand but no photo-reduction occurs with imidazole or 1-MeIm as axial ligands under similar conditions which form six coordinate low spin complexes with Fe(PPDME). In order to gain insight into the mechanism of photo-reduction of [Fe^{III}(PPDME)][2-MeIm], we monitored the changes in the RR spectral features as a function of concentration of 2-MeIm as shown in Figure 4.6. As the concentration of 2-MeIm increases

from 0 to 5 mM from Figure 4.6A to 4.6D, the spectral pattern becomes more complicated due to contributions from the oxidized, reduced and presumably intermediate species as well. For instance, the spectrum in Figure 4.6C shows band centres at 1634, 1631 and 1604 cm^{-1}; 1572, 1562 and 1547 cm^{-1}; 1508, 1493 and 1474 cm^{-1} which can be associated with the ν_{10}, ν_2, and ν_3 modes respectively, for various species. In Table 4.1, we give the frequencies and their most probable assignment based on other model systems[12d,13,17] where we could identify at least two bands at 1634 and 1508 cm^{-1} which can be associated with the ferrous intermediate spin complex. It is known[13,17c] that Fe^{III}(PPDME)(2-MeIm) does not form a low spin complex with 2-MeIm under the present concentrations used. We therefore infer that intermediate species formed during photo-reduction is four coordinated Fe^{II}(PPDME) of intermediate spin with no axial ligand. The weak feature at 1622 cm^{-1} in the spectra of oxidized form of [Fe^{III}(PPPDME)][2-MeIm] develops into a well defined peak without shift in its position on reduction. Therefore this band has been indentified as originating from the vinyl group $\nu_{C=C}$ stretching mode.

The time resolved studies on iron porphyrins[18] indicate very short relaxation time of the excited singlet state (pico sec. range). The absence of luminiscence by excitation in the Soret region also implies a rapid deactivation of the (π, π^*) excited state via short-lived and low lying ring $\longleftrightarrow$ metal (d_π, e_g (π^*)) or (a_{2u} (π), d_z2) charge-transfer (C T), or

ligand field (d_π , d_z2) states. As the d_z2 orbital is antibonding towards the σ-bonded nitrogenous bases, excitation in the Soret region may excite the [Fe^{III}(PPDME)][(2-MeIm)] complex to the d_z2 orbital directly by electronic excitation from the porphyrin a_{2u} (π) or from the axial ligand (2-MeIm) to the d_z2 orbital. The axial ligand in this excited state may dissociate by donating its electron to the d_z2 orbital which may relax to the d metal orbital to give transient intermediate spin species. Based on these considerations, the following mechanism for photo-reduction of [Fe^{III}(PPDME)][2-MeIm] may be suggested.

$$Fe^{III}(PPDME)Cl + 2\text{-MeIm} \xrightarrow{\text{Alcohol}} Fe^{III}PPDME\text{-}2\text{-MeIm} \xrightarrow{h\nu}$$

$$[\ Fe^{II}\ (PPDME)\ \ 2\text{-MeIm}^{+}\ ] \rightleftharpoons [\ Fe^{II}\ \ PPDME\ ] \longrightarrow$$

$$Fe^{II}\ (PPDME)\text{-}2\text{-MeIm}.$$

Light irradiation of Fe^{III}(PPDME)(2-MeIm) in the Soret region excites the system to the d_z2 orbital where coordinated 2-$MeIm^{+}$ dissociates, donating its charge to Fe^{III}(PPDME). This excitation follows an instantaneous charge separation. The Fe^{II}(PPDME) and 2-$MeIm^{+}$ diffuse away and coordination of another molecule of 2-MeIm from the solution results in the formation of the stable [Fe^{II}(PPDME)][2-MeIm] complex. When the concentration of 2-MeIm is too low, a sufficient amount of [Fe^{III}(PPDME)][2-MeIm] is not available for photo-reduction explaining the dependence of photo-reduction on concentration of

2-MeIm. Similar mechanism may be operative in primary alcohols without 2-MeIm. The presence of alcohols may accelerate the process of photo-reduction in the following ways: Firstly, because of their polarity, they facilitate the charge separation while the non-polar solvents accelerate the cage recombonation processes which will suppress the process of photo-reduction. Secondly, the presence of alcohols or other polar solvents may displace the Cl^- from the coordination sphere of iron, where alcohol first coordinates with iron displacing halide ion and then facilitating coordination of 2-MeIm in its place at lower concentration of alcohols which act as directing ligand.[16a] This will decrease the electron density on iron and enhance its electron accepting ability to facilitate photo-reduction. Thirdly, the O-H group of alcohols and the N_δ- H group of 2-MeIm can form stronger hydrogen bonds leading to an increase in charge delocalization and electron donating ability of the 2-MeIm ring. This will accelerate the charge transfer process from axial ligand to iron centre. In the case of 1,2-Me_2Im , hydrogen bonding would be very weak but the methylation of the N_δ - H proton shall increase the charge density on the imidazole ring due to increased π - overlap of the nitrogen lone-pair electrons with the imidazole ring. This electronic effect alongwith increased steric interactions are expected to reduce activation energy for photodissociation of 1,2-Me_2Im axial ligand during photoexcitation of the Fe^{III}(PPDME)-(1,2-Me_2Im) complex. Addition of imidazole or 1-MeIm produce six

coordinate, low spin complexes with Fe(PPDME). These stronger bases increase electron density at iron centre with significant decrease in its ability to accept electrons.

There is a significant difference in the extent of photo-reduction of the Fe^{III}(PPDME) and Fe^{III}(OEP) complexes under aerobic conditions. Perhaps the vinyl groups accelerate the formation of -oxo-bridged dimers or aggregates of Fe^{III}(PPDME) by interaction between and stacking of the porphyrin rings[19a-c], it is likely that the life time of the intermediate species formed during photo-reduction under aerobic conditions for the aggregated forms is enhanced compared to the monomeric form. This may facilitate the build-up of enough population in the transient intermediate state for the dimeric form which may explain the difference in phtoreducibility of the [Fe^{III}(PPDME)][2-MeIm] and [Fe^{III}(OEP)][2-MeIm] complexes. Direct evidence for the formation of aggregated species in aerobic solution of [Fe^{III}(PPDME)]Cl in CH_2Cl_2 comes from enhanced RR intensity of the 1492 cm^{-1} band compared to the 1372 cm^{-1} band for aggregated form in comparison to their ratio for the monomeric species[20a-c] under anaerobic conditions as shown in Figure 4.7.

We can summarize our main findings as follows:
The primary alcohols and some other polar solvents accelerate the process of photoreduction by facilating charge separation. The primary step involved in photoreduction appears to be the

dissociation of axial ligand in the excited state of iron-porphyrins, most likely the dissociative d_z2 orbital of iron, and the photoreduction process is coupled to the electronic trnasition in the Soret region. The energies associated with excitation in the CT region from axial ligand to iron may be inadequate for axial ligand dissociation and thus giving no photoreduction. Moreover, we have deduced that the fraction of the sample reduced upon illumination for a particular time varies exponentially on the rate of photoreduction. These findings are at variance with the earlier reported results[7] where it was imlicitly assumed that the fraction of sample reduced is directly proportional to the rate of photoreduction which is not valid under the conditions of these experiments.

REFERENCES

1. Augustin, M.A.; Yandell, J.K. *Inorg. Chim. Acta.* 37, 11, 1979.
2. Wherland, S.; Gray, H.B. *Proc. Natl. Acad. Sci. U.S.A.* 73, 2950, 1976.
3. Mauk,A.G.; Gray, H.B. *Biochem. Biophys. Res. Commun.* 86, 206, 1979.
4. Eguchi, L.A.; Saltman, P. *J. Biol. Chem.* 259, 14337, 1984.

5a. Kitagawa, T.; Orii, Y. *J. Biol. Chem. (Tokyo)* 84, 1245, 1978.

b. Kitagawa, T.; Nagai, K. *Nature,* 281, 503, 1979.

c. Kitagawa, T.; Chihara, S.; Fushitani, K.; Morimoto,H. *J. Am. Chem. Soc.* 106, 1860, 1984.

d. Sage, J.T.; Morkis, D.; Champion, P.M. *J. Chem. Phys.* 90, 3015, 1989.

6a. Hariman, A.; Porter, G. *J. Chem. Soc. Faraday. Trans.* 75, 1543, 1979.

b. Bartocci, C.; Scandola, F.; Ferri, A.; Carassitti, V. *J. Am. Chem. Soc.* 102, 7067, 1980.

c. Bizet, C.; Morliere, P.; Brault, D.; Delgado, O.; Bazin, M.; Santus, R. *Photo chem. Photo biol.* 34, 315, 1981.

d. Bartocci, C.; Maldotti, A.; Traverso, O.; Bignozzi, C.A.; Carassitti, V. *Polyhedron.* 2, 97, 1983.

7. Ozaki, Y.; Iriyama, K.; Ogoshi, H.; Kitagawa, T. *J. Am. Chem. Soc.* 109, 5583, 1987.

8a. Furhop, J.H.; Smith, K.M. *"Porphyrins and Metalloporphyrins"* Smith, K.M., Ed., American Elsevier, New York, p. 835, 1975.

b. Ogoshi, H.; Sugimoto, H.; Yoshida, Z. *Bull. Chem. Soc. Jpn.* 54, 3414, 1981.

9a. Kitagawa, T.; Ogoshi, H.; Watanabe, E.; Yoshida, Z. *Chem. Phys. Lett.* 30, 451, 1975.

b. Kitagawa, T.; Ogoshi, H.; Watanabe, E.; Yoshida, Z. *J. Phys. Chem.* 79, 2629, 1975.

c. Kitagawa, T.; Abe, M.; Ogoshi, H. *J. Chem. Phys.* 69, 4516, 1978.

d. Abe, M.; Kitagawa, T.; Kyogoku, Y. *J. Chem. Phys.* 69, 4526, 1978.

10a. Choi, S.; Spiro, T.G.; Langry, K.C.; Smith, K.M.; Budd, D.L.; LaMar, G.N. *J. Am. Chem. Soc.* 104, 4345, 1982.

b. Choi, S.; Spiro, T.G.; Langry, K.C.; Smith, K.M. *J. Am. Chem. Soc.* 104, 4337, 1982.

11a. Ozaki, Y.; Iriyama, K.; Ogoshi, H.; Ochiai, T.; Kitagawa, T. *J. Phys. Chem.* 90, 6105, 1986.

b. Kim, D.; Oliver Su, Y.; Spiro, T.G. *Inorg. Chem.* 25, 3988, 1986.

c. Ozaki, Y.; Kitagawa, T.; Ogoshi, H. *Inorg. Chem.* 18, 1772, 1979.

12a. Yamamoto, T.; Palmer, G.; Gili, D.; Salmeen, I.T.; Rimai, L. *J. Biol. Chem.* 248, 5211, 1973.

b. Verma, A.L.; Bernstein, H.J. *J. Raman. Spectrsc.* 2, 163, 1974.

12c. Spiro, T.G.; Strekas, T. *J. Am. Chem. Soc.* 96, 338, 1974.

d. Spiro, T.G. in *Iron Porphyrins*, Lever, A.B.P.; Gray, H.B. Eds., Addison-Wesley, Reading, M.A, Part II, p. 91, 1983.

13a. Kitagawa, T.; Ozaki, Y. *Structure and Bonding*, 64, 71,1987.

b. Hori, H.; Kitagawa, T. *J. Am. Chem. Soc.* 102, 3608, 1980.

14. Verma, A.L.; Chaudhury, N.K.; Saini, G.S.S. in *"Recent trends in Raman Spectroscopy"* Banerjee, S.B.; Jha, S.S. Eds., World Scientific Publishing Co., Singapore, p. 192, 1989.

15a. The authors are grateful to Prof. T. Kitagawa for informing us that the CH_2Cl_2 used in their studies in ref.7 contained methanol impurity. The following work appeared when we completed our studies.

b. Fidler, V.; Ogura, T.; Ozaki, Y.; Kitagawa, T. *Chem. Phys. Letts.* 169, 457, 1990.

16a. Pavlovic, D.; Asperger, S.; Dokuzovic, Z.; Jurisic, B.; Ahmeti, X.; Sertic, M.; Murati, I. *J. Chem. Soc. Dalton Trans.* 1095, 1985.

b. Collman, J.P.; Brauman, J.L.; Collins, T.J.; Iverson, B.L.; Lang, G.; Pettman, R.B.; Seccler, J.L.; Walters, M.A. *J. Am. Chem. Soc.* 105, 3038, 1983.

17a. Spiro, T.G.; Strong, J.D.; Stein, P. *J. Am. Chem. Soc.* 101, 2648, 1979.

b. Teraoka, J.; Kitagawa, T. *J. Phys. Chem.* 84, 1928, 1980.

c. Kitagawa, T.; Teraoka, J. *Chem. Phys. Lett.* 63, 443, 1979.

18a. Huppert, D.; Straub, K.D.; Rentzupis, P.M. *Proc. Natl. Acad. Sci. U.S.A.* 74, 4139, 1977.

b. Liang, Y.; Negus, D.K.; Hochstrasser, R.M.; Gunner M.; Dulton, D.L. *Chem. Phys. Lett.* 84, 236, 1981.

c. Kim, D.; Kiramier, C.; Holten, D. *Chem. Phys.* 75, 305, 1983.

19a. Momenteau, M. *Biochem. Biophys. Acta* 304, 814, 1973.

b. LaMar, G.N.; Viscio, D.B. *J. Am. Chem. Soc.* 96, 7354, 1974.

c. Doughty, D.A.; Dwiggins(jr), C.W. *J. Phys. Chem.* 73, 423, 1969.

20a. Smulevich, G.; Spiro, T.G. *J. Phys. Chem.* 89, 5168, 1985.

b. Sanchez, L.A.; Spiro, T.G. *J. Phys. Chem.* 89, 763, 1985.

c. Hofmann, J.A.; Bocian, D.F. *J. Phys. Chem.* 88, 1472, 1984.

Table 4.1

Observed RR frequencies of different vibrational modes for the ferric and ferrous complexes of Fe(PPDME)

Mode number and assignment(a)	Ferric	Ferrous	
	High Spin (cm^{-1})	Intermediate spin (cm^{-1})	Photoreduced and chemically reduced High spin (cm^{-1})
ν_{10}, $B_{1g}(C_a\ C_m)$	1631	1634	1605
$\nu_{C=C}$, Vinyl mode	1622	1622	1622
ν_{37}, $Eu(C_b - C_b)$	1590	Overlapping	1586
ν_2, $A_{1g}(C_b\ C_b)$	1572	Overlapping	1562
ν_{11}, $B_{1g}(C_b\ C_b)$	1555	Overlapping	1555
ν_{38}, Eu (C_aC_m)	1521	1526	1526
ν_3, $A_{1g}(C_aC_m)$	1493	1508	1471
ν_4 ,$A_{1g}(C_aN)$	1372	Overlapping	1355

(a) Mode numbering is in accordance with ref nos.9-10.

(b) The ν_{10} and ν_3 modes have shown distinct features assignable to the intermediate spin, ligand free Fe^{II}(PPDME) species.

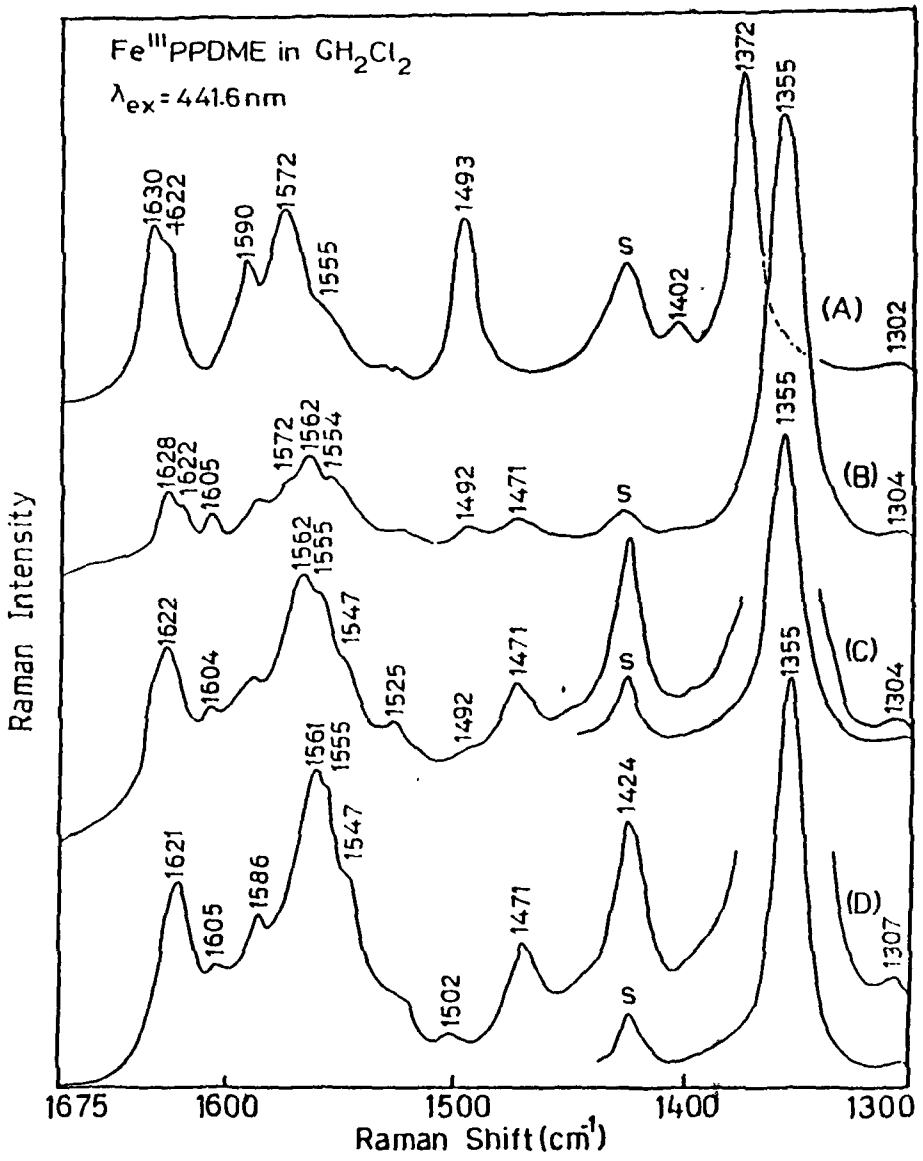

Fig.4.1 RR spectra of Fe^{III}(PPDME)Cl in CH_2Cl_2 and its photoreduced and chemically reduced species with excitation at 441.6 nm. (A) Fe^{III}(PPDME)Cl in CH_2Cl_2 in aerobic condition. Sensitivity, 1000 counts/sec; Scan speed, 25 cm^{-1}/min; Time constant, 3.2 sec; Laser power 30 mW; Slit width, 200μm. (B) The same solution of (A) but containing trace amount of MeOH and excess 2-MeIm in aerobic condition. Experimental conditions are identical to (A). (C) Fe^{III}(PPDME)Cl in CH_2Cl_2 containing 2-MeIm (150 mM) and trace amount of MeOH under anaerobic condition. (D) Chemically reduced Fe^{II}(PPDME)(2-MeIm) in CH_2Cl_2. Experimental conditions for (C) and (D) are same as for (A) except the sensitivity was 500 counts/sec and slit width, 140 μm. The concentration of Fe^{III}(PPDME)Cl is 0.5mM for all spectra.

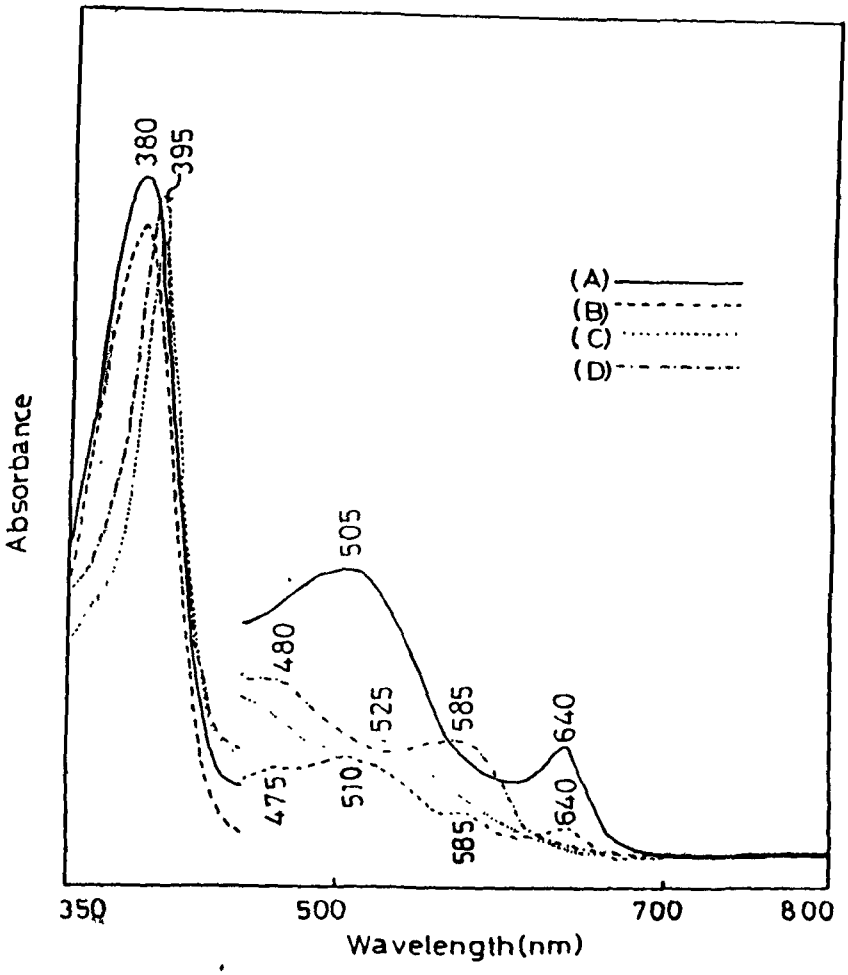

Fig.4.2 Absorption spectra of $Fe^{III}(OEP)I$ in CH_2Cl_2 solution under different conditions: (A) $Fe^{III}(OEP)I$ in CH_2Cl_2 + methanol (0.1% v/v); (B) $Fe^{III}(OEP)I$ in CH_2Cl_2 + methanol (10% v/v); (C) $Fe^{III}(OEP)I$ in CH_2Cl_2 + 2-MeIm (100 mM); (D) Same solution as in (C) + methanol (1% v/v). The concentration of $Fe^{III}(OEP)$ is about 1 mM for all the spectra.

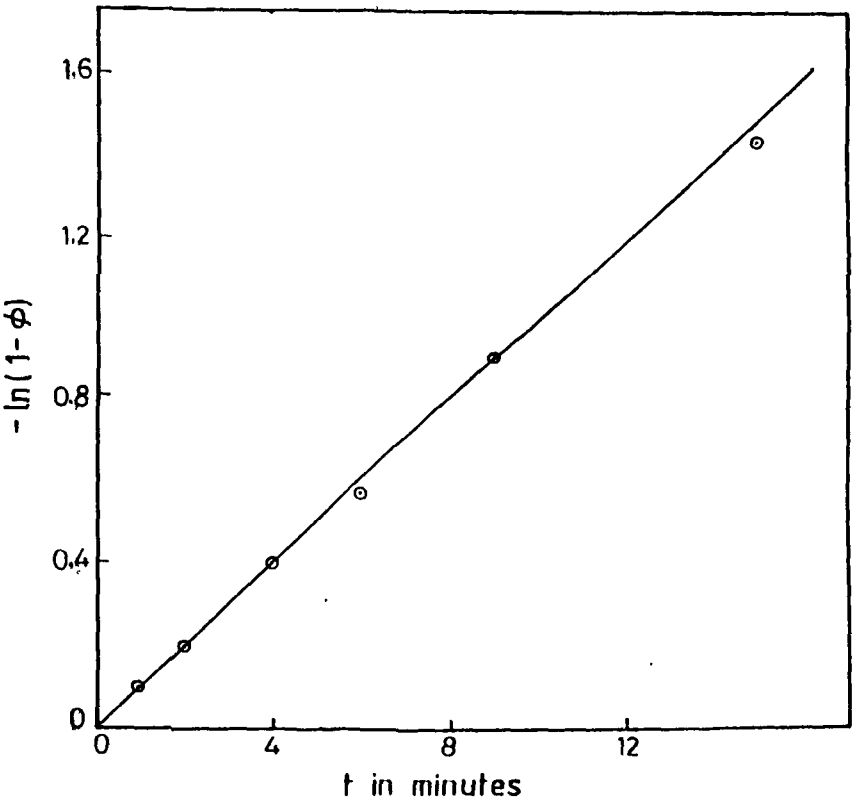

Fig.4.3 Plot of $-\ln(1-\phi)$ vs time of irradiation for a degassed solution (10^{-4} Torr) of Fe^{III}(PPDME)-(2-MeIm) in CH_2Cl_2 with a trace amount of MeOH after illumination by a white light source through the L-38 short-cut filter. $\phi = (1 - e^{-k_R t}) = [Fe^{II}(PP)]/[Fe^{Tot}(PP)]$ represents the fraction of reduced species upon illumination for time t.

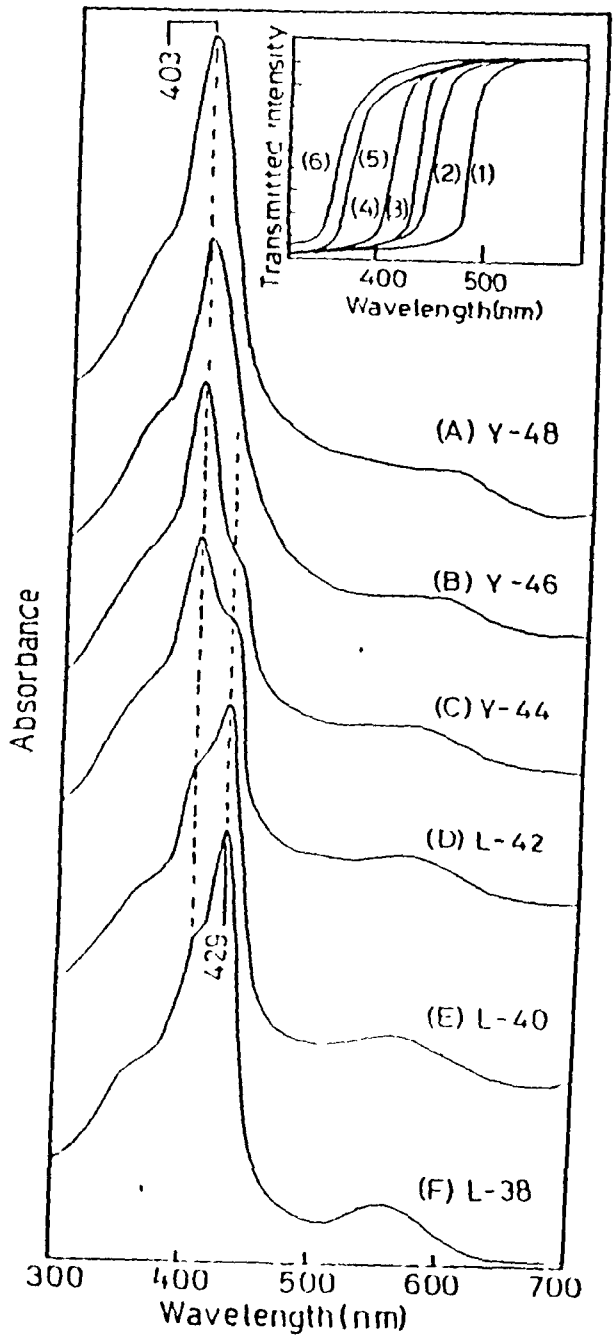

Fig.4.4 Visible absorption spectra of Fe^{III}(PPDMF)(2-MeIm) in CH_2Cl_2 containg trace amount of MeOH, illuminated by a projector lamp for 5 minutes through the designated short-cut filters. The inset figure shows the spectra of the illuminated light specified by the short-cut filters; (1), (2), (3), (4), (5) and (6) corresponding to Y-48, Y-46, Y-44 , L-42, L-40 and L-38 respectively. The spectral intensity changes also reflect the output profile of the projector lamp.

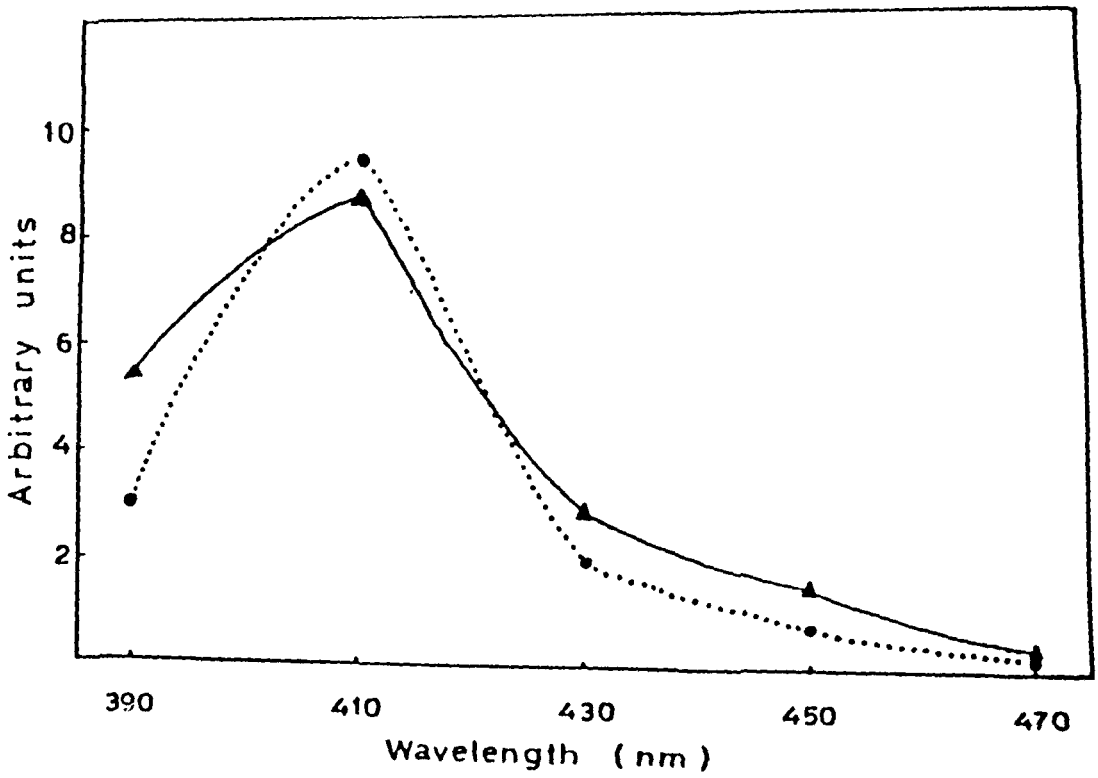

Fig.4.5 Action spectrum and relative quantum yield for photoreduction of Fe^{III}(PPDME)(2-MeIm) in CH_2Cl_2 with MeOH. The closed circles represent the ln of absorbances $|A_{R\lambda} - A_{\lambda_2}|/|A_{R\lambda} - A_{\lambda_1}|$ at 429 nm obtained from Fig.4.3 and the absorption spectra of the fully oxidized and reduced forms, plotted against illumination wavelength λ. The data for the absorbance ratios at λ_1 and λ_2 are located at $(\lambda_1 + \lambda_2)/2$ of the abscissa. The data represented by triangles are obtained after dividing the raw data by the relative number of photons between λ_1 and λ_2 corrected for the spectral response of the monochronator and detection system. The ordinate scale for the final relative quantum yield represented by triangles is 10^{-5} times the scale for the raw data.

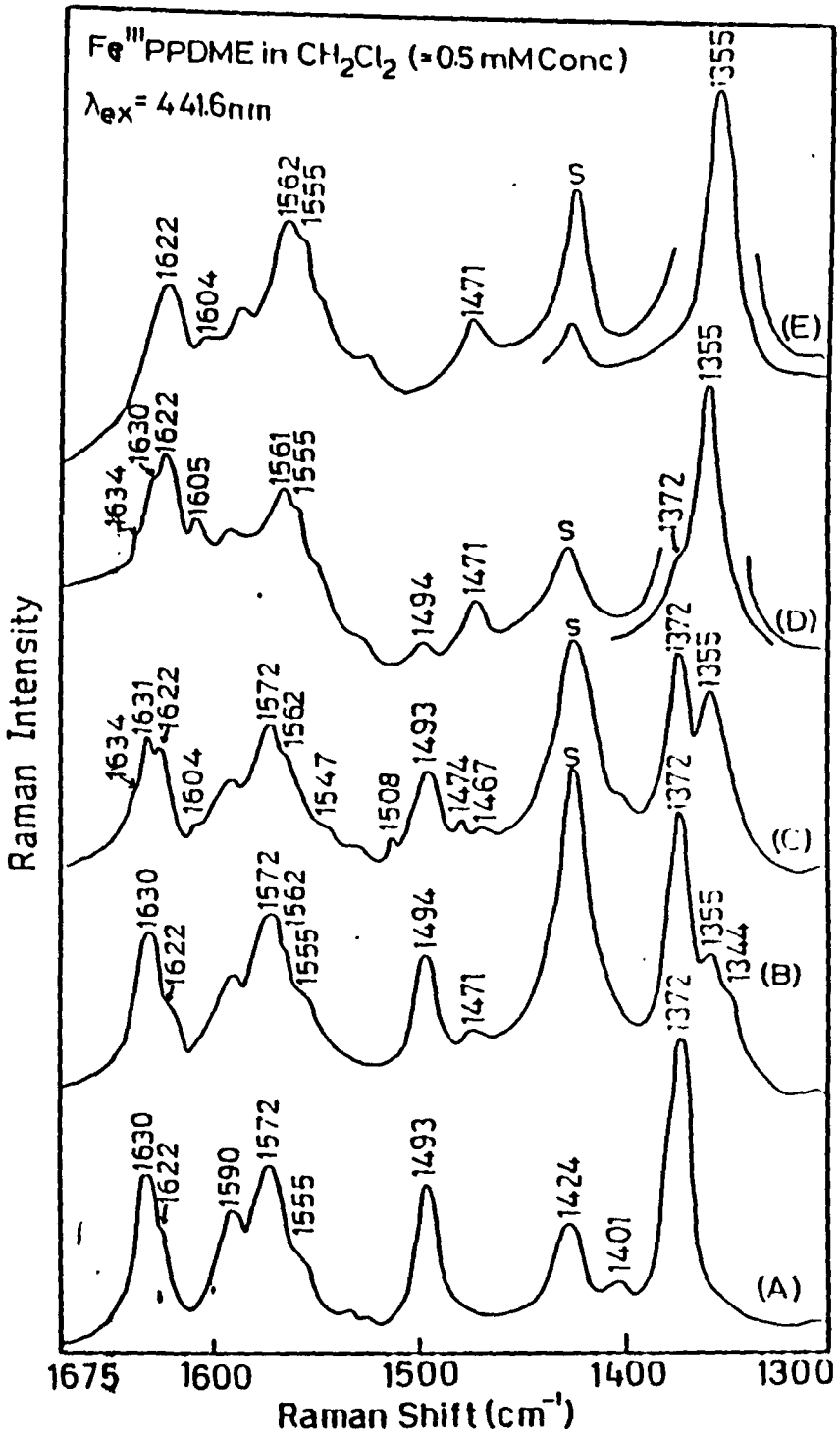

Fig.4.6 RR spectra of anaerobic solution of Fe^{III}(PPDME)Cl (0.5mM) in CH_2Cl_2 and MeOH containing different amounts of 2-MeIm obtained with 441.6nm excitation. The concentration of 2-MeIm is as follows: (A) 0mM, (B) 0.1mM, (C) 0.5mM, (D) 5.0mM and (E) 50mM. Experimental conditions, sensitivity, 500 counts/sec; Scan speed 10 cm^{-1}/min; Time constant, 3.2 sec; Laser power 30 mW; Slit width, 200 μm.

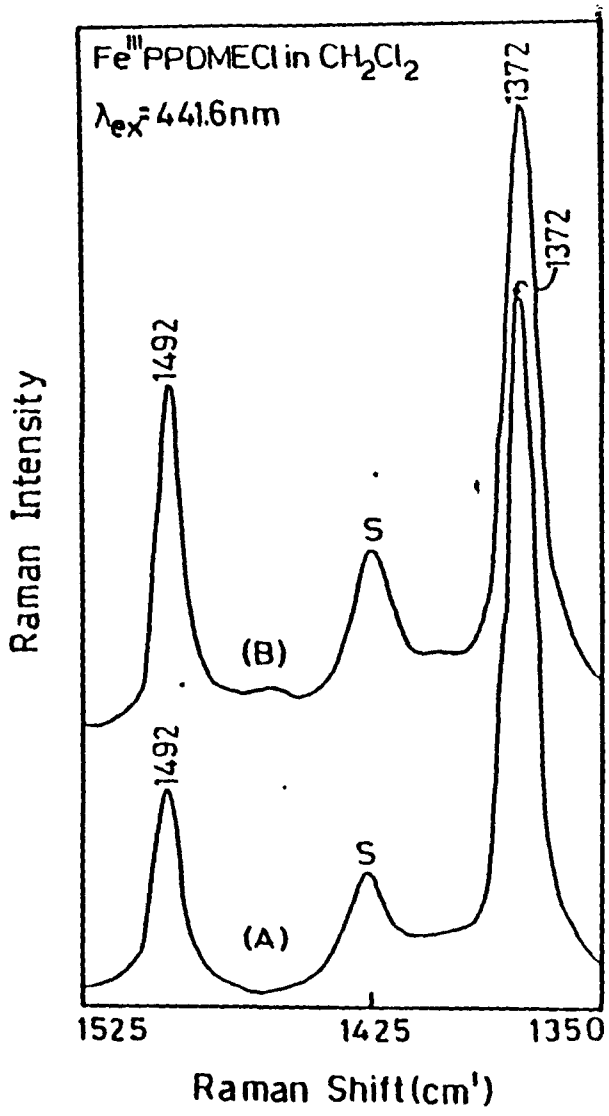

Fig.4.7 RR spectra of anaerobic (A) and aerobic (B) solutions of Fe^{III}(PPDME)Cl in CH_2Cl_2 (0.5mM conc.) using 441.6nm excitation. The higher ratio of RR intensities of the 1492 and 1372 cm^{-1} bands in spectrum (B) compared to that in spectrum A) indicate formation of aggregated species of Fe^{III}(PPDME)Cl in aerobic solution.

Temperature Dependent Axial Ligation Changes and Photoreduction of Iron protoporphyrin-IX dimethyl ester chloride at Low Temperatures Monitored by Resonance Raman Technique*

Abstract

We report here our resonance Raman studies of photoreduction of iron protoporphyrin-IX dimethyl ester chloride [$Fe^{III}PP(Cl)$] in the presence of 1,2-dimethylimidazole [1,2-Me_2Im] in dimethylsulfoxide [DMSO] matrix at low temperatures by excitation in the Soret region. By comparison of the RR marker bands of chemically reduced complex at low temperature, the photoreduced species has been identified as six-coordinated, intermediate spin, $Fe^{II}PP(DMSO)_2$ complex in the soft matrix at ~100K. Non-photoreducibility of $Fe^{III}PP(1,2\text{-}Me_2Im)$ in the hard glassy matrix of DMSO at ~20K, support the short range electron transfer process involved in photoreduction while quantum mechanical electron tunneling is insignificant. A temperature dependent change in axial ligation has been observed in the photoreduced $Fe^{II}PP(DMSO)_2$ in the relatively warm DMSO matrix at ~250K, where 1,2-Me_2Im coordinates at the fifth ligand position in the reduced complex. In solution at room temperature, the yield of photoreduction appears to be dependent on the polarity of the solvent which facilitates the solvent-induced dissociation of ion-pair created by electron transfer.

---

*Based on this study, the following paper has been communicated (a) Chaudhury, N.K.; Saini, G.S.S.; Verma, A.L. *Chem. Phys. Lett.* (Submitted).

5.1 Introduction

The properties and reactivities of iron porphyrins are subjects of continuing importance, because of their various roles as prosthetic group in heme-proteins.[1] Among the various physico-chemical reactions displayed by these iron-porphyrins are oxygen binding for transport and storage as in hemoglobins and myoglobins, electron-transfer reactions in cytochromes etc. For a number of these processes, it is the reduced iron(II)porphyrins which play all the important roles. Thus, characterization of the iron(II)porphyrins and related mechanism involved in reduction process are of intrinsic importance from the point of view of physico-chemical and bio-chemical functions. Various techniques[2-4] have been utilized for the characterization of iron(II)-porphyrins and for understanding the reduction mechanisms. Photoreduction technique[5,6] is being employed as a very efficient method to achieve reduction at the iron centre of porphyrin complexes. However, the mechanism is yet to be understood properly. To get further insight into the mechanism of photo-reduction and the role of solvents on its yield of photoreduction, we have undertaken this study.

The resonance Raman (RR) studies on iron-protoporphyrin-IX dimethylester chloride [Fe^{III}PP(Cl)] complexes in the presence of axial ligands like 1,2-Me_2Im and 2-MeIm, performed at low temperature have revealed the occurrence of photo-reduction of Fe^{III}PP(1,2-Me_2Im) in the soft matrix of DMSO where axial ligation change also takes place. We have identified

the photo-reduced iron porphyrin complex as six coordinated, intermediate spin, $Fe^{II}PP(DMSO)_2$ as the predominant species in the soft matrix. A distinct change in the axial ligation has been observed with increase in temperature of the soft matrix, where coordinated DMSO is replaced by 1,2-Me_2Im forming Fe^{II}PP-(1,2Me_2Im) species at a temperature of ~250K in the cold solution. The photoreduction at low temperature in the soft matrix was obtained irrespective of the presence of alcohols.

We also report here preliminary investigations on the effect of different solvents on the yield of photoreduction of iron-porphyrins at room temperature. It is not possible to correlate the yield of photoreduction with the known relationships on solvent parameters but it appears to be a complex function of different solvent parameters. The extent of photoreduction is most likely dependent on the ability of the solvent to displace the halide ion from the coordination sphere of iron and thus facilitating coordination of 1,2-Me_2Im.

5.2 Experimental Procedure

Iron(III) insertion into free base protoporphyrins-IX dimethyl ester was achieved by the literature methods.[11] Free base protoporphyrins-IX dimethyl ester (PP) was purchased from Sigma Chemical Co. (U.S.A.) and used without further purification. 2-methylimidazole (2-MeIm) and 1,2-dimethylimidazole (1,2-Me_2Im) were purchased from Aldrich Chemical Co. and were recrystallized before use. All solvents used were of spectroscopic grade from

SISCO (India). The solutions for low temperature Raman measurements, were thoroughly deoxygenated by purging N_2 gas and then sealed into a quartz capillary. The quartz capillary is then mounted with the help of a conducting glue on the sample holder made of copper which is mechanically connected to the second stage heat station of the vacuum shroud Model DMX 1E. Low temperatures upto ~20K were obtained by using a closed-cycle Helium cryocooler Displex Model CSA 202E which consists of a compressor Model 202 and the DE 202 expander module. The temperature controller readings were calibrated with respect to the known melting point of different substances and accordingly temperature readings were corrected.

Chemical reduction of $Fe^{III}PP$ complex was achieved by adding excess solid sodium dithionite ($Na_2S_2O_4$), obtained from BDH, in a thoroughly degassed iron(III)porphyrin in dimethyl sulfoxide solution and then shaken vigorously. The reduced iron porphyrin complexes were identified from known oxidation, spin and coordination state marker Raman bands[7-9] and absorption spectra.

Raman spectra were recorded with the help of a SPEX 1403 Ramalog Spectrometer equipped with cooled RCA-31034A photomultiplier and photon counting electronics. Data processing and spectrometer control were achieved through a micro processor based SPEX Datamate. Excitation lines were provided by Liconix Model 4240 He-Cd and Spectra-Physics Model 165-09 Argon ion

lasers. Solution spectra at room temperature were recorded with the help of a stationary cell. Calibration of the spectrometer was performed with Indene[12] and very often with known Raman lines of solvents used in these studies.

5.3 Results

Figure 5.1 shows the RR spectra of FePP(1,2-Me_2Im) complex in the 1300 - 1675 cm^{-1} region in dimethyl sulfoxide (DMSO) solvent matrix at low temperatures obtained with 441.6 nm excitation line. Figure 5.1A shows the RR spectral pattern in the 1300 - 1675 cm^{-1} region at 50K. The frequency positions for the various marker bands are found to be distinctly different from the usual reduced iron porphyrin complexes.[8-10] The most prominent feature in the spectral region is due the oxidation state marker band which appeared at 1363 cm^{-1}. This frequency is distinctly different from that expected for a five-coordinated, high spin oxidized or reduced species for which the ν_4 mode is generally observed at 1372 and 1355 cm^{-1} respectively for the FePP(1,2-Me_2Im) complexes.[7,13] The ν_3 mode appears at 1495 cm^{-1}. The bands corresponding to the ν_2 and ν_{10} modes also broaden which indicate probable coexistence of more than one species at low temperature. At relatively higher temperature of 75K, the spectral pattern corresponding to the various marker bands ν_4, ν_3, ν_2 and ν_{10} are identical to that in Figure 5.1A. At 125K the spectral pattern deviates from the previous spectra in the ν_2 region, as shown in Figure 5.1B. The relative

intensity of the ν_{37} mode at 1580 cm^{-1} becomes higher than that of the ν_2 mode at 1561 cm^{-1}. The band at 1571 cm^{-1} either disappears or is overlapped by the more intense band at 1580 cm^{-1}. Another important observation is the decrease in the bandwidth (FWHM) of the ν_4 mode (1363 cm^{-1}) from 22 cm^{-1} (Figure 5.1A) to 15 cm^{-1}. This bandwidth shows once again an increase in value to 20 cm^{-1} at 175K (Figure 5.1C), with simultaneous observation of two bands in the ν_3 region at 1495 and 1471 cm^{-1}. This observation once again indicates the presence of two different species. At relatively higher temperature of ~250K, the position of all the marker bands correspond to a completely photo-reduced, five-coordinated high-spin $Fe^{II}PP(1,2\text{-}Me_2Im)$ complex as shown in Figure 5.1D. At room temperature, remarkably different spectral pattern is observed that correspond to the partially photo-reduced and partially oxidized five-coordinated, high spin iron porphyrin complexes (Figure 5.1E).

Figure 5.2 shows the Raman spectra in the low frequency region around $Fe\text{-}N_{Im}(1,2\text{-}Me_2Im)$ stretching mode for the corresponding situations of Figure 5.1. The $Fe\text{-}N_{Im}(1,2\text{-}Me_2Im)$ stretching band is observed at 195 cm^{-1} with a medium intensity at 175K (Figure 5.2C) while it is absent at lower temperatures. The intensity of this band increases on increasing the temperature with concomitant increase in the yield of the five-coordinated photo-reduced $Fe^{II}PP(1,2\text{-}Me_2Im)$ complex without showing any change or shift in the position within experimental errors.

In order to understand the specific role of alcohol on the yield of photo-reduction of iron porphyrin complexes at room temperature, we have performed a systematic resonance Raman study on the yield of photo-reduction of iron protoporphyrin complexes with 2-MeIm as axial ligand in different solvents.

Figure 5.3 shows the RR spectra of FePP(2-MeIm) in a variety of solvents under anaerobic conditions. As is evident from Figure 5.3, only partial photo-reduction occurs in pure solvents like DMSO (Figure 5.3F), acetone (Figure 5.3D), dimethyl-formamide (Figure 5.3E) and ethyl acetate (Figure 5.3C). Where as no photo-reduction is observed in other pure solvents like acetonitrile (Figure 5.3A), in mixed solution of tetrahydrofuran and dichloromethane (Figure 5.3B) also in carbon disulphide and in dichloromethane (spectra not shown). The yield of photo-reduction is not possible to correlate with any of the known expression involving solvent parameters like dielectric constant, polarity, viscosity, refractive index but it appears to be a complicated function of all these parameters. The corresponding low frequency region from 100 - 500 cm^{-1} is shown in Figure 5.4.

Figures 5.5 and 5.6 show the RR spectra of photo-reduced $Fe^{II}PP(2\text{-MeIm})$ complex containing varying quantity of methanol in the same solution as used for Figures 5.3 and 5.4 in the 1300 - 1675 cm^{-1} and 100 - 500 cm^{-1} regions respectively. Figure 5.5A shows the RR spectra of FePP(2-MeIm) in acetonitrile containing $\sim$5% v/v MeOH in anaerobic condition. The spectrum

corresponds to the totally photo-reduced five-coordinated high spin species. The corresponding Fe-N_{Im}(2-MeIm) stretching region is shown in Figure 5.6A. Figures 5.5 and 5.6 show that complete photo-reduction can take place irrespective of the nature of solvent (provided the iron protoporphyrin is soluble in that solvent) if it contains a small quantity of primary alcohol. Therefore, the importance of alcohol in the photo-reduction of iron porphyrins is once again demonstrated.

5.4 Discussion

The observation of unusual frequency pattern for the various marker bands in the low temperature RR spectra of FePP(1,2-Me_2Im) in DMSO matrix in Figure 5.1 has prompted us to identify the nature of the species present at such temperatures more carefully. The oxidation state (ν_4) and spin state (ν_3) marker bands appear at 1363 cm^{-1} and 1495 cm^{-1} respectively. The other spin state and coordination state marker bands appear at 1561, 1571 cm^{-1} and 1617, 1605 cm^{-1}. None of this set of RR bands corresponds to any single known five-coordinated oxidized or reduced species.[7,13] Thus, in order to characterize these bands, we have recorded the RR spectrum of chemically reduced Fe^{II}PP-(1,2-Me_2Im) using solid sodium dithionite in DMSO at low temperature (50K) (Figure 5.1F). Table 5.1 gives the position of various marker bands obtained from RR spectra of FePP under different chemical and physical conditions. The spectral features broadly coincided with those in Figures 5.1A and 5.2A. This

comparative study thus indicate the photo-reducibility of $Fe^{III}PP(1,2\text{-}Me_2Im)$ at low temperatures where the matrix formed by DMSO at ~50K becomes soft due to absorption and heating of the laser light . The oxidation state and spin state marker bands at 1363 and 1495 cm^{-1} correspond to the photo-reduced species. However, in a frozen solid matrix of $FePP(1,2\text{-}Me_2Im)$ in DMSO at 20K, the RR spectrum obtained with much lower (~ 5 mW) laser power indicates almost no photoreduction. Moreover, the absence of any band around 195 cm^{-1} in the photoreduced or chemically reduced species at 50K, indicate the absence of five coordinated $Fe^{II}PP$ complex with $1,2\text{-}Me_2Im$ at the fifth ligand position. It is possible that 195 cm^{-1} band may not be observable due to the formation of bis-ligated species of $1,2\text{-}Me_2Im$ resulting into low spin complex. One such case has been observed in a temperature dependent magnetic moment study in "pocket" porphyrin with 1-MeIm as axial ligand by Mossbauer spectroscopy.[14] But no such spin state change has been reported with highly sterically hindered ligand like $1,2\text{-}Me_2Im$. The absence of detectable low-spin species formation was reported in the case of 2-MeIm with iron porphyrin complexes from low temperature ESR[15] and Mossbauer[16] investigations. The validity of this result was again tested by *LaMar et al*[17] using NMR technique where no low spin species were detected with sterically hindered $1,2\text{-}Me_2Im$ ligand. From our RR study and known marker bands, we have not detected formation of any such low spin complexes. We have also performed similar temperature dependent RR experiments with 2-MeIm as axial ligand

and the spectral pattern is almost identical to that with 1,2-Me_2Im thereby ruling out the possibility of bis-ligation of either 2-MeIm or 1,2-Me_2Im within 100 mM concentration range used in all these studies. The chemically reduced $Fe^{II}PP$ in DMSO in the presence of 1,2-Me_2Im has also indicated the replacement of 1,2-Me_2Im from its axial ligand position by DMSO in the soft matrix at low temperature of ~50K. The chemically reduced $Fe^{II}PP$ in DMSO in the absence of nitrogenous bases like 1,2-Me_2Im at 50K shows Raman bands, Figure 5.1F, as observed under similar experimental conditions of Figure 5.1A and 5.2A. The same chemically reduced solution at room temperature in the presence of 1,2-Me_2Im gives a set of RR bands assignable to a five coordinated, high spin, reduced species. Table 5.1 shows different RR marker bands at various temperatures in the chemically reduced species with or without nitrogenous ligands and also $Fe^{III}PP(Cl)$ in DMSO. Thus at low temperature at ~50K (Figure 5.1A and 5.2A) both the axial ligand positions of iron(II)porphyrin are most likely occupied by DMSO molecules. Coordination of DMSO at both the axial positions had been reported in an NMR study by *LaMar et al*[18] in FeTPP(Cl) complex. In a recent study, *Spiro et al*[19] have associated the ν_4 mode at 1365 cm^{-1} in the chemically reduced FePPDME in DMSO with a reduced, intermediate spin and six coordinated species with DMSO occupying both the ligation positions. Based on these considerations, we therefore, characterized the predominant photo-reduced species in the soft matrix showing marker bands

ν_4, ν_3, ν_2 and ν_{10} at 1363, 1495, 1560 and 1605 cm^{-1} respectively as the reduced, intermediate spin,[10b,20] six coordinated, $Fe^{II}PP(DMSO)_2$. The observation of an extra band at 1571 cm^{-1} and a broad ν_{10} mode at 1617 cm^{-1} alongwith an increased band width of the ν_4 mode (22 cm^{-1}, FWHM) at 50K (Figure 5.1A) indicates simultaneous occurrence of another species alongwith the dominant $Fe^{II}PP(DMSO)_2$ complex. The RR spectrum of $Fe^{III}PP$ in pure DMSO at 50K (Table 5.1) did not show any of these bands and thereby ruling out the presence of $Fe^{III}PP(DMSO)_2$ complex. Thus, we attribute these additional features due to presence of either the $Fe^{III}PP(1,2\text{-}Me_2Im)$ species or $Fe^{III}PP(1,2\text{-}Me_2Im)$ species with very weakly bound DMSO at the vaccant sixth ligand position[7,9], which may be very unlikely due to steric interaction with $1,2\text{-}Me_2Im$.

On gradual increase of temperature upto 125K (Figure 5.1B) all the spectral features remained unaltered, except for the decrease in the band width of the ν_4 mode (15 cm^{-1}, FWHM) and enhanced relative intensity of the ν_{37} (E_u) mode at 1580 cm^{-1}. The enhanced intensity of the ν_{37} mode of E_u symmetry in iron protoporphyrin complexes may be the result of asymmetric disposition of vinyl groups which may experience larger distortions at low temperatures and thereby destroy the inversion centre of the chromophore inducing Raman activity for the infrared active modes (E_u in D_{4h} symmetry).[1b] The RR spectra of chemically reduced $Fe^{II}PP(1,2\text{-}Me_2Im)$ in soft DMSO at low temperature (125K), infact coincides exactly in frequency

positions and relative intensities of the ν_4, ν_3, ν_2 and ν_{10} modes with the photoreduced spectrum shown in Figure 5.1B. Thus at this temperature the spectral pattern corresponds to only the photo-reduced, intermediate spin, $Fe^{II}PP(DMSO)_2$ complex and hence complete photoreduction occur at temperature around 125K (Figure 5.1B). At higher temperature of ~175K, where matrix is relatively much softer, change in axial ligation is observed with concomitant observation of the $\nu_{Fe-N_{Im}}$ (1,2-Me_2Im) stretching band at 195 cm^{-1} (Figure 5.2C) along with increase in band width of the ν_4 mode at 1363 cm^{-1} (~20 cm^{-1},FWHM) as shown in Figure 5.1C. The observation of the $Fe-N_{Im}$ band suggests gradual replacement of DMSO from its coordination position by 1,2-Me_2Im and this conversion becomes complete at 250K (Figure 5.1D and 5.2D) in the cold solution. The photo-reduced species corresponds to a high-spin, five coordinated $Fe^{II}PP$(1,2-Me_2Im) complex. The same solution at room temperature showed spectral features that are indicative of a mixture of five coordinated high-spin, oxidized and reduced FePP(1,2-Me_2Im) complexes. The same solution containing a trace amount of alcohol (0.1% v/v) showed complete photoreduction in DMSO at room temperature where as the presence or absence of alcohols gave identical spectral pattern at low temperatures.

The role of alcohol was also observed in our previous RR study on the mechanism of photo-reduction of iron porphyrins.[22]

We have observed partial photoreduction of iron porphyrins in the presence of electron donors like 2-MeIm under anaerobic conditions in pure solvents like acetone, ethylacetate, dimethylformamide, dimethylsulfoxide etc., at room temperature without alcohol as shown in Figure 5.3 and 5.4. It was not possible to explain the yield of photoreduction using known formulations such as Marcus parameter γ,[22] Gutmann acceptor number[23] etc., involving complex solvent parameters like dielectric constant, refractive index, viscosity and polarizability. Thus the extent of photoreduction appears to be a more complicated process in different solvents. However, irrespective of the nature of the solvent, addition of a trace amount of alcohol gives fully reduced $Fe^{II}PP(2\text{-MeIm})$ complex under anaerobic conditions by excitation in the Soret region. In order to elucidate the reaction mechanism of $Co^{II}(PP)X$ with axial ligands like 3-Chloropyridine, 2-MeIm etc., in protic solvents, *Pavlovic et al*[24] have recently suggested a reversible binding of alcohol to facilitate binding of nitrogenous ligands by displaying halide ion from the coordination sphere of metal-porphyrins. Based on these considerations, we propose the following mechanism for binding of axial ligands like 2-MeIm, 1,2-Me_2Im where primary alcohols at very low concentrations(.01% v/v) act as "directing ligands"

$$Fe^{III}PP(Cl) + ROH \rightleftharpoons Fe^{III}PP(ROH) + Cl^- \qquad ----5.1$$

$$Fe^{III}PP(ROH) + 2\text{-MeIm} \longrightarrow Fe^{III}PP(2\text{-MeIm}) + ROH \qquad ----5.2$$

The partial photoreduction observed in some pure solvents like acetone, ethyl acetate, dimethylformamide and DMSO with 2-MeIm thus appears to depend upon the ability of these solvents to displace halide ion from the coordination sphere of iron either by ion-pair separation or by a similar mechanism as shown in Eqn. 5.1 and 5.2. Protic solvents like primary or secondary alcohols are therefore found to be most effective in displacing halide ion by acting as directing ligands.

The temperature-dependent photoreduction results on $Fe^{III}PP(1,2\text{-}Me_2Im)$ in DMSO solvent can be understood and rationalized as follows:

In liquid solution at room temperature, the laser excitation in the Soret region excites the $Fe^{III}PP(1,2\text{-}Me_2Im)$ system to the antibonding state where the coordinated $1,2\text{-}Me_2Im$ dissociates donating its charge to the iron atom.[22] The yield of photoreduction is expected to increase with the increase in the polarity of the solvents which help in the solvent-induced dissociation of ion-pairs created by electron transfer. However, the yield of photoreduction also depends on the power density of irradiation which decreases due to fast diffusion of molecules at room temperature resulting in only partial photoreduction. As the temperature is decreased to $\sim$250K, molecular motion becomes restricted which may result in higher effective power density at the sample and almost complete photoreduction. The coordinated $1,2\text{-}Me_2Im$ dissociates in the excited state donating its charge to

the iron atom, the $(1,2\text{-}Me_2Im)^+$ diffuses away and another molecule of $1,2\text{-}Me_2Im$ from the solution is attached to the iron giving rise to the $Fe^{II}PP(1,2\text{-}Me_2Im)$ complex as the photoreduced species. As the temperature is further reduced to $\sim$50K, a glassy solid matrix is obtained. However, the absorption of laser light raises the temperature of the matrix converting it to a soft matrix in which the molecular motion becomes further restricted and viscosity of the medium increases considerably. The laser irradiation and subsequent photoreduction results in the charge separated electron transfer products and the solvent reorganization around the solvent-separated ion pairs stabilizes the electron-transfer products. The steady state charge separation is maintained as the concentration of the photostationary state increases dramatically with decrease in temperature. The laser irradiation of the $Fe^{III}PP(1,2\text{-}Me_2Im)$ complex in the DMSO soft and viscous matrix conditions produces solvent separated $Fe^{II}PP$ and $1,2\text{-}Me_2Im^+$ ion-pairs. The diffusion of $1,2\text{-}Me_2Im^+$ is severely restricted and DMSO molecules in the vicinity of the iron coordinate at the fifth and sixth ligand positions producing intermediate spin, reduced $Fe^{II}PP(DMSO)_2$ species as the photoreduced product. Due to restricted diffusion of $1,2\text{-}Me_2Im^+$, back electron transfer reaction also takes place giving rise to the $Fe^{III}PP(1,2\text{-}Me_2Im)$ species, as observed. When the temperature is reduced further to $\sim$20K and lower laser power ($\sim$5 mW) is used maintaining rigid solid matrix, the solvent reorganization and diffusion of dissociated

1,2-Me_2Im is not possible with the result that no photoreduction is observed. These observations give strong support for short-range electron transfer process as the dominant mechanism during photoreduction and the long-range quantum mechanical electron tunneling process is insignificant. The non-photoreducibility of Fe^{III}PP(1,2-Me_2Im) in the soft DMSO matrix by excitation in the α-β absorption region once again support our conclusions that the charge-transfer process is coupled to Soret electronic transitions.

We can summarize our results as follows:

1. We have observed photoreduction and axial ligation changes for Fe^{III}PP(1,2-Me_2Im) complex in DMSO matrix at low temperatures. In the solid rigid matrix at ~20K, diffusion of charged species is improbable and back electron transfer takes place without any photoreduction. This supports short-range electron transfer process responsible for photoreduction.

2. As the temperature is increased to ~100K, absorption of laser light warms up the glassy material converting it into a soft matrix. Laser irradiation of Fe^{III}PP(1,2-Me_2Im) complex in DMSO produces solvent separated Fe^{II}PP and $(1,2\text{-}Me_2Im)^+$ ion pairs and solvent reorganization around the ion pairs produces $Fe^{II}PP(DMSO)_2$ as well as Fe^{III}PP(1,2-Me_2Im) due to back electron transfer.

3. At relatively higher temperature of ~250K, the molecular motion becomes comparatively easier. The coordinated (1,2-Me_2Im) donates it electron to iron and diffuses away while another molecule of (1,2-Me_2Im) from solution coordinates to iron giving reduced $Fe^{II}PP(1,2\text{-}Me_2Im)$ complex.

4. At room temperature, the laser excitation in the Soret region excites the system where the coordinated (1,2-Me_2Im) dissociates in the excited state donating its charge to the iron atom. The yield of photoreduction appears to depend on the polarity of the solvents which facilitate the solvent-induced dissociation of ion-pairs created by electron transfer.

These low temperature studies lend strong support to our proposed mechanism of photoreduction of iron-porphyrins as discussed in Chapter - IV.

References

1a. Drabkin, D.L. in *"The Porphyrins"*, Dolphin, D. Ed., Academic Press, New York, Vol. I, p. 29, 1978.

b. Spiro, T.G. in *"Iron Porphyrins"*, Lever, A.B.P.; Gray, H.B., Eds., Addison Wesley, M.A. Part II, p. 89, 1983.

2a. Bartocci, C.; Maldotti, A.; Traversso, O.; Bignozzi, C.A.; Carassitti, V. *Polyhedron*, 2, 97, 1983.

b. Bartocci, C.; Scandala, F.; Ferri, A.; Carassitti, V. *J. Am. Chem. Soc.* 102, 7067, 1980.

c. Bizet, C.; Morliere, P.; Brault, D.; Delgado, O.; Bazin, M.; Santus, R. *Photochem. Photobiol.* 34, 315, 1981.

3a. Kim, D.; Miller, L.A.; Rakhit, G.; Spiro, T.G. *J. Phys. Chem.* 90, 3320, 1986.

b. Lexa, D.; Momenteau, M.; Mispelter, J. *Biochem. Biophys. Acta* 338, 151, 1974.

c. Wolberg, A. *Isr. J. Chem.* 12, 1031, 1974.

d. Bottomely, L.A.; Kadish, K.M. *Inorg. Chem.* 20, 1348, 1981.

4a. Maldotti, A.; Bartocci, C.; Amadelli, R.; Carassitti, V. *Inorg. Chemica. Acta.* 74, 275, 1983.

b. Imamura, T.; Jin, T.; Suzuki, T.; Fujimoto, M. *Chem. Lett.* 847, 1985.

5a. Kitagawa, T.; Orii, Y. *J. Biochem. (Tokyo)* 84, 1245, 1978.

b. Salmeen, I.; Rimai, L.; Babcock, G.T. *Biochemistry*, 17, 800, 1978.

c. Kitagawa, T.; Nagai, K. *Nature*, 281, 503, 1979.

5d. Yoshikawa, S.; Mochizuki, H.; Chihara, S.; Hogihara, B.; Kitagawa, T. *Biochim. Biophys. acta.* 786, 267, 1984.

6. Ozaki, Y.; Iriyama, K.; Ogoshi, H.; Kitagawa, T. *J. Am. Chem. Soc.* 109, 5583, 1987.

7a. Spiro, T.G.; Strekas, T.C. *J. Am. Chem. Soc.* 96, 338, 1974.

b. Yamamoto, T.; Palmer, G.; Gill, D.; Salmeen, I.T.; Rimai, L. *J. Biol. Chem.* 248, 5211, 1973.

c. Choi, S.; Spiro, T.G.; Langry, K.C.; Smith, K.M.; Budd, D.L.; LaMar, G.N. *J. Am. Chem. Soc.* 104, 4345, 1982.

d. Choi, S.; Spiro, T.G.; Langry, K.C.; Smith, K.M. *J. Am. Chem. Soc.* 104, 4337, 1982.

8a. Spiro, T.G. *Biochim. Biophys. Acta.* 416, 169, 1975.

b. Felton, R.H.; Yu, N.T. in *"The Porphyrins"*, Dolphin, D. Ed., Academic Press, New York, Vol. III, Ch. III, 1978.

c. Kitagawa, T.; Ozaki, Y.; Kyogoku, Y. *Adv. Biophys.* 11, 153, 1978.

9. Kitagawa, T.; Ozaki, Y. in *"Structure and Bonding"*, 64, 71, 1987.

10a. Verma, A.L.; Bernstein, H.J. *J. Raman Spectrosc.* 2, 163, 1974.

b. Spiro, T.G.; Burke, J.M. *J. Am. Chem. Soc.* 98, 5482, 1976.

c. Kitagawa, T.; Ogoshi, H.; Watanabe, E.; Yoshida, Z. *J. Chem. Phys. Letts.* 30, 451, 1975.

d. Kitagawa, T.; Ogoshi, H.; Watanabe, E.; Yoshida, Z. *J. Phys. Chem.* 79, 2629, 1975.

10e. Burke, J.M.; Kincaid, J.R.; Spiro, T.G. *J. Am. Chem. Soc.* 100, 6077, 1978.

f. Kitagawa, T.; Abe, M.; Kyogoku, Y.; Ogoshi, H.; Watanabe, E.; Yoshida, Z. *J. Phys. Chem.* 80, 1181, 1976.

g. Spaulding, L.D.; Chang, C.C.; Yu, N.T.; Felton, R.H. *J. Am. Chem. Soc.* 97, 2517, 1975.

11a. Fuhrhop, J.H.; Smith, K.M. in *"Porphyrins and Metalloporphyrins"*, Smith, K.M. Ed., American Elsevier, New York, p. 835, 1975.

b. Ogoshi, H.; Sugimoto, H.; Yoshida, Z. *Bull. Chem. Soc. Jpn.* 54, 3414, 1981.

12. Hendra, P.J.; Loader, E.J. *Chem. Ind. (London)* 7, 18, 1968.

13a. Kitagawa, T.; Abe, M.; Ogoshi, H. *J. Chem. Phys.* 69, 4516, 1978.

b. Abe, M.; Kitagawa, T.; Ogoshi, H. *J. Chem. Phys.* 69, 4526, 1978.

14. Collman, J.P.; Brauman, J.I.; Collins, T.J.; Iverson, B.L.; Lang, G.; Pettman, R.B.; Sessler, T.L.; Walters, M.A. *J. Am. Chem. Soc.* 105, 3038, 1983.

15. Peisach, J.; Blumberg, W.E.; Adler, A. *Ann. N. Y. Acad. Sci.* 206, 310, 1973.

16. Straub, D.K.; Conner, W.M. *Ann. N. Y. Acad. Sci.* 206, 383, 1973 .

17. Satterlee, J.D.; LaMar, G.N.; Frye, J.S. *J. Am. Chem. Soc.* 98, 7275, 1976.

18. Zobrist, M.; LaMar, G.N. *J. Am. Chem. Soc.* 100, 1944, 1978.

19. Anzenbacher, P.; Evangelista-Kirkup, R.; Schenkman, J.; Spiro, T.G. *Inorg. Chem.* 28, 4491, 1989.

20. Teraoka, J.; Kitagawa, T. *J. Phys. Chem.* 24, 1928, 1980.

21a. Verma, A.L.; Chaudhury, N.K.; Saini, G.S.S. in *"Recent Trends in Raman Spectroscopy"*, Banerjee, S.B.; Jha, S.S. Eds., World Scientific Pub. Co., Singapore, p. 192, 1989.

b. Verma, A.L.; Saini, G.S.S.; Chaudhury, N.K. *Proc. Ind. Acad. Sci. (Chem. Sci.)* 102, 291, 1990.

c. Verma, A.L.; Chaudhury, N.K.; Saini, G.S.S. in *"XIIth International Conference on Raman Spectroscopy"*, Durig, J.R.; Sullivan, J.F. Eds., John Wiley and Sons, New York, P. 592, 1990.

d. Verma, A.L.; Chaudhury, N.K. *J. Raman Spectrosc.* (submitted)

22. Marcus, R.A.; Sutin, N. *Inorg. Chem.* 14, 213, 1975.

23a. Gutmann, V. *Electrochem. Acta.* 21, 661, 1976.

b. Gutmann, V. in *"The Donor-Acceptor Approach to Molecular Interactions"*, Plenum Press, New York, 1978.

24a. Pavlovic, D.; Asperger, S.; Domi, B. *J. Chem. Soc. Dalton Trans.* 2535, 1986.

b. Pavlovic, D.; Asperger, S.; Dokuzovic, Z.; Jurisic, B.; Ahmeti, X. *J. Chem. Soc. Dalton Trans.* 1095, 1985.

Table - 5.1

Comparison of various RR marker bands of iron protoporphyrin complexes under different chemical and physical environments.

Iron porphyrin complexes	$\nu_4(A_{1g})$	$\nu_3(A_{1g})$	$\nu_2(A_{1g})$	$\nu_{37}(E_u)$	$\nu_{10}(B_{1g})$	$\nu_{C=C}$ (Vinyl modes)	$\nu_{Fe-N_{Im}}$	Characterization[a]
$Fe^{III}PP(Cl)$ in DMSO at 50K	1370	1480	1561	1586	1610	1621	-	Six coordinated, oxidized, high spin.
$Fe^{III}PP(Cl)$ in DMSO at room temperature	1370	1481	1561	1585	1609	1621	-	Six coordinated, oxidized, high spin.
$Fe^{II}PP$, chemically reduced in DMSO (with 1,2-Me_2Im) at 50K	1364	1495	1561	1584	1625	Overlapped	-	Six coordinated, reduced, intermediate spin.
$Fe^{II}PP$, chemically reduced in DMSO (with 1,2-Me_2Im) at room temperature	1355	1470	1560	1584	1604	1620	195	Five coordinated, reduced, high spin.
$Fe^{II}PP$, chemically reduced in DMSO (with out 1,2-Me_2Im) at 50K	1364	1495	1560	1586	1625	Overlapped	-	Six coordinated, reduced, intermediate spin.
$Fe^{II}PP$, chemically reduced in DMSO (with out 1,2-Me_2Im) at room temperature	1355	1470	1562	1584	1604	1620	-	Five coordinated, reduced, high spin.

(a) The different species have been characterized in accordance with ref. No. 10, 19 and 20.

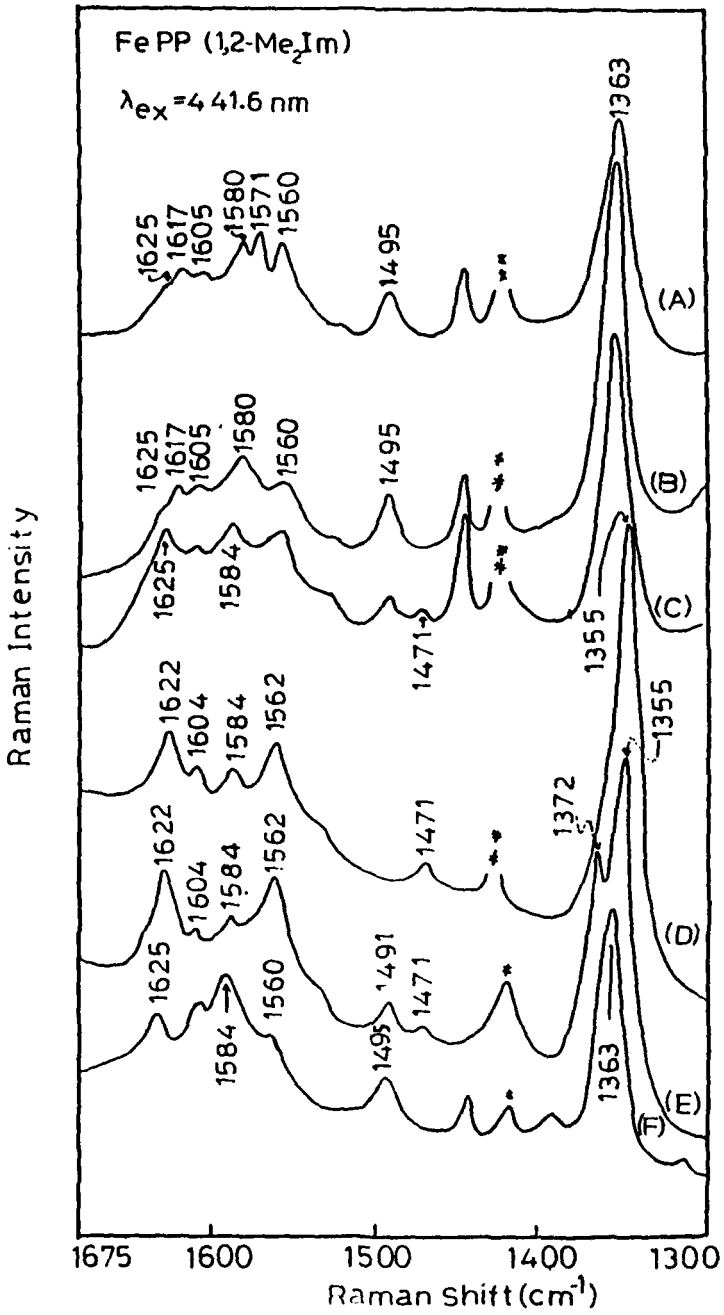

Fig. 5.1 RR spectra of FePP(1,2-Me_2Im) in DMSO matrix at low temperatures in the (1300 - 1675) cm^{-1} region. The concentration of FePP(1,2-Me_2Im) (0.5 mM) and 1,2-Me_2Im (50 mM) are kept constant for various temperatures: (A) 50K; (B) 125K; (C) 175K; (D) 250K and (E) room temperature. (F) At T = 50K, the chemically reduced Fe^{II}PP(1,2-Me_2Im) in DMSO. Experimental conditions: Excitation wavelength, 441.6 nm; Laser power 30 mW; Scan speed, 12 cm^{-1}/min.; Time constant, 2 sec.; Slit width, 200 μm; Sensitivity 1000, counts/sec. Plasma lines and solvent bands are marked by double and single asterisk respectively.

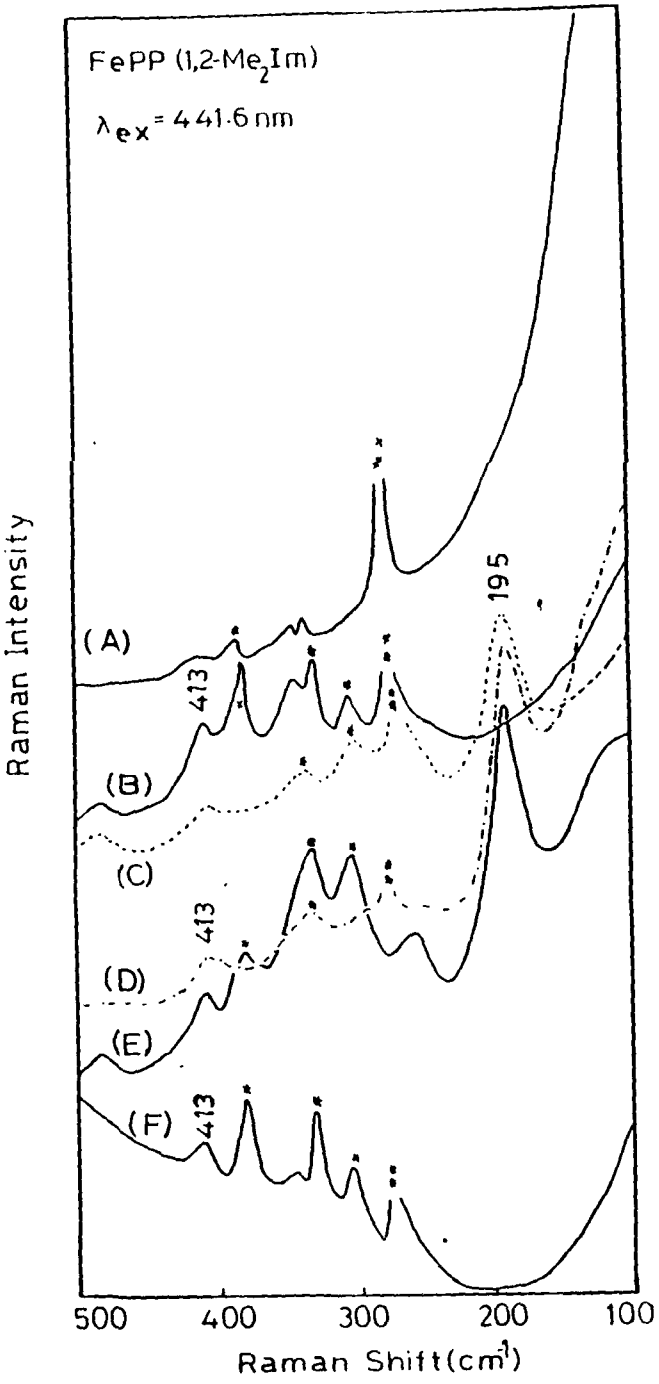

Fig. 5.2 RR spectra of FePP(1,2-Me_2Im) in DMSO matrix in the (100 - 500) cm^{-1} region, at various temperatures: (A) 50K; (B) 125K; (C) 175K; (D) 250K; (E) room temperature and (F) the chemically reduced species at 50K. All the experimental conditions are identical to that in Fig. 5.1, except for sensitivity, 500 counts/sec. Plasma lines and solvent bands are marked by double and single asterisk respectively.

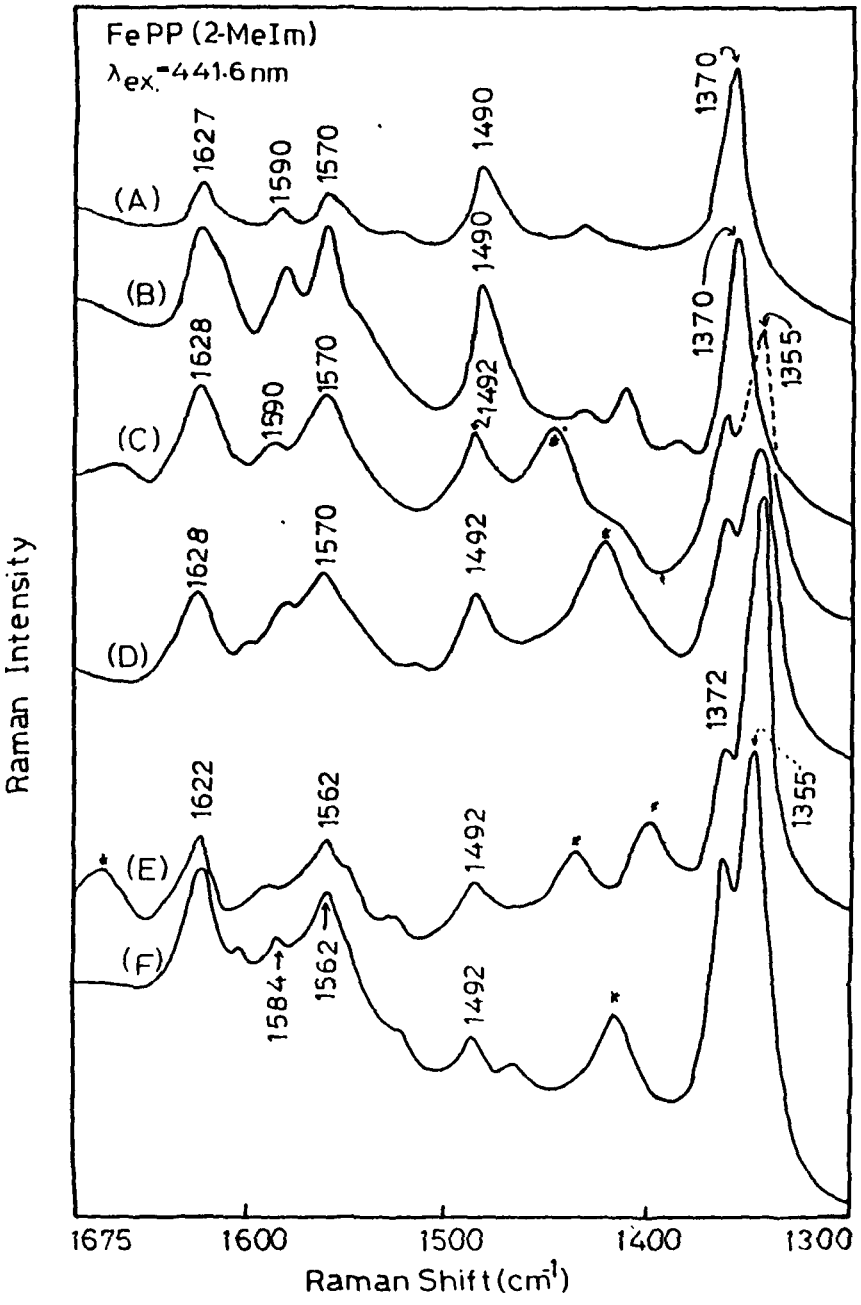

Fig. 5.3 RR spectra of FePP(2-MeIm) in different of solvents under anaerobic conditions in the (1300 - 1675) cm^{-1} region. The various solvents are (A) Acetonitrile; (B) 50:50 (v/v) mixture of Tetrahydrofuron and Dichloromethane; (C) Ethylacetate; (D) Acetone; (E) Dimethylformamide and (F) Dimethyl sulfoxide. All the experimental conditions are identical to Fig. 5.1. Respective solvent bands are marked by asterisk. Concentration of FePP and 2-MeIm are 0.5 mM and 50 mM respectively.

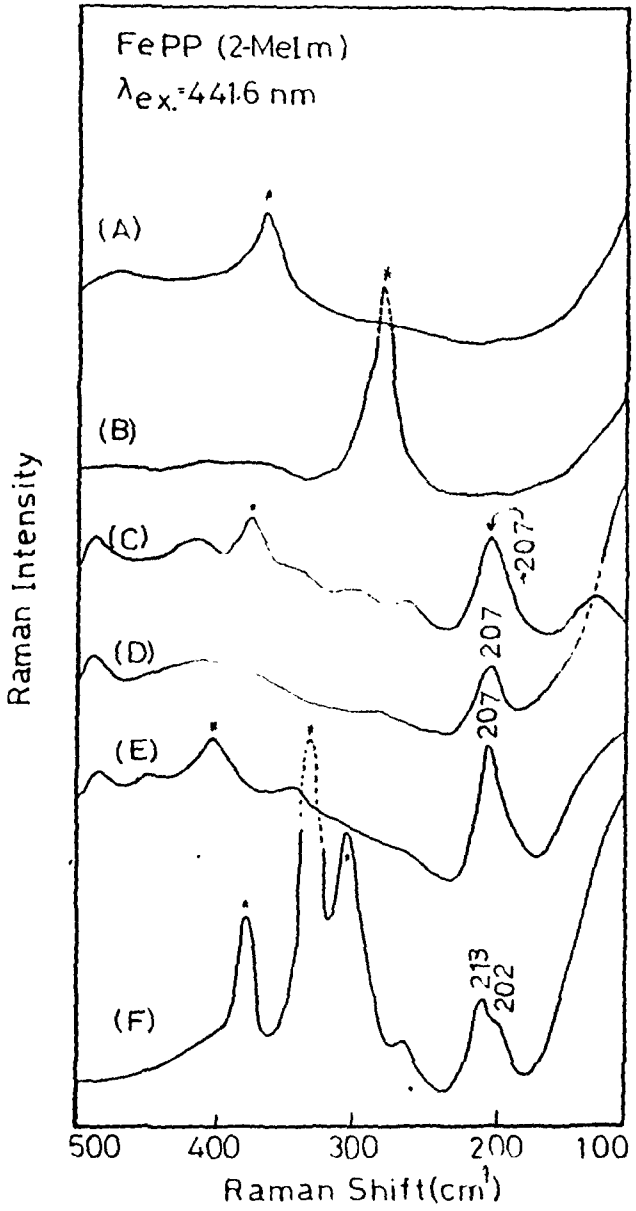

Fig. 5.4 RR spectra of FePP(2-MeIm) in the (100 - 500) cm^{-1} region under anaerobic condition in different solvents: (A) Acetonitrile; (B) 50:50 (v/v) mixture of Tetrahydrofuran and Dichloromethane; (C) Ethylacetate; (D) Acetone; (E) Dimethylformamide and (F) Dimethylsulfoxide. Experimental conditions are same as in Fig. 5.1 except for sensitivity as 500 counts/sec. Solvent bands are marked with asterisk.

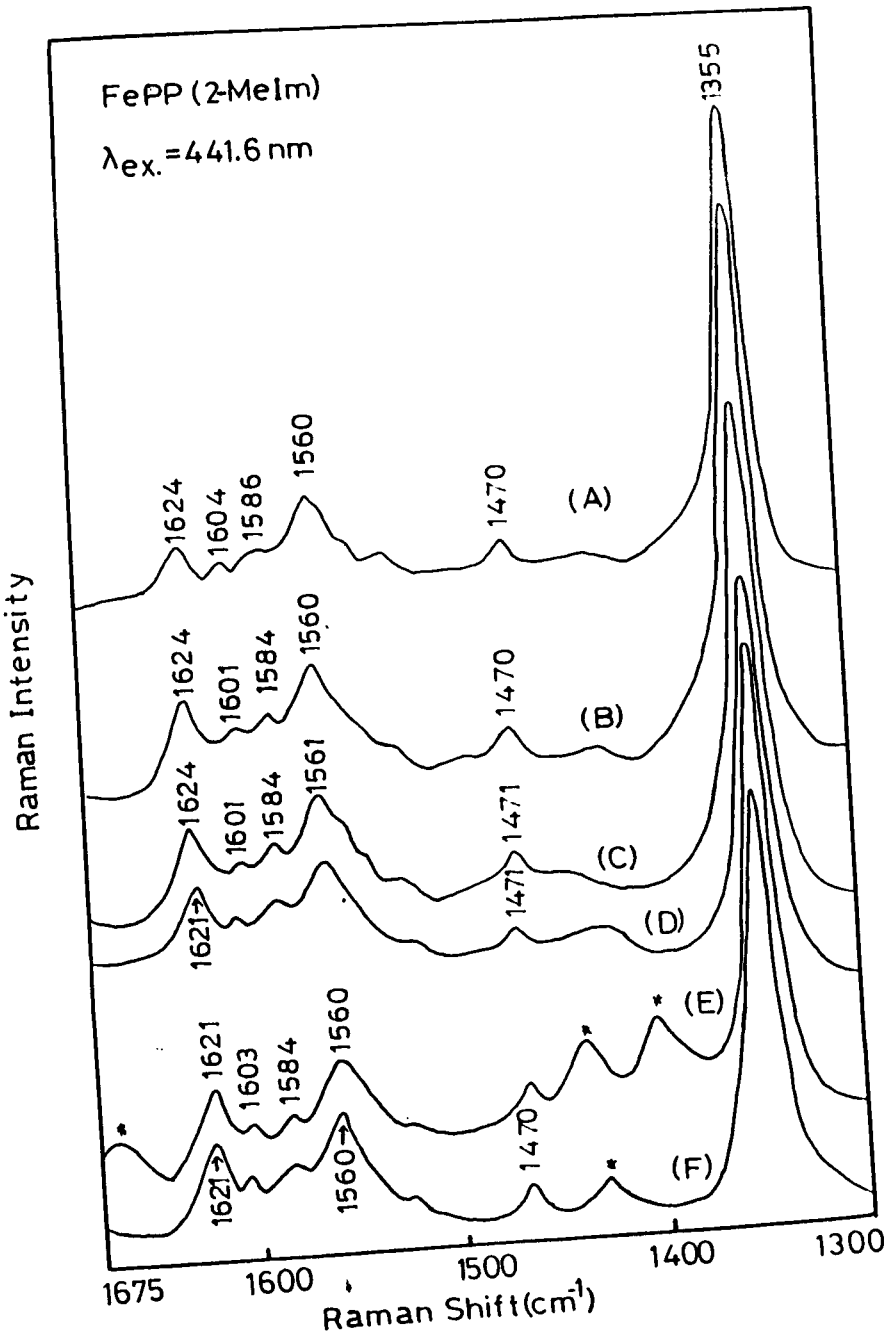

Fig. 5.5 RR spectra of the same FePP(2-MeIm) solutions used in Fig. 5.3 under similar experimental conditions in the (1300 - 1675) cm^{-1} region, containing trace amount (v/v) of methanol in respective solvents as (A) 5%; (B) 2%; (C) 2%; (D) 5%; (E) 2% and (F) 0.1%. Respective solvent bands are marked by asterisk.

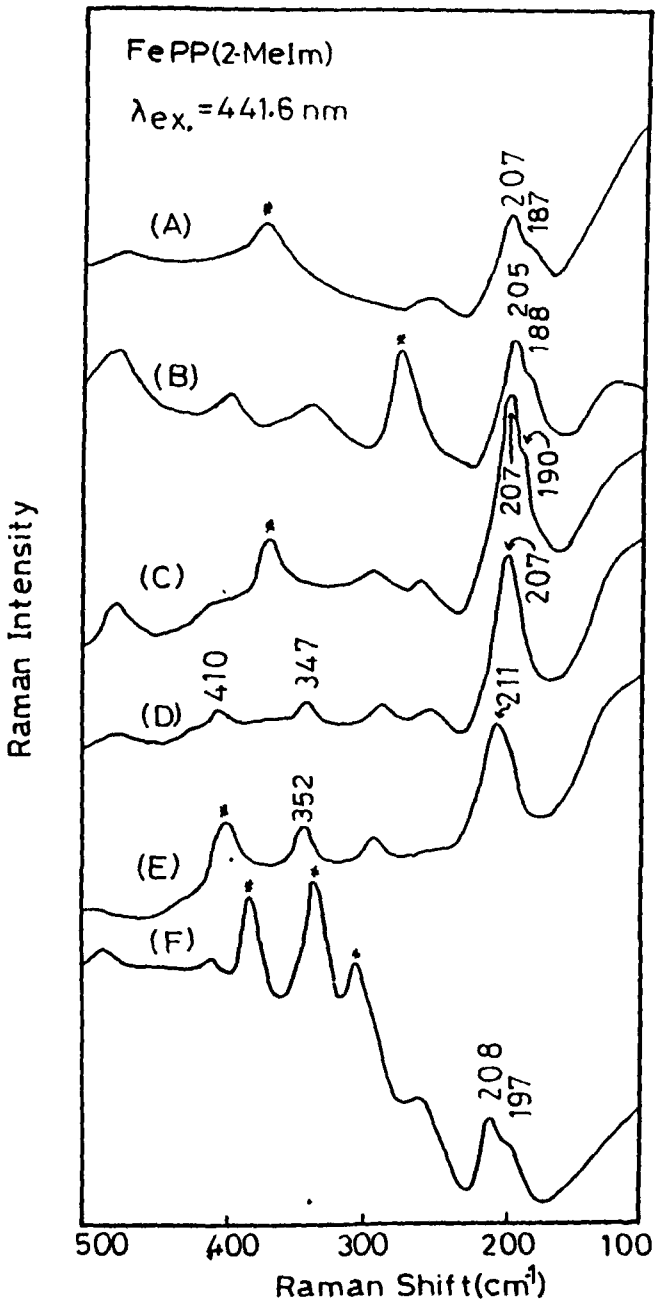

Fig. 5.6 RR spectra of the same FePP(2-MeIm) solution used in Fig. 5.5 in the (100 - 500) cm^{-1} region and under identical experimental conditions of Fig. 5.5 except for sensitivity 500 counts/sec. Asterisk denote respective solvent bands.

Nature of Iron-ligand Bond in Ferrous Iron-porphyrins Probed by Resonance Raman Scattering*

ABSTRACT

We report the concentration dependent resonance Raman (RR) studies of the Fe-N_{Im} stretching modes in the photo-reduced iron-octaethyl porphyrin [Fe^{II}OEP] and iron-protoporphyrin-IX dimethylester [Fe^{II}PPDME] complexes with 2-MeIm and 1,2-Me_2Im as axial ligands. The Fe-N_{Im} stretching modes in both the iron complexes have revealed two components due to co-existence of the upright and tilted configurations of the Fe-N_{Im} bond with respect to normal to the heme plane. The frequencies of the two components in both the complexes shift to higher side with an increase in concentration of 2-MeIm as axial ligand. With more sterically hindered 1,2-Me_2Im as axial ligand, the Fe^{II}OEP(1,2-Me_2Im) complex exists mainly with the tilted configuration of the Fe-N_{Im} bond while the upright configuration is the dominant species in the Fe^{II}PPDME(1,2-Me_2Im) complex. From the comparative study, we infer that the vinyl groups in the protoporphyrin complex play dominant role in non-bonded interactions with the sterically hindered axial ligands in stabilizing the specific configurations.

---

* Based on this study, the following paper has been communicated. (a) Chaudhury, N.K.; Saini, G.S.S.; Verma, A.L. *Inorg. Chem.* (submitted).

6.1 INTRODUCTION

Understanding the physico-chemical properties and reactivities of iron porphyrins is an area of great interest because of their active role in heme proteins. In most of the heme proteins, one of the coordination sites of the iron of heme acts as the binding site for active molecules such as O_2, CO etc. The other coordination site is occupied by amino acid residue, most often by an imidazole nitrogen of histidine residue. The state of the two axial ligands and the nature of iron-ligand bonds greatly influence the structure-function relationship in heme proteins. Resonance Raman (RR) spectroscopy has provided significant information about the active site of heme proteins[1] because of its structural specificity of vibrational frequencies.

In the present RR study made at higher resolution, we have focussed our attention on the iron-ligand stretching mode $\nu_{Fe-N_{Im}}$ of photo-reduced Fe^{II}OEP and Fe^{II}PPDME with varying concentrations of axial ligands like 2-methylimidazole (2-MeIm) and 1,2-dimethylimidazole (1,2-Me_2Im). This iron-ligand stretching mode ($\nu_{Fe-N_{Im}}$) has been well characterized by earlier workers.[2] In the subsequent studies on different model systems[3], it was observed that the position of the $\nu_{Fe-N_{Im}}$ mode varies under different conditions. The various explanations for understanding the causes for this variation are rather controversial. In some studies[3c] of hindered imidazole complexes

of Fe^{II}PPDME and Fe^{II}OEP, the variation was attributed due to H-bonding between the N_δ -H group of the imidazole and H-bond acceptor which could be another free imidazole itself; while *Champion et al*[4] have suggested its origin due to rotation of the tilted configuration of the ligated 2-MeIm or 1,2-Me_2Im. The importance of the changes in the frequency of the $\nu_{Fe-N_{Im}}$ stretching band in relation to quaternary structural changes from R to T states of hemoglobin were emphasized by several workers.[5] The careful monitoring of the changes in this stretching mode frequency will be of great help in understanding the iron-ligand interactions. In this study, we have monitored this band as a function of the concentration of axial ligands and have observed two components in the region of $\nu_{Fe-N_{Im}}$ stretching mode in the Fe^{II}PPDME and Fe^{II}OEP complexes. These two components have been suggested to arise from the upright and tilted configurations of the ligated 2-MeIm and 1,2-Me_2Im with respect to the normal to the heme plane. The larger shift for the Fe^{II}PPDME compared to the Fe^{II}OEP complex for the same concentrations of the 2-MeIm is suggested to arise from additional non-bonding interactions between the vinyl groups and imidazole ring alongwith contribution due to H-bonding of the N_δ -H group of 2-MeIm. With more sterically hindered ligand 1,2-Me_2Im we have observed a distinct influence of the vinyl groups in contributing towards non-bonding interactions where we have found that the upright configuration of the 1,2-Me_2Im ligand is favoured in the Fe^{II}PPDME complex while the configuration with

tilted 1,2-Me_2Im is a predominant species in the Fe^{II}OEP complex.

6.2 EXPERIMENTAL PROCEDURE

Fe^{III}PPDME(Cl) and Fe^{III}OEP(I) were synthesized in accordance with the procedure described elsewhere.[6] The 2-MeIm was recrystallized before use and 1,2-Me_2Im was used as received from Aldrich Chemical Co. All solvents were of spectroscopic grade and were used without further purification. All solutions were degassed with a fore pressure of 10^{-4} Torr using freeze and thaw cycles before Raman measurements unless otherwise stated. The Raman spectra were recorded in 90^{o} scattering geometry with a SPEX Ramalog 1403 triple monochromator equipped with a cooled RCA 31034 photomultiplier and photon counting arrangement. The spectrometer control and data processing were achieved with the help of a microprocessor based SPEX datamate. A Liconix model 4240 He-Cd laser (40 mW) was used as excitation source and Raman shifts were calibrated with CCl_4 lines.

As we have shown in our previous study[15], the photo-reduction of iron-porphyrins with 2-MeIm or 1,2-Me_2Im as axial ligands in pure CH_2Cl_2 under anaerobic conditions takes place only in the presence of trace amount of alcohols and in some other polar solvents, all the photo-reduction experiments in this study were carried out with a trace amount of methanol. The concentration of methanol was kept constant (~0.1% v/v) in the solution of iron-porphyrins for all the experiments.

6.3 RESULTS

Figure 6.1 shows the RR spectra of anaerobically photoreduced Fe^{II}OEP(2-MeIm) in CH_2Cl_2 with a trace amount (.1% v/v) of methanol in the 100-250 cm^{-1} and 1300-1400 cm^{-1} regions with 441.6 nm excitation line. We observe a prominent band at 206 cm^{-1} alongwith a shoulder around 190 cm^{-1} in the region of the $Fe-N_{Im}$ stretching mode.[7] When the concentration of the 2-MeIm is increased from 1 to 100 mM, the position of the two components varies from 204 to 211 cm^{-1}, and 190 to 196 cm^{-1} respectively. The 1300 - 1400 cm^{-1} spectral region shows the corresponding ν_4 mode for the oxidized (1374 cm^{-1}) and photo-reduced (1360 cm^{-1}) species, indicating the fraction of photo-reduced species.

Figure 6.2 shows the RR spectra in the 150-250 cm^{-1} and 1300 - 1400 cm^{-1} regions for the photo-reduced Fe^{II}PPDME(2-MeIm) under similar experimental conditions except for the concentrations of 2-MeIm as smaller quantities of 2-MeIm were required for the corresponding extent of photo-reduction shown in Figure 6.1 for FeOEP complexes. When the concentration of 2-MeIm is increased from 0.1 mM (Figure 6.2A) to 1mM (Figure 6.2B) the $\nu_{Fe-N_{Im}}$ stretching band shifts from 197 cm^{-1} to 201 cm^{-1}. At relatively higher concentrations of 2-MeIm (5 mM; Figure 6.2C), the $Fe-N_{Im}$ band appears at 202 cm^{-1} alongwith a weak shoulder at 186 cm^{-1}. When the concentration of 2-MeIm is further increased to 40 mM, (Figure 6.2E), both the bands shift upward to 205 cm^{-1} and 199 cm^{-1}. The higher frequency band showed gradual

increase in intensity but the lower frequency band did not change in its intensity. At higher concentration (100 mM) of 2-MeIm, the lower frequency shoulder is almost suppressed by the strong band at higher frequency. The magnitude of the shift in frequency of the bands in the $Fe\text{-}N_{Im}$ stretching region is, however, greater for the FePPDME(2-MeIm) complex than that observed for the FeOEP(2-MeIm) complex in the similar concentration range of 2-MeIm studied. The presence of two bands in the region of $\nu_{Fe\text{-}N_{Im}}$ stretching mode is further confirmed in the chemically reduced Im species, Figure 6.2H. Under aerobic conditions with higher concentration of 2-MeIm (100 mM), the spectral pattern changes as shown in Figure 6.2G showing three components at 199, 205 and 210 cm^{-1}. For each of the above concentrations of 2-MeIm, the corresponding ν_4 band has been shown in Figures 6.2A' to 6.2E'. The ν_4 band for the reduced species is observed at 1355 cm^{-1} without any detectable shift in its position.

We have performed similar experiments with more sterically hindered ligand like 1,2-Me_2Im where hydrogen bonding is not expected. Figure 6.3 gives the RR spectra of Fe^{II}OEP(1,2-Me_2Im) complex with different concentrations of 1,2-Me_2Im and the corresponding ν_4 band region is also shown. When the concentration of 1,2-Me_2Im is increased, we have observed an intense band at 186 cm^{-1} alongwith a shoulder at 207 cm^{-1} and their positions remained invariant with increase in concentration of axial ligand upto 100 mM. Figure 6.4 gives similar RR spectra of Fe^{II}PPDME(1,2-Me_2Im) complex with varying amounts of

1,2-Me_2Im. In this case, a strong band is observed at 194 cm^{-1} with a weak shoulder at 184 cm^{-1} whose position also remains invariant as the concentration of 1,2-Me_2Im is increased. Figure 6.5 gives RR spectra of Fe^{II}PP(2-MeIm) complex in the 100-250 cm^{-1} region at low temperatures. We have observed only single band at 216 cm^{-1} at 150K (Figure 6.5A) which shifts to 209 cm^{-1} at 250K (Figure 6.5C). This increase in frequency position at lower temperature (150K) is due to enhanced H-bonding between N_δ - position of ligated 2-MeIm of FePP(2-MeIm) complex and free 2-MeIm. The spectrum at room temperature (Figure 6.5D) shows doublet features at 197 and 208 cm^{-1}. We also observed a single band at 194 cm^{-1} in the low temperatures RR spectra of FePP(1,2-Me_2Im) complex without any frequency shift. The results for different complexes as a function of concentration of axial ligands are compared in the Table 6.1.

6.4 DISCUSSION

The electronic absorption spectra of FeOEP(I) and FePPDME(Cl) complexes in pure CH_2Cl_2 and after addition of 0.1% v/v methanol are found exactly identical. This rules out the possibility of coordination of methoxy radical in place of halide ion or at the vaccant sixth ligand position at this concentration of methanol. However, at much higher concentration of methanol (>10% v/v) the 640 nm charge-transfer band disappears and a new band at 595 nm in the absorption spectra grows in intensity indicating that the halide ion is replaced by methoxy radical.[8]

The hindered ligands like 2-MeIm and 1,2-Me_2Im upto 200mM concentration when added to a solution of 1mM concentration of FeOEP(I) or FePPDME(Cl) in CH_2Cl_2 with 0.1% v/v methanol replace halide ion forming five coordinate ferric high spin species as revealed by electronic absorption and RR spectra without any indication of six coordinated species.[2a,8,9] Moreover, all experiments were carried out under anaerobic conditions on freshly prepared solutions; the absence of a band around 363 cm^{-1} due to Fe-O-Fe symmetric stretch and other expected spectral changes in the RR and electronic absorption spectra in the Soret region did not indicate any presence of μ-oxo-bridged dimeric or higher aggregated species. On the other hand, the low spin or the oxidized high spin iron porphyrin complexes do not show Fe-axial ligand stretching modes in non-aqueous solutions with hindered ligands.[10] Therefore, the μ-oxo-bridged dimer or higher aggregates or six coordinated species can be ruled out as a possible source for the appearance of two bands in the Fe^{II}-axial ligand stretching region of these systems. If structures such as Fe-(2-MeIm)----(2-MeIm) and Fe-(2-MeIm) coexist in solution, one would expect the $\nu_{Fe-N_{Im}}$ band arising from the first structure to shift in frequency while the other component due to the second structure should be unaffected with change in concentration of the axial ligand. This is contrary to our observations ruling out this possibility for the doublet structure. There is yet another possibility of aggregation among the porphyrins mediated by H-bonding between the axial ligands

(structures like Fe-(2-MeIm)----(2-MeIm)-Fe) which may induce a component on the higher energy side of the $Fe-N_{Im}$ stretch due to the Fe-(2-MeIm) form even at the lowest concentration of the axial ligand. Observation of only one component at low concentration of 2-MeIm and a doublet structure with the non-hydrogen bonding 1,2-Me_2Im as axial ligand rules out this as a likely source for the appearance of two bands in the $Fe-N_{Im}$ stretching region. We have also detected two components at 188 and 201 cm^{-1} in the chemically reduced Fe^{II}PPDME(2-MeIm) complex.

Other possibility for the doublet structure in the $Fe-N_{Im}$ stretching frequency region may be due to Fermi Resonance between the $Fe-N_{Im}$ stretch and porphyrin mode or overtone/combination of some low frequency modes as suggested by *Collman et al.*[3a] The out of plane (oop) porphyrin modes are likely to be more effective in coupling with the $\nu_{Fe-N_{Im}}$ mode. In principle, the oop modes in RR scattering can be activated due to deviations in planarity of the porphyrin structure thereby coupling them with the porphyrin $\pi - \pi^*$ transitions. Recently, *Czernuszewicz et al*[11b] have assigned most of the low frequency skeletal and oop modes based on RR studies of the highly ruffled forms of NiOEP. An extremely weak feature is observed at 201 cm^{-1} in the tetragonal form of solid NiOEP (S_4 symmetry) by excitation in the Soret region (λ_{ex} = 406.7 nm) while no such feature is observable in the CH_2Br_2 solution (Fig. 6.7 in Ref. 11b). On the other hand, very weak and depolarized features at 202 and 212

cm^{-1} have been reported for the tetragonal form due to the ν_{34} (B_{2g} C_β-ethyl) and ν_{53}(E_u, Pyrrole transl.) in-plane skeletal modes respectively. The oop modes in the RR spectra of NiOEP have been identified at 230 and 127 cm^{-1} corresponding to the γ_{24}(E_g, $C_\alpha - C_m$) and γ_{17}(B_{2u}, C_β C_1) modes respectively none of which lie in the Fe-N_{Im} stretching region. The position of oop modes may be expected to vary with the porphyrin structure. As the γ_{24} mode of E_g symmetry involves contributions from $C_\alpha - C_m$ atoms, its frequency should differ for the iron complexes of the OEP and PocPiv- systems with similar axial ligands because of very different substituents at the C_m positions in the two cases. Observation of weak features centred around 200 cm^{-1} in both the systems makes it unlikely to associate them with the γ_{24} mode. In our study, we have found that both the components in the $\nu_{Fe-N_{Im}}$ region are polarized and therefore Fermi resonance with the depolarized in-plane porphyrin modes or with modes of symmetry species different from that of the Fe-N_{Im} mode in this frequency region can be ruled out. In the event of a Fermi Resonance[3a], the low frequency component at 187 cm^{-1} in the Fe^{II}PPDME(2-MeIm) would be expected to increase in intensity and shift to lower frequency on replacing 2-MeIm by 1,2-Me_2Im while the higher frequency band at 202 cm^{-1} for 2-MeIm should have been observed above 194 cm^{-1} in the corresponding 1,2-Me_2Im complex as the 202 cm^{-1} band for 2-MeIm complex is expected to shift down to 195 cm^{-1} for the 1,2-Me_2Im complex on the basis of mass effect. These predictions are contrary to our experimental

observations as is evident from Figures 6.2 and 6.4. Moreover, both the components in the $\nu_{Fe-N_{Im}}$ region show almost identical frequency shift to higher side with increase in concentration of 2-MeIm implying similar origin for both the components. As in the case of NiOEP, if the iron complexes also contain a range of coexisting ruffled structures in solution, then the presumed porphyrin skeletal mode around 200 cm^{-1} should have shown higher intensity with concomitant broadening of the ν_{10} mode at 1606 cm^{-1} with increase in ligand concentration. This was not observed in the present work. Moreover, any weak feature due to a porphyrin mode in the $\nu_{Fe-N_{Im}}$ region was expected to gain in intensity in the RR spectrum of the low temperature solidified sample. We did not observe any features in the solidified sample at 60K in the 180-250 cm^{-1} region. Instead, we have observed only a single band at 216 cm^{-1} (Figure 6.5A) at 150K in the soft matrix while the spectrum of the same solution at room temperature revealed the doublet structure (Figure 6.5D). Based on these considerations, similar upward frequency shifts for both the components of the $\nu_{Fe-N_{Im}}$ band in the iron OEP and PPDME complexes with increase in concentration of the 2-MeIm axial ligand, frequency-intensity pattern of the features etc., it is clear that the weak feature in the $Fe-N_{Im}$ stretching frequency region can not be associated with any of the porphyrin modes in Fermi resonance with the $\nu_{Fe-N_{Im}}$ band which should otherwise be also observable for the oxidized species of iron-porphyrin complexes with these ligands.

In order to ascertain the origin of the doublet structure in $\nu_{Fe-N_{Im}}$ region, we note that the high resolution X-ray Studies[12] on Im deoxyhemoglobin and myoglobin have indicated that the Fe-His bond is tilted off the normal to the porphyrin plane and the orientation is specified by the polar angle $\theta \sim 10^{o}$ for deoxy structure which decreases to $\sim 0^{o}$ upon oxygen binding. The azimuthal angle, ϕ is 15-25^{o} in the deoxy structure and decreases to a small value of 0^{o} upon oxygenation where the histidine plane eclipses the N_1 - N_3 axis (Figure 6.6). The other X-ray crystallographic study[14a] on $FeT_{piv}P$(2-MeIm).EtOH indicate that the imidazole unit is infact tilted off the normal to the porphyrin plane so as to accommodate the sterically hindered axial ligand. In a recent X-ray study on five coordinated mono(imidazole)iron(III)porphyrin complexes by *Scheidt et al*[14b], the $Fe-N_{Im}$ vector was found to be tilted off the porphyrin plane by 5^{o} in FeOEP(2-MeIm). There have been few more such studies[14c] on the FeTPP(2-MeIm) and FePF(2-MeIm) complexes where the $Fe-N_{Im}$ vector was found substantially tilted by 10.3^{o} and 9.6^{o} respectively.

Apart from these X-ray studies, quite a few spectroscopic studies have been performed with a view to ascertain the axial ligand plane orientation. The NMR studies[18a] on iron proto-porphyrin derivatives containing imidazole as axial ligands indicate specific rotational orientation of the axial ligands with respect to the normal to the porphyrin plane. In other NMR studies[18b,c] elongation of

the $Fe-N_{Im}$ bond or tilting of this bond from the vertical axis was suggested. However, the EPR studies of low spin Fe^{III}_{TPP} imidazole complexes[18d] could not detect any changes in the axial ligand plane orientation. The observation of large 'g' values in the different type of cytochrome model complexes b_T and b_K was again suggested to be due to tilted orientation of the axial ligands with respect to each other or porphyrin plane.[18d]

The time resolved Raman studies[13] of the deoxy R and T quaternary structures of hemoglobin have revealed a tilted configuration of the proximal histidine with respect to the normal to the heme plane in the T-state and the frequency of the iron-proximal histidine stretching mode, $\nu_{Fe-N_{Im}}$, increases in going from T to R state where the $Fe-N_{His}$ bond becomes nearly upright. An increase in the tilt angle would increase the non-bonded interaction between the $-CH_3$ group of the 2-MeIm and the pyrrole nitrogens or side chain substituents of the heme which would weaken the Fe-axial ligand bond. The two components in the $Fe-N_{Im}$ stretching frequency region show almost similar upward shift with increase in concentration of 2-MeIm and therefore we suggest that both the bands arise due to the $Fe-N_{Im}$ stretching mode. The stronger band at higher frequency is associated with the upright configuration while the lower frequency weaker component arises due to a tilted configuration of the $Fe-N_{Im}$ bond with respect to the normal to the heme plane and both configurations co-exist in solution. The energetically favourable configuration is stabilized in the low temperature solid form at

150K showing only a single band. The relative RR intensities of the two components in both the complexes in solution indicate that the upright configuration with 2-MeIm is the predominant species. The upward shift in frequency of the $\nu_{Fe-N_{Im}}$ modes with increase in concentration of 2-MeIm can be explained[3c] due to hydrogen-bonding of the ligated 2-MeIm to a H-bond acceptor which could also be the free 2-MeIm molecules present in the solution. The H-bonding would increase the electron donating propensity of the N_δ atom and thus strengthen the $Fe-N_{Im}$ bond.

Although the general features of the frequency shift of the $Fe-N_{Im}$ mode for the Fe^{II}PPDME(2-MeIm) complex are similar to that for the Fe^{II}OEP(2-MeIm) complex, its magnitude is much larger for the former ($\Delta_{Fe-N_{Im}} = 13\ cm^{-1}$) than for the later ($\Delta_{Fe-N_{Im}} = 7\ cm^{-1}$) complex in the same concentration range of axial ligands. This difference reflects additional contributions to frequency shift in the case of Fe^{II}PPDME(2-MeIm) complexe other than H-bonding effect. The asymmetric placement of vinyl groups in the protoporphyrin system with their out-of-plane orientation[16] would increase non-bonded repulsive interaction with the $-CH_3$ group of the imidazole ring thereby changing the tilt angle and the strength of the $Fe-N_{Im}$ bond. This interaction may be responsible for larger displacement of the iron atom from porphyrin plane for Fe^{II}PPDME(2-MeIm) compared to the case of Fe^{II}OEP(2-MeIm) complex[17] resulting in the expanded core size for the former complex and lower frequencies. In the

case of Fe^{II}PPDME(2-MeIm) complex, the weak feature at lower frequency due to a tilted configuration was observable with moderate concentration of 2-MeIm (5mM) and was not clear in the totally photo-reduced species (Figure 6.2E) indicating that the major species exist with the upright configuration. On the other hand, the Fe^{II}OEP(2-MeIm) complex shows a predominant band due to upright configuration along with a substantial contribution from the tilted configuration at slightly higher concentrations of 2-MeIm as is clear from Figures 6.1B-6.1E. The RR spectra of the aerobic solution of Fe^{II}PPDME(2-MeIm) (Figure 6.2G) show change in relative intensities of the bands and an extra feature at 205 cm^{-1} which may arise from μ-oxo-bridged or higher aggregated species.[15]

Further insight into the specific effects of side-chain substituents of the porphyrin ring is obtained by observation of the $Fe-N_{Im}$ stretching bands with more sterically hindered 1,2-Me_2Im as axial ligands. The RR spectra of Fe^{II}OEP(1,2-Me_2Im) complex given in Figures 6.3A to 6.3E show a strong band at 186 cm^{-1} due to tilted configuration alongwith a weaker component at 206 cm^{-1} due to upright configuration. Because of the symmetrically placed ethyl substituents at the porphyrin periphery, the ligated 1,2-Me_2Im favours a tilted configuration and the intensity of the $Fe-N_{Im}$ band due to this configuration increases with the increase in concentration of the axial ligand. Because of the absence of N_δ-H proton, there is no hydrogen bonding and therefore there is no variation in the frequency of

the $Fe-N_{Im}$ stretching mode with concentration of $1,2-Me_2Im$. The situation is, however, different in the Fe^{II}PPDME($1,2-Me_2Im$) complex. The enhanced non-bonded interactions between the vinyl groups at the porphyrin periphery and the methyl substituents of the axially ligated $1,2-Me_2Im$ restrict its orientation to an upright configuration giving rise to a strong RR band at 194 cm^{-1} due to $Fe-N_{Im}$ stretch with a weak shoulder at 184 cm^{-1} due to tilted configuration. In the totally photo-reduced species, Figure 6.4F, the lower frequency band due to tilted configuration disappears altogether indicating that only upright configuration is stabilized.

The frequencies of the ν_4 mode for the Fe^{II}OEP and Fe^{II}PPDME complexes have not shown any detectable shift with change in concentration of axial ligands and are observed at 1360 and 1355 cm^{-1} for the OEP and PPDME -complexes respectively with 2-MeIm or $1,2-Me_2Im$ as axial ligands. It is expected that the ν_4 and the $Fe-N_{Im}$ stretching mode frequencies would show opposite shift if the azimuthal angle Φ (Figure 6.6) varies due to change in orientation of the plane of the axial ligand with respect to the N_1 - N_3 line. A decrease in the angle ϕ would lead to a decrease in the electron density in the $\sigma^*_{Fe-N_{Im}}$ orbital because of increased overlap between the $\sigma^*_{Fe-N_{Im}}$ and π^*_{por} antibonding orbitals which would shift the $Fe-N_{Im}$ stretching mode towards higher frequency. The simultaneous increased electron density in the antibonding π^*_{por} orbitals would decrease the ν_4 mode frequency. In this study, we have not observed any such

variation in the ν_4 mode frequency with change in concentration of 2-MeIm which indicates that the azimuthal angle is greater than 25^{o} and does not vary with concentration of axial ligands.[4]

The main findings of the concentration dependent RR studies of the Fe-N_{Im} stretching modes in the FeOEP and FePPDME complexes with different axial ligands can be summarized as follows: We have observed two bands in the region of Fe-N_{Im} stretching modes in both the Fe^{II}OEP(2-MeIm) and Fe^{II}PPDME(1,2-Me_2Im) complexes due to coexistence of the upright and tilted configurations of the Fe-N_{Im} bond with respect to the normal to the heme plane, the upright configuration being predominant species in both the complexes. The frequencies of both the components move upward with increase in concentration of 2-MeIm due to H-bonding of ligated 2-MeIm and other molecules of 2-MeIm in the solution. With more sterically hindered axial ligand 1,2-Me_2Im, again both the upright and tilted configurations co-exist but the tilted configuration is the predominant species in the case of Fe^{II}OEP(1,2-Me_2Im) while the upright configuration is the major species for the Fe^{II}PPDME(1,2-Me_2Im) complex. The vinyl groups in the PPDME-complex play dominant role in non-bonded interactions with the sterically hindered axial ligands in stabilizing the specific configurations.

REFERENCES

1. Spiro, T.G. in *"Iron Porphyrins"*, Lever, A.B.P.; Gray, H.B., Eds.; Addison-Wesley, Reading, MA, Part II, p. 89, 1983.

2a. Hori, H.; Kitagawa, T. *J. Am. Chem. Soc.* 102, 3608, 1980.

b. Nagai, K.; Kitagawa, T. *Proc. Natl. Acad. Sci, U.S.A.* 77, 2033, 1980.

3a. Collman, J. P.; Brauman, J.I.; Collins, T.J.; Iverson, B.L.; *Lang, G.; Pettman, R.B.; Sessler, J.L.; Walters, M.A. J. Am. Chem. Soc.* 105, 3038, 1983.

b. Scott, T. W.; Friedman, J.M. *J. Am. Chem. Soc.* 106, 5677, 1984.

c. Stein, P.; Mitchell, M.; Spiro, T.G. *J. Am. Chem. Soc.* 102, 7795, 1980.

d. Choi, S.; Lee, J.J.; Wei, Y. H.; Spiro, T. G. *J. Am. Chem. Soc.* 105, 3692, 1983.

e. Landrum, J.T.; Hatano, K.; Scheidt, W.R.; Reed, C.A. *J. Am. Chem. Soc.* 102, 6729,1980.

4. Bangcharoenpaurpong, O.; Schomacker, K. T.; Champion, P. M. *J. Am. Chem. Soc.* 106, 5688, 1984.

5. Freidman, J. F. *Science*, 228, 1273, 1985

6a. Fuhrhop, J.H.; Smith, K.M. in *"Porphyrins and Metalloporphyrins"* Smith, K. M. Ed., American Elsevier, New York, p. 835, 1975.

6b. Ogoshi, H.; Sugimoto, H.; Watanabe, E.; Yoshida, Z.; Maeda, Y.; Sakai, H. *Bull. Chem. Soc. Jpn.*, 54, 3414, 1981.

7a. Kincaid, J. R.; Stein, P; Spiro, T. G. *Proc. Natl. Acad. Sci.* U.S.A. 76, 549, 1979.

b. Kitagawa, T.; Nagai, K.; Tsubaki, M. *FEBS Lett.* 104, 376, 1979.

8. Yoshimura, T.; Ozaki, T. *Bull, Chem. Soc. Jpn.* 52, 2268, 1979.

9. Satterlee, J. D.; LaMar, G. N.; Frye, J. S. *J. Am. Chem. Soc.* 98, 7275, 1976.

10a. Mitchell, M. L.; Li, X. Y.; Kincaid, J. R.; Spiro, T. G. *J. Phys. Chem.* 91, 4690, 1987.

b. Ozaki, Y.; Iriyama, K.; Ogoshi, H.; Kitagawa, T. *J. Am. Chem. Soc.* 109, 5583, 1987.

11a. Li, X. Y.; Czernuszewicz, R. S.; Kincaid, J. R.; Spiro, T.G. *J. Am. Chem. Soc.* 111, 7012, 1989.

b. Czernuszewicz, R.S.; Li, X.Y; Spiro, T.G. *J. Am. Chem. Soc.* 111, 7024, 1989.

c. Spiro, T.G.; Czernuszewicz, R.S.; Li, X.Y. *Coord. Chem. Rev.* 100, 541, 1990.

12a. Takano, T. *J. Mol. Biol.* 110, 569, 1977.

b. Phillips, S. E. V. *J. Mol. Biol.* 142, 531, 1980.

13. Scott, T. W.; Friedman, J. M. *J. Am. Chem. Soc.* 106, 5677, 1984.

14a. Jameson, G. B.; Molinaro, F. S.; Ibers, J. A.; Collman, J. P.; Brauman, J. I.; Rose, E.; Suslick, K. S. *J. Am. Chem.*

Soc. 102, 3224, 1980.

14b. Scheidt, W.R.; Geiger, D.K.; Lee, Y.J.; Reed, C.A.; Lang, G. *J. Am. Chem. Soc.* 107, 5693, 1985.

c. Scheidt, W.R.; Gouterman, M. in *"Iron Porphyrins"*, Lever, A.B.P.; Gray, H. B.; Eds.; Addison-Wesley, Reading, MA, Part I, p. 1, 1983.

15. Verma, A.L.; Chaudhury, N.K. *J. Raman Spectrosc.* (submitted).

16. Sarkar, M.; Verma, A.L. *J. Raman Spectrosc.* 17, 407, 1986.

17. Choi, S.; Spiro, T. G.; Langry, K. C.; Smith, K. M.; Budd, D. L.; LaMar, G. N. *J. Am. Chem. Soc.* 104, 4345, 1982.

18a. Goff, H.M. in *"Iron Porphyrins"* , Lever, A.B.P.; Gray, H.B., Eds., Addison Wesley, Reading, MA, Part I, p. 239, 1983.

b. Goff, H. *J. Am. Chem. Soc.* 102, 3252, 1980.

c. Walker, F.A. *J. Am. Chem. Soc.* 102, 3254, 1980.

d. Walker, F.A.; Reis, D.; Balke, L.V. *J. Am. Chem. Soc.* 106, 6888, 1984.

TABLE - 6.1

Concentration dependence of the $\nu_{Fe-N_{Im}}$ stretching frequencies in the photoreduced $Fe^{II}OEP$ and $Fe^{II}PPDME$ in CH_2Cl_2 containing 0.1% (v/v) methanol under anaerobic condition in the presence of axial ligands.

Conc.of axial ligands (mM)	with 2-MeIm				with 1,2-Me_2Im			
	$Fe^{II}OEP$		$Fe^{II}PPDME$		$Fe^{II}OEP$		$Fe^{II}PPDME$	
	(a)	(b)	(a)	(b)	(a)	(b)	(a)	(b)
0.1	-	-	197(w)	-	-	-	194(w)	-
1	-	190(w)	201(mw)	-	-	187(vw)	194(mw)	-
5	204(mw)	190(sh)	202(mw)	186(sh)	207(w)	184(w)	194(ms)	184(sh)
10	205(ms)	193(sh)	202(ms)	187(Sh)	207(sh)	186(ms)	194(ms)	183(sh)
40	-	-	205(ms)	199(sh)	-	-	-	-
50	207(ms)	197(sh)	-	-	207(sh)	186(ms)	194(ms)	-
100	211(ms)	196(sh)	210(ms)	-	207(sh)	186(ms)	-	-

(a) and (b) represent the upright and tilted configurations repectively of the axial ligands.

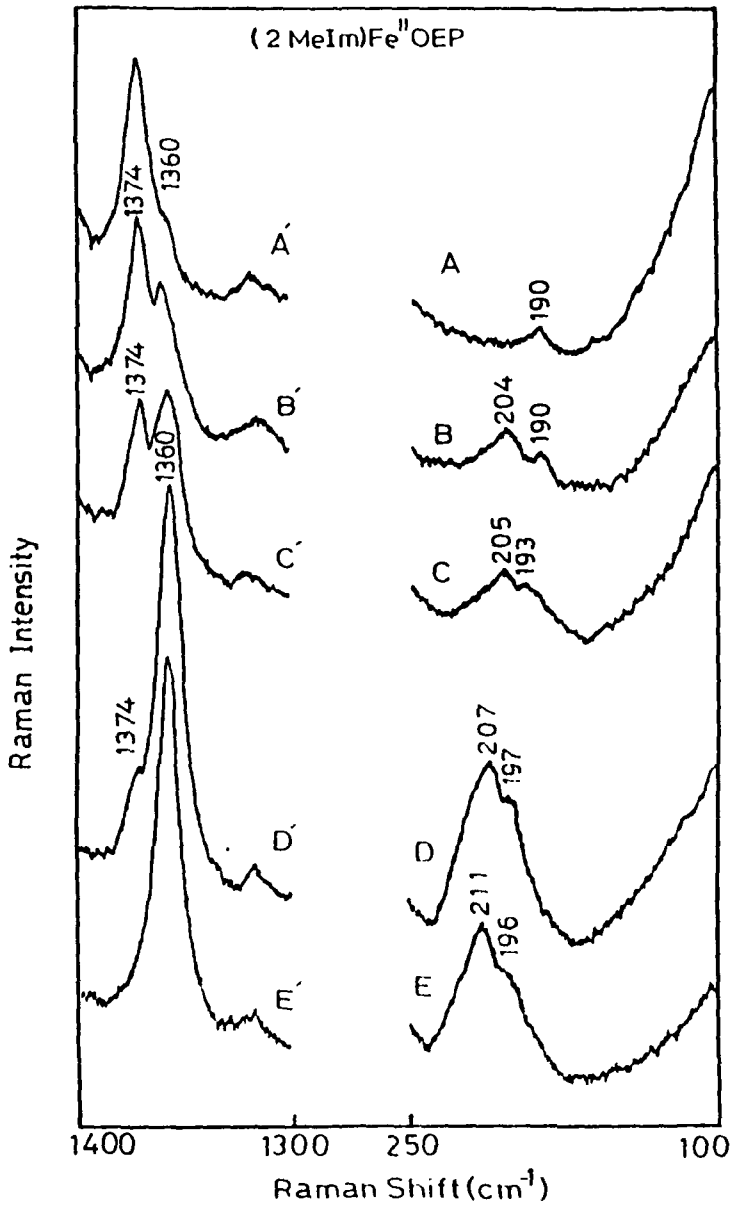

Fig. 6.1 RR spectra of anaerobically photoreduced Fe^{II}OEP(2-MeIm) in CH_2Cl_2 solution in the (100 -250 cm^{-1}) region at different concentrations of 2-MeIm: (A) 1 mM; (B) 5 mM; (C) 10 mM; (D) 50 mM; (E) 100 mM. The corresponding ν_4 regions (1300-1400 cm^{-1}) are shown in Figures 6.1A' to 6.1E'. Experimental conditions: Scan speed, 12cm^{-1}/min.; Time constant, 2 sec; Slit width, 200 μm; Excitation line, 441.6 nm; Laser power, 30 mW; Sensitivity for Figures 6.1A to 6.1E was 500 counts/sec. and for the Figures 6.1A'-6.1E' was 1000 counts/sec. concentration of (I)FeOEP was 1 mM for all the spectra.

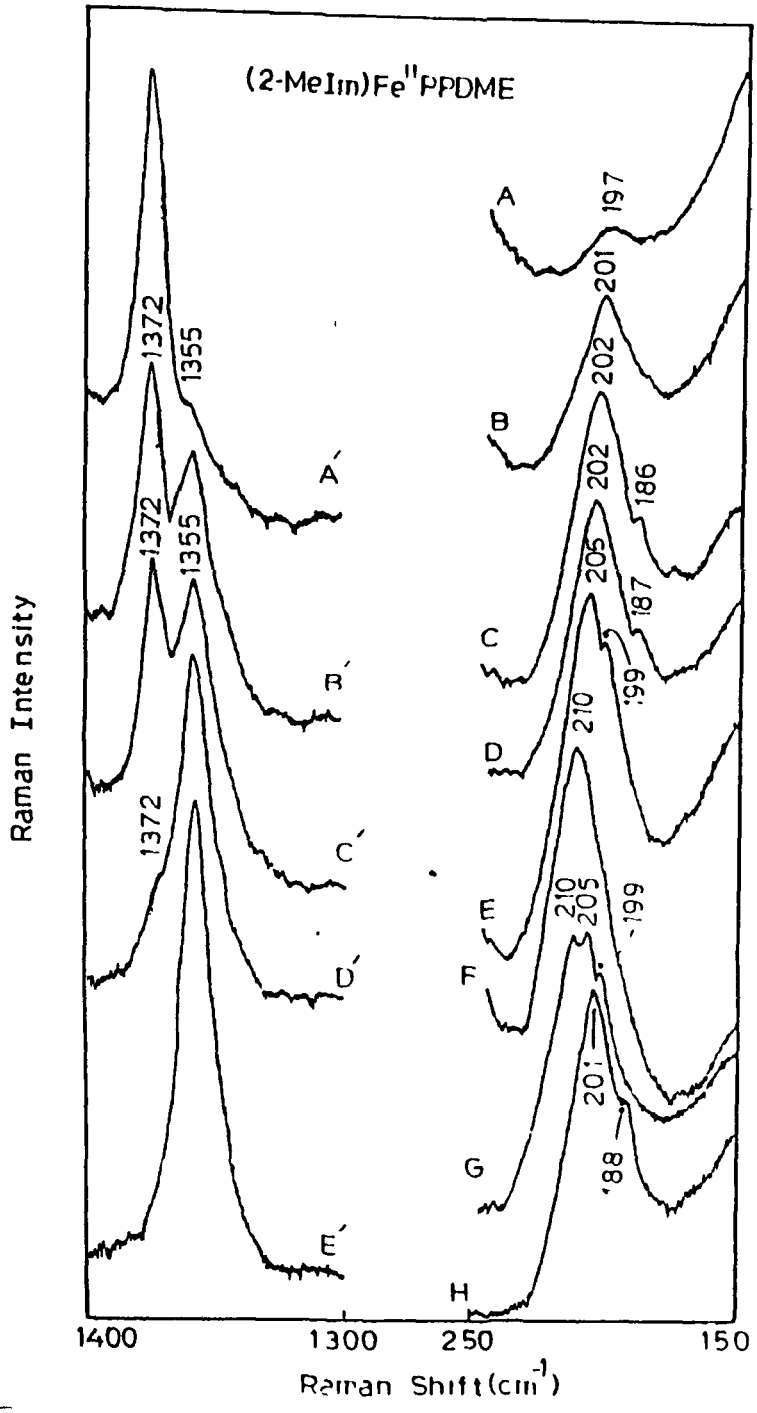

Fig. 6.2 RR spectra of anaerobically photoreduced Fe^{II}PPDME(2-MeIm) in CH_2Cl_2 solution in the (150-250 cm^{-1}) region at different concentrations of 2-MeIm: (A) 0.1 mM; (B) 1 mM; (C) 5 mM; (D) 10 mM; (E) 40 mM; (F) 100 mM; (G) excess 2-MeIm (200 mM) for aerobic photo-reduction and (H) 10 mM for chemical reduction by $Na_2S_2O_4$. The corresponding ν_4 mode regions (1300-1400 cm^{-1}) are shown in Figures 6.2A' to 6.2E'. The spectral features in the ν_4 mode region were identical for Figures 6.2E to 6.2H and thus shown by Fig. 6.2E' only. Experimental conditions were the same as for Fig. 6.1 except for the scan speed, 25 cm^{-1} min and Time constant, 3.2 sec. Concentration of (Cl)FePPDME was 0.5 mM.

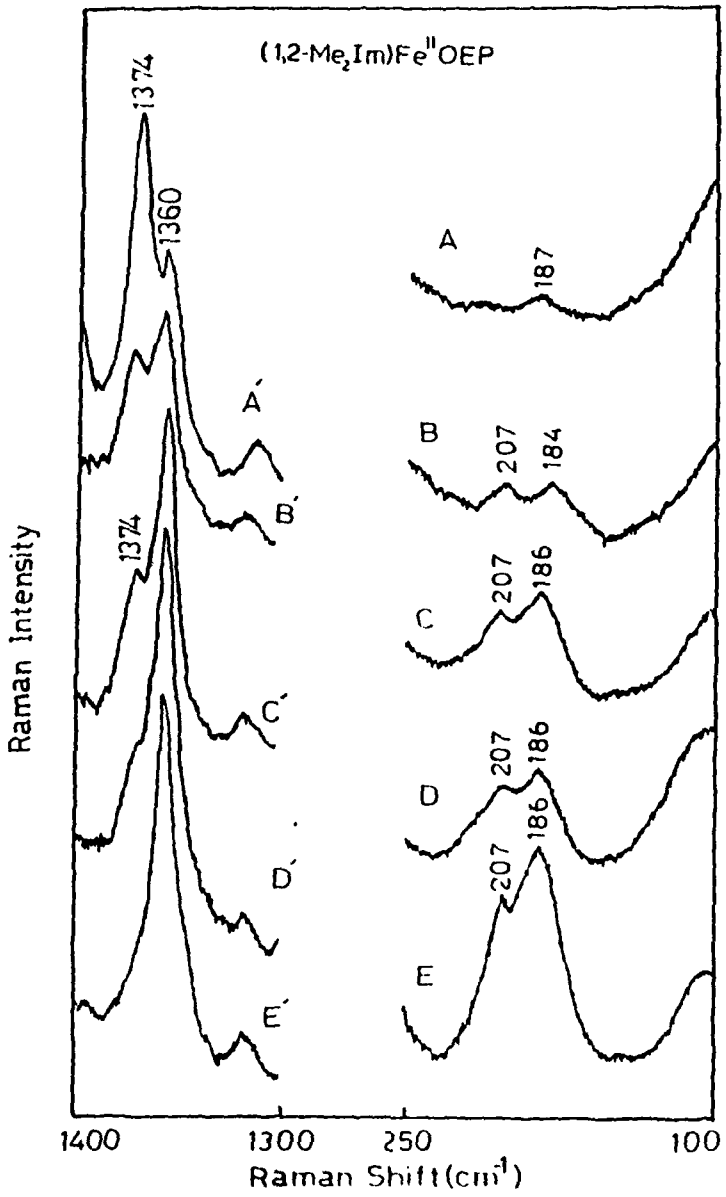

Fig.6.3 RR spectra of anaerobically photoreduced $Fe^{II}OEP(1,2\text{-}Me_2Im)$ in CH_2Cl_2 solution in the (100-250 cm^{-1}) region at different concentrations of $1,2\text{-}Me_2Im$: (A) 1 mM; (B) 5 mM; (C) 10 mM; (D) 50 mM; (E) 100 mM. The corresponding ν_4 mode regions (1300-1400 cm^{-1}) are shown in Figures 6.3A' to 6.3E'. Experimental conditions were the same as in Fig. 6.1.

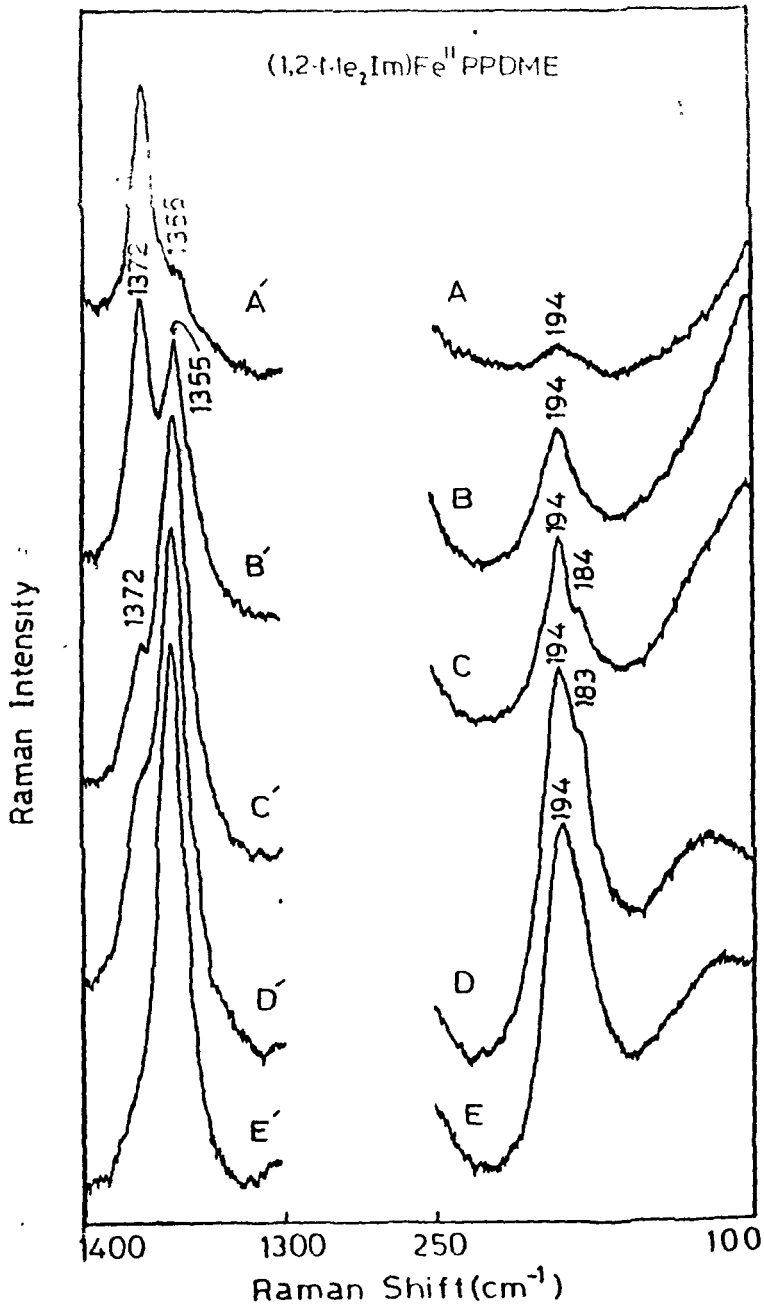

Fig.6.4 RR spectra of anaerobically photoreduced Fe^{II}PPDME(1,2-Me_2Im) in CH_2Cl_2 solution in the (100-250 cm^{-1}) region. The concentrations of 1,2-Me_2Im are: (A) 0.1 mM; (B) 1 mM; (C) 5 mM; (D) 10 mM; (E) 50 mM. The corresponding ν_4 mode regions (1300-1400 cm^{-1}) are shown in Figures 6.4A' to 6.4E'. Experimental conditions were same as in Fig. 6.1.

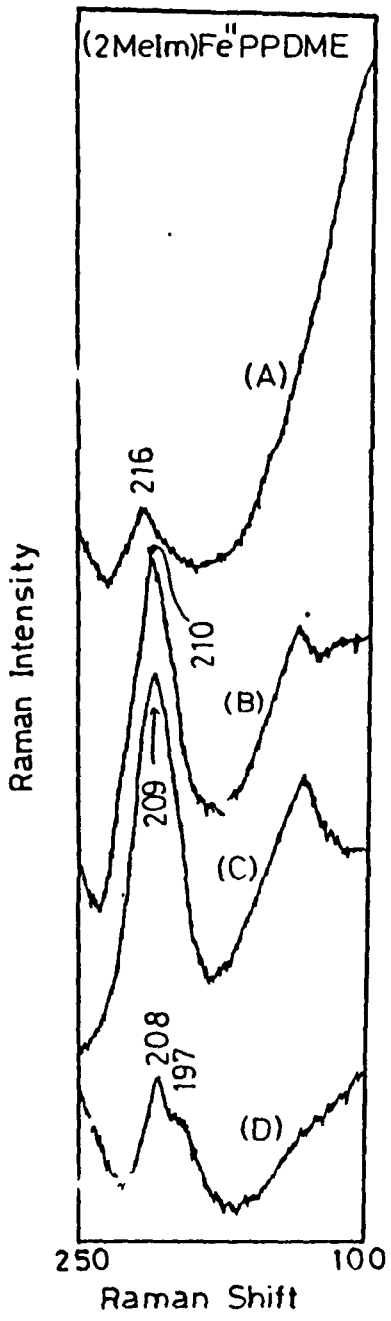

Fig. 6.2 RR spectra of photo-reduced Fe^{II}PPDME(2-MeIm) in dimethylsulfoxide solution at low temperatures in the (100-250 cm^{-1}) region. The concentrations of Fe(PPDME) and 2-MeIm are kept Constant at ~0.5 mM and 50 mM respectively for the various temperatures. (A) 150K; (B) 200K; (C) 250K; (D) 300K. Other experimental conditions are identical to that of Fig. 6.1.

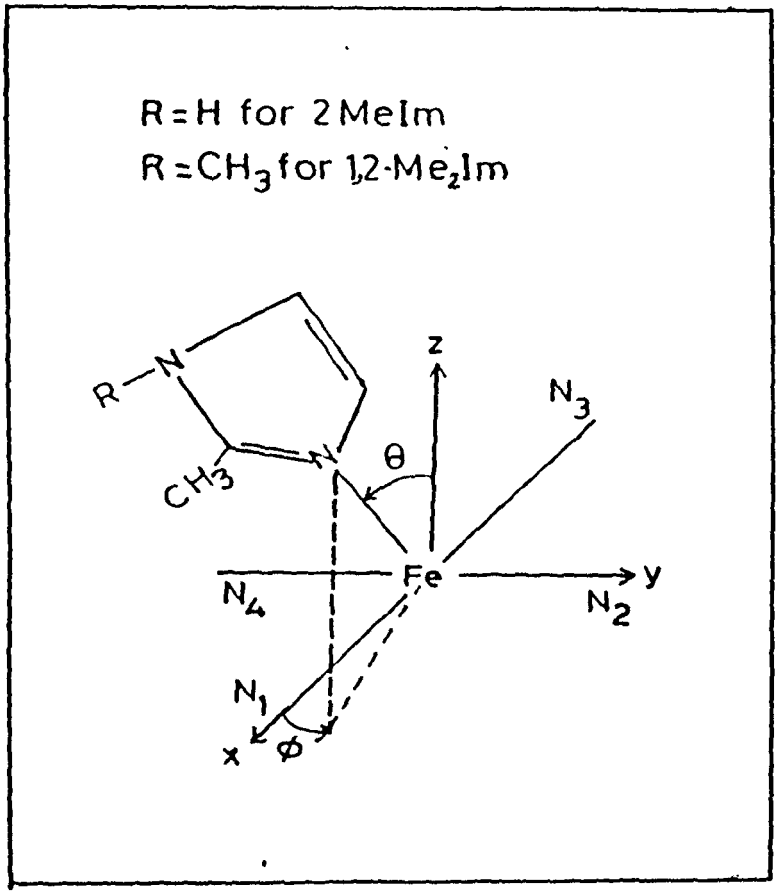

Fig. 6.6 A diagramatic representation of the axial ligand showing polar angle and azimuthal angle Φ, with respect to the normal to the porphyrin plane. θ 0° corresponds to upright configuration and any other value of corresponds to tilted configuration of the ligand with nearly same value of $\phi = 15^{\circ}$ - 25°.

SUMMARY AND CONCLUSIONS

The scope of this thesis is to elucidate the basic steps involved in the mechanism of photo-reduction of iron porphyrins and related stereochemical aspects of axial ligation as probed by resonance Raman technique from the point of view of understanding various functions of heme-related proteins. The continuing research interest on iron porphyrins stems from the fact that they form the active site for a variety of biochemical processes such as oxygen binding in hemoglobin and myoglobin in the reduced state. This discriminating behaviour is not followed by other small ligands, e.g.; carbonmonoxide, imidazole, nitrogen monoxide etc., all of which bind the iron in both the ferric and ferrous states. Over the years, various workers have been trying to explain this selective nature of binding of O_2 in iron(II) state. Therefore, it is of crucial importance to understand the reduction mechanism involved in the redox processes, electron distribution and structural implications at the active site in iron porphyrin complexes.

We have therefore undertaken systematic resonance Raman (RR) studies on some model complexes such as iron-protoporphyrin-IX dimethylester chloride [Fe(PPDME)Cl] and iron-octaethyl porphyrin iodide [Fe(OEP)I] in the presence of biologically relevant axial ligands like, 2-methylimidazole (2-MeIm), 1,2-dimethylimidazole (1,2-Me_2Im), imidazole (Im) and 1-methylimidazole (1-MeIm) to understand the mechanism of

photoreduction and stereochemistry of axial ligation which may be helpful in gaining insight on the electron transfer processes and other structure-function relationships in various heme-related proteins.

Many extensive reviews on iron-porphyrins have been cited in Chapter I. Special emphasis has been given on the stereochemical aspects of iron porphyrins alongwith discussion based on various spectroscopic techniques. The importance of RR studies on related model complexes was emphasized for obvious reasons. The basis for employing photo-reduction technique and in situ monitoring of the reduction process probed by RR technique has also been emphasized with various advantages over conventional chemical, electrochemical and other available techniques.

Chapter II presents pertinent theoretical background to understand the absorption and resonance Raman spectra of iron porphyrins. Further theoretical description of iron porphyrins has been incorporated in this chapter.

Chapter III gives details of different experimental techniques used in this study along with preparation of samples and degassing of solutions used in recording Raman spectra. Some details of other instruments and accessories have also been covered in this chapter.

In Chapter IV, we give details of our RR studies on the

mechanism of photoreduction of iron-protoporphyrin-IX dimethylester chloride Fe^{III}(PPDME)Cl in the presence of axial ligands like 2-MeIm, 1,2-Me_2Im, Im etc. In this study, we have observed that in pure CH_2Cl_2 solution, the iron porphyrins containing 2-MeIm or 1,2-Me_2Im as electron donors do not photoreduce even under anaerobic conditions upon laser excitation in the Soret region. But the same solution containing a trace amount of alcohol (primary or secondary) is photoreduced completely. This specific catalytic effect of alcohol has been termed as "directing ligand", where alcohol helps removing halide ion from the coordination sphere of iron and then facilitating coordination of 2-MeIm or 1,2-Me_2Im. The dependence of photo-reduction on excitation wavelength was also ascertained from action spectra, where the yield of photoreduction was found to be maximum on excitation in the Soret absorption region. The rate constant for photo-reduction, k_R^{-1} was calculated to be 10 minute from action spectra in the UV-visible region of anaerobic solutions of iron-porphyrins by irradiation with a white light source for different times in the presence of a short-cut filter L-38. By monitoring the extent of photoreduction of Fe(PPDME)Cl in anaerobic conditions as a function of concentration of 2-MeIm, we have identified ligand free, four coordinated, intermediate spin-complex as the transient species involved in the photoreduction process. Based on this and excitation wavelength dependent action spectra of photoreduction, we have proposed the following mechanism for photoreduction. By irradiation of

Fe^{III}PPDME-(2-MeIm) in the Soret region, the system is excited to the $e_g(\pi^*)$ or the antibonding d_z2 orbital, where coordinated 2-MeIm dissociates, donating its charge to the iron centre. The resulting 2-MeIm^+ diffuses away from the coordination sphere of the iron-porphyrin. The ligand free Fe^{II}PPDME is then stabilized by coordination of another 2-MeIm from the solution at the fifth ligand position stabilizing the high spin, five coordinated Fe^{II}PPDME(2MeIm) complex as the final photoreduced product.

Further studies by other spectroscopic techniques like time resolved RR spectroscopy might help in understanding the mechanism of photo-reduction in greater details, especially to establish the nature of transient species involved in the photo-reduction process. Measurement of magnetic moments of the various products involved in the photo-reduction process and careful chemical analysis of the products formed would also strengthen our proposed mechanism. The origin of Soret coupled charge-transfer transitions also need to be delineated clearly in any further study.

We have extended our RR studies as discussed in Chapter V to low temperatures in order to characterize the photoreduced product and to understand the mechanism of electron transfer process. We have discovered that the Fe^{III}PPDME(1,2-Me_2Im) complex in DMSO at low temperature in the soft matrix is photoreduced and we have identified the six-coordinated, intermediate spin, $Fe^{II}PPDME(DMSO)_2$ as the prominent

photoreduced species in the soft matrix. The same solution cooled to ~20K could not be photoreduced at lower levels of laser power (5 mW) at 441.6 nm where the DMSO matrix remains solidified and thus restricting diffusion of detached 1,2-Me_2Im^+ ligand in the excited state. This implies that only short-range electron transfer is responsible for photoreduction. The non-photoreducibility in even the soft matrix by excitation with about 200 mW laser power in the α - β absorption region once again suggests that the charge transfer process is coupled to the Soret transition. On increasing the temperature of the soft matrix, a distinct change in the axial ligation has been observed where the Fe^{II}PPDME(DMSO)$_2$ species converts to Fe^{II}PPDME(1,2-Me_2Im) complex at a temperature of ~250K in the cold solution. The photoreduction at low temperatures in the soft matrix was obtained irrespective of the presence of alcohols. We also report our preliminary investigations on the effect of different solvents on the yield of photoreduction of iron-porphyrins at room temperature. It is not possible to correlate the yield of photoreduction with the known relationships on solvent parameters like Marcus parameter or the Gutmann solvent acceptor number but it appears to be a complex function of different solvent parameters.

Although, we have identified intermediate spin state Fe^{II}PPDME(DMSO)$_2$ as the final species after photoreduction from our present RR study, if the same study can be carried out in some suitable non-coordinating solvents at low temperatures, it

may be possible to delineate the nature of transient species involved at low temperature. A much improved device for low temperature arrangement in which solid matrix formation is realized even after prolonged laser irradiation, would help to elucidate the effect of short-range electron transfer process. The solvent dependent study on the yield of photoreduction is yet to be clearly understood.

In Chapter VI, we discuss details of stereochemical aspects of axial ligation in photoreduced iron porphyrins. The concentration dependent RR studies of the $Fe-N_{Im}$ stretching modes in the model complexes FeOEP and FePPDME with different axial ligands like 1,2-Me_2Im and 2-MeIm have revealed doublet structure in the $Fe-N_{Im}$ stretching region. This doublet structure has been suggested to arise as a result of coexistence of the upright and tilted configurations of the $Fe-N_{Im}$ bond with respect to the normal to the porphyrin plane. The upright configuration is predominant in iron porphyrin complexes with 2-MeIm as the axial ligand. However, with more sterically hindered ligand 1,2-Me_2Im tilted configuration is found to be favoured in FeOEP complex, where as upright configuration is predominant in FePPDME complex. This effect was ascribed to the specific effect of substituents at the macrocycle where vinyl groups are asymmetrically disposed and thus play key role in stabilizing the specific configuration in the (1,2-Me_2Im) iron complexes. In case of (2-MeIm) iron porphyrins complexes , both the frequency components of $Fe-N_{Im}$ stretching modes showed

upshift with increase in concentration of 2-MeIm due to H-bonding with the N_δ-H proton of the coordinated 2-MeIm with free 2-MeIm. The extent of frequency shift is higher in case of PP complex, which once again is attributed to the specific effect of vinyl group substituents.

The coexistence of both the upright and tilted configurations of axial ligands in solution has been characterized by our RR study. Further work by NMR, ESR and other techniques will help to understand the other stereochemical parameters responsible for coexistence of both the configurations.